Performance Analysis for the RIS and the AmBC Systems at the Short Blocklength Regime

Likun Sui

A thesis submitted in fulfilment of the requirements

for the degree of

DOCTOR OF PHILOSOPHY

School of Electrical and Information Engineering

The University of Sydney

February 2023

To my beloved parents and fiancée,
Yishan Sui, Sihui Tan, and Chenmeng Wang

Abstract

This thesis focuses on the study of the performance of a reconfigurable intelligent surface (RIS) system and ambient backscatter communication (AmBC) system with multiple input and output antennas. The RIS has been regarded as a bright technology in the field of communication. It is of the utmost importance to be used to overcome the limitations of current fifth-generation (5G) wireless networks, which, for instance, are that high-frequency signals are highly sensitive to obstacles such as walls, trees, and buildings to deteriorate line-of-sight (LOS) links. Unlike existing relay technologies, RIS uses a massive array of reflecting elements to alleviate the negative environment. By manipulating the phase shift and the upcoming wave's angle of reflection, and the angle of the incident through software, the transmitted signal quality can be significantly improved. In the meantime, at the receiver side, the multipath propagation can be minimized. Furthermore, AmBC is an innovative communication method that provides a cost-effective, energy-efficient, and spectrum-efficient approach to transmitting data. Due to these advantages, AmBC has emerged as a competitive solution for building and deploying the Internet of Things (IoT) in the future. The AmBC system allows devices such as tags and sensors to utilize radio frequency (RF) signals that are present in their surrounding environment to transmit information signals to tags and sensors by harvesting power from these signals. Speaking of the difference between the radio frequency

identification (RFID) communication system and an AmBC system, its benefit is to collect the information by utilizing ambient RF source signals in lieu of creating an information-bearing signal.

In order to analyze the performance of the systems mentioned above, two main fundamental mathematical theories are included. The first theory is the Polyanskiy-Poor-Verdú (PPV) bound that new achievability and converse bounds for general channel classes are presented, which are more precise than previous bounds for a range of relevant parameters. The PPV bound demonstrates that when an average or maximal error probability is given and a blocklength is set, there always exists the maximal achievable channel coding rate and shows that the maximum achievable rate can be accurately approximated for moderate and short blocklengths. In this theory, a channel property, known as channel dispersion, determines the convergence speed towards capacity. The second theory is the sphere-packing bound, which is the most precise formula for the case in which all codewords require equal energy for transmission with Phase-Shift Keying (PSK) modulation. In this theory, all possible codewords with equal transmitting energy form a multidimensional sphere. A Voronoi cell is used to define a single codeword situated on the sphere. Sphere-packing means that every cell has the same radius and different solid angle, and then every cell can be treated as a polyhedron in the sphere. The additive white Gaussian noise (AWGN) modifies the area of the polygon base, i.e., more noise means a larger size of the area. The error probability of the maximum likelihood (ML) decoder occurs when the AWGN causes the area of the polygon base of one codeword to overlap that of another codeword. Thus, by applying the sphere-packing theory to the AWGN channel with the PSK modulation scheme, the tightest lower bound for the specific channel is obtained.

This thesis investigates and analyzes the performances of the RIS and AmBC

systems, and three main research works are involved. The first research work of this thesis is to present the decoding error probability bounds for the optimal code in an RIS system within the short blocklength regime and given a code rate and signal-to-noise ratio (SNR). The approach uses sphere-packing techniques to derive the main results, with the Wald sequential t-test lemma and the Riemann sum serving as the primary tools for obtaining the closed-form expressions for both the upper and lower bounds. The numerical results are demonstrated to illustrate the performance of the findings.

The second research work focuses on examining the maximal achievable rate for a given maximum error probability and blocklength in a system that employs RIS to aid a multiple-input and multiple-output (MIMO) communication system. The findings of this research include finite blocklength and finite alphabet constraints channel coding achievability and converse bounds, which are established through the use of the Berry-Esseen theorem, the Mellin transform, and the closed-form expression of the mutual information and the unconditional variance. The numerical analysis indicates that the maximum achievable rate is reached rapidly as the blocklength increases. Additionally, the channel variance accurately reflects the deviation from the maximum achievable rate due to the finite blocklength.

The third research work investigates the maximum achievable rate in an AmBC MIMO system, given a fixed blocklength and maximum error probability. Additionally, both achievability and converse bounds for the specific channel coding with finite blocklength and finite alphabet constraints are established. The bounds are based on the same mathematical theories as the previous research focus, such as the Neyman-Pearson test, the Berry-Esseen theorem, and the Mellin transform. Then a closed-form expression for the mutual information and information variance is derived, which simplifies the computation process.

To explore the relationship between the error probability of the RF source signal and the error probability of the tag symbol with respect to the blocklength in the AmBC MIMO system, we apply low-complexity ML detection. The numerical evaluation demonstrates that as the blocklength increases, there is a fast convergence to the maximum achievable rate. Additionally, we prove that the information variance is an accurate measure of the backoff from the maximal achievable rate due to finite blocklength.

Acknowledgments

I would like to express my sincere gratitude to those who have supported me during this unforgettable research journey. It would be impossible for me to walk this journey alone without their selfless help, support, and encouragement.

First and foremost, an immense thanks and deepest regards to my PhD supervisor, Dr. Zihuai Lin. I am eternally grateful to him for offering me the opportunity to study under his supervision. Support and guidance throughout the whole candidacy from you have been invaluable. Dr. Zihuai is a father figure to me. He has been invaluable to my research work, consistently demonstrating a willingness to lend a listening ear, engage in fruitful discussions, and provide constructive advice. Beyond his role as my supervisor, he has taken on the role of a mentor, offering guidance that extends far beyond the confines of my academic pursuits. Dr. Zihuai's philanthropic spirit and obliging nature have had a profound impact on me, inspiring me to be more appreciative and compassionate towards those around me. His approach to life has imbued me with the strength to face challenges and overcome obstacles. I am confident that this mindset will continue to motivate me as I navigate future challenges.

I would like to take a moment to express my heartfelt appreciation to Prof. Branka Vucetic, Dr. Peng Wang and Dr. Ming Ding. Their unwavering support and boundless patience have been instrumental in helping me overcome the various

obstacles I faced during my research. Their guidance and encouragement, coupled with their profound knowledge and insightful ideas, have been a constant source of motivation and inspiration for me. I am deeply grateful for the constructive feedback and suggestions they provided, without which my research would not have been possible.

I also would like to thank all my colleagues at the Center of Excellence in Telecommunications, the University of Sydney, Yunkai Hu, Jichao Leng, Xucun Yan, Shuang Liu, etc. I am delighted to have had the opportunity to share a joyful moment with all of you. Although I may not have mentioned every individual by name, please know that each and every one of you will hold a special place in my memories.

Last but not least, I would like to thank my beloved parents and fiancée, Sihui Tan, Yishan Sui, and Chenmeng Wang, who always support me and have faith in me all the time.

I would like to extend my deepest appreciation to all those who have been a source of strength and support, enabling me to face each new day with renewed vigour. My gratitude is truly immeasurable, and words cannot fully convey the extent of my appreciation.

Likun Sui

Sydney Australia

February 2023

Statement of Originality

I, Likun Sui, declare that this thesis, submitted in fulfilment of the requirements for the degree of Doctor of Philosophy in the School of Electrical and Information Engineering, the University of Sydney, is the original work of the author unless otherwise stated. The document has not been previously submitted for the award of any other qualification at any educational institution. Most of the results contained herein have been published, accepted for publication, or submitted for publication in journals or conferences of international standing. My contribution in terms of published material is listed in the Chapter "Publications".

These studies were conducted under the supervision of Dr. Zihuai Lin and Prof. Branka Vucetic from the University of Sydney.

Likun Sui

School of Electrical and Information Engineering

The University of Sydney

February 2023

Publications

The following is a list of publications in refereed journals and conference proceedings produced during my Ph.D. candidature.

Journal Papers

[J1] L. Sui, Z. Lin, "Analytical Bounds for the Optimal Code over the Reconfigurable Intelligent Surface at a Short Blocklength", *IEEE Wireless Communications Letters*, [Early Access], Jun. 2023. doi: 10.1109/LWC.2023.3283528.

[J2] L. Sui, Z. Lin, P. Xiao, and B. Vucetic, "Performance Analysis for Reconfigurable Intelligent Surface Assisted MIMO Systems", *IEEE Transaction on Wireless Communications*, [Early Access], May. 2023. doi: 10.1109/TWC.2023.3277887.

[J3] L. Sui, Z. Lin, P. Xiao, H. V. Poor, and B. Vucetic, "Performance Analysis of Multiple-Antenna Ambient Backscatter Systems at Finite Blocklengths", *IEEE Internet of Things Journal*, [Early Access], Apr. 2023.
doi: 10.1109/JIOT.2023.3267130.

[J4] L. Sui, Z. Lin, "Probability of Error for Optimal Codes in a Reconfigurable Intelligent Surface Aided URLLC System". *IEEE Communications Letters*, [Early Access], Jun. 2023. doi: 10.1109/LCOMM.2023.3289195.

Contents

List of Figures

List of Tables

List of Abbreviations

AFSS	Active Frequency Selective Surfaces
AmBC	Ambient Backscatter Communication
AP	Access Point
AWGN	Additive White Gaussian Noise
BCH	Bose-Chaudhuri-Hocquenghem
BER	Bit Error Rate
BPSK	Binary Phase Shift Keying
B-DMS	Binary-Input, Discrete, Memoryless Symmetric
CMA	Coverage Maximization Algorithm
CR	Cognitive Radio
CSI	Channel State Information
DT	Dependent Test
EM	Electromagnetic
FECC	Forward Error Control Coding
ISPB	Improved Sphere-Packing Bound
IoT	Internet of Things
i.i.d.	Independent and Identically Distributed
LOS	Line-of-sight
LDPC	Low-density Parity-check

ML	Maximum Likelihood
MMSE	Minimum-mean-square-error
MIMO	Multiple-input-multiple-output
MISO	Multiple-input-single-output
PDF	Probability Density Function
PPV	Polyanskiy-Poor-Verdú
PSK	Phase-Shift Keying
PTx	Primary Transmitter
P2P	Point-to-point
QPSK	Quadrature Phase Shift Keying
RF	Radio Frequency
RFID	Radio Frequency Identification
RIS	Reconfigurable Intelligent Surface
RV	Random Variable
SCL	Successive Cancellation List
SIC	Successive Interference Cancellation
SIMO	Single-input-multiple-output
SNR	Signal-to-noise-ratio
SPB59	1959 Sphere-Packing Bound
SPB67	1967 Sphere-Packing Bound
SR	Symbiotic Radio
SRx	Second Receiver
STx	Second Transmitter
ULAs	Uniform Linear Arrays
WLAN	Wireless Local Area Networks
3G	Third-generation

5G	Fifth-generation
6G	Sixth-generation

List of Notations

u	a variable
$\mathbf{u}$	a vector
$\mathbf{U}$	a matrix
$\mathcal{S}$	a set
$\mathbb{R}$	the real number field
$\mathbb{C}$	the complex number field
$GF(2)$	the Galois field of two element
$\mathrm{Re}\{u\}$	the real part of complex variable u
$\mathrm{Im}\{u\}$	the imaginary part of complex variable u
$\|u\|$	the absolute value of complex variable u
$\angle u$	the angle of the complex variable u
$\|\|\mathbf{u}\|\|$	the Euclidean norm of vector $\mathbf{u}$
$\mathbf{U}^\top$	the transpose of $\mathbf{U}$
$\mathrm{Trace}\{\mathbf{A}\}$	the trace of a square matrix A
$\mathbf{U}^\mathrm{H}$	the conjugate transpose of $\mathbf{U}$
$\|\mathcal{S}\|$	the cardinality of a set $\mathcal{S}$
$\mathbb{E}[u]$	the statistical expectation of u
$\mathbb{P}[A]$	the probability of an event A
$\exp\{u\}$	the exponential of u

$\log u$	the logarithm base 2 of u
$f_A(x)$	the PDF of A
$\max\{u, v\}$	the maximal number amongst u and v
$\min\{u, v\}$	the minimal number amongst u and v
$[u]^+$	the maximal number amongst u and 0
$< \cdot, \cdot >$	the inner product
$\otimes$	the vector multiplication over $GF(2)$
$P(A, B)$	the joint probability of events A and B
$P(A\|B)$	the probability of event A conditioned on event B
$B \setminus A$	the set of elements in B that are not in A
$\bigcup$	the union operator
I_n	the identity matrix of size n
$Q(x)$	the Craig's formula of Q-function, $Q(x) = \frac{1}{\pi}\int_0^{\pi/2} e^{-x^2/2sin^2(\theta)}d\theta$
$\mathcal{O}(\cdot)$	the big o notation
$\Gamma(a, b)$	the upper incomplete Gamma function, $\Gamma(a, b) = \int_b^\infty t^{a-1}e^{-t}dt$
$I_0(x)$	the modified Bessel function of first kind of order 0
$K_0(x)$	the modified Bessel function of second kind of order 0
${}_1F_1(a, b, c)$	the Kummer confluent hypergeometric function
$G_{c,d}^{a,b}\left(\cdot \middle\| \cdot\right)$	the Meijer G-function
$\lceil \cdot \rceil$	the ceiling function
$(\cdot)!$	the factorial function
$(\cdot)!!$	the double factorial function
$\binom{n}{k}$	the binomial coefficient, $\binom{n}{k} = \frac{n!}{k!(n-k)!}$
$Leb(\cdot)$	the Lebesgue measure

Chapter 1

Introduction

This chapter briefly describes the history of several communication systems and mathematical theories. Furthermore, it will step into the backgrounds and main motivations. In the third part, the main contributions of this thesis are summarized.

1.1 History of Reconfigurable Intelligent Surface

The advancements in fifth-generation (5G) wireless networks are uncovering various limitations. One of them is the sensitivity of high-frequency signals to obstacles like walls, trees, and buildings, which makes it difficult to establish reliable line-of-sight (LOS) links, leading to a drop in signal quality and coverage. Reconfigurable Intelligent Surface (RIS) has been regarded as another bright technology to tackle these limitations and pave the way for 5G and sixth-generation (6G) networks, garnering substantial attention from the wireless communication research community.

The introduction of Reconfigurable Intelligent Surfaces (RIS) [1] in wireless communication systems has changed the definition of radio propagation from passive to active. The concept of a smart radio environment where RIS can actively influence radio propagation has been established. The roots of RIS can be traced back to the

early research on Active Frequency-Selective Surfaces (AFSS) [2–4]. By controlling the PIN diodes integrated into AFSS, it is possible to perform spatial diversity and filter the specific frequencies from the incoming electromagnetic (EM) waves. This increases cell coverage, reduces interference between the EM waves, and optimizes the quality of service.

An RIS is designed to improve the signal quality at the receiver when the line-of-sight path is obstructed or weak. Unlike traditional relay technologies, an RIS can improve signal quality without requiring extra power or complicated signal processing. By adjusting the phase and angle of the incident and reflecting waves on each reflective element in a software-controlled manner, the reflected signals can be optimized to minimize the multipath effect on the received signals. This can result in amplifying the signal strength or reducing multipath interference by combining the reflected signals constructively or destructively.

1.2 History of Backscatter Communication

The landscape of wireless networking is undergoing a transformation, moving from simple point-to-point (P2P) communications to multi-functional systems that cater to a diverse range of user cases. The IoT is a crucial part of the future of wireless communication and is expected to encompass billions of connected devices. However, this presents three major challenges for the design of IoT networks: cost efficiency, spectrum efficiency, and energy efficiency. With a significant proportion of these devices relying on limited spectrum resources and some being ultra-low-power or battery-free, Ambient Backscatter Communication (AmBC) has been seen as an encouraging solution to provide numerous benefits, such as decreasing the cost, expanding the spectrum efficiency, and increasing the energy efficiency in the wireless

communication systems and the future IoT networks.

The concept of backscatter communication has roots dating back to World War II when it was used to detect enemy aeroplanes by reflecting radar signals. In 1948, Stockman [5] introduced backscatter communication as a technique that transmits data by modulating and reflecting received RF signals in lieu of generating them independently. Based on the configuration, backscatter communication can be classified into two main types: ambient backscatter communication systems and symbiotic radio systems.

1.2.1 Ambient Backscatter Communication

Recently, a new communication technology called ambient backscatter [6–13] has gained attention as a solution to the limitations of conventional backscatter communication systems. In AmBC systems, backscatter devices can transmit their own information symbols to other devices or readers by harnessing existing RF source signals. This eliminates the need for an extra frequency spectrum. At the receiver end, useful information can be decoded from the received signals by extracting the ambient backscatter signal out of the RF source signal. This means that backscatter transmitters can transmit data even when the receiver is not initiated, as long as they have enough energy from the RF source [14]. This capability makes the AmBC system a promising technology for various practical applications.

AmBC has enormous potential as a low-energy communication technology, especially for the IoT, but it is still facing several challenges. The transmission efficiency of an AmBC system is heavily dependent on the type of ambient source, whether indoor or outdoor. As a result, AmBC systems must be tailored to specific ambient sources. Another challenge is to optimize the scheduling of data transmission in order to make the most of the ambient signals, which are dynamic in nature. More-

over, the communication protocols of AmBC systems must be designed to avoid interfering with the transmissions of licensed users. Substantial research has been conducted to address these challenges and enhance AmBC systems in various aspects.

1.2.2 Symbiotic Radio System

Symbiotic radio (SR) is defined in [15] as a cutting-edge backscattering communication system. It absorbs the benefits of cognitive radio (CR) and AmBC while addressing their drawbacks. The basic SR system is comprised of two parts: the primary system and the secondary system. Unlike CR, SR employs backscattering radio technology, which applies no additional power in the ambient backscatter devices, to make the secondary transmission from the STx to the second receiver (SRx) become possible instead of utilizing the active RF source signal at both the primary transmitter (PTx) and second transmitter (STx) and consuming significant power. Specifically, the STx transmits its own information to the SRx by modulating and reflecting the RF signals received from the PTx, allowing the secondary system to increase spectrum and energy efficiency effectively.

In SR, the two systems operate cooperatively on both the transmitter ends, and the receiver ends. By leveraging the collaborative decoding process at the SRx, it becomes possible to decode primary and secondary information simultaneously, effectively avoiding interference between the primary and secondary signals and establishing highly reliable backscattering communications. The secondary system would be seen as multipath compared with the primary system, which is similar to the MIMO system, to increase the spectrum efficiency. This is what makes SR a prime example of cognitive backscattering communications, achieving two critical objectives for wireless communications, which are improved spectrum efficiency

through mutually beneficial usage of the same spectrum and increased power efficiency by utilizing dependable backscattering communications.

1.3 History of the Channel Coding in Finite Blocklength

In 2010, Yury Polyanskiy, H. Vincent Poor and Sergio Verdú published the epic work. In this paper, their focus was on determining the maximal achievable channel coding rate that can be accomplished for an arbitrary blocklength and a given error probability. The achievability and converse bounds were presented for general channel classes, which are more precise than previous bounds for a wide range of relevant parameters. The results indicated that the maximum achievable rate could be accurately approximated for the short blocklengths. Additionally, the authors analytically demonstrated that the maximal achievable channel coding rate with a specific blocklength and error probability could be tightly estimated by the expression as $C - \sqrt{\frac{V}{n}}Q^{-1}(\epsilon)$, where C represents the channel capacity, V is a channel property known as channel dispersion, n denotes the blocklength, ϵ is the error probability, and Q is the complementary Gaussian cumulative distribution function.

Ever since Shannon [16] demonstrated that there exists a feature of convergence from optimal channel coding rate towards capacity, there have been efforts to understand the impact of finite blocklength. One of the earliest contributions in this area was by Shannon himself in [16], who derived a tight bound for the AWGN channel, which was later investigated significantly. With the advent of sparse-graph codes, more recent work has focused on evaluating the signal-to-noise-ratio (SNR) compensation which can be regarded as a function of blocklength to assess the suboptimality of a specific code easily. Rather than focusing on the asymptotic limit

represented by channel capacity, this approach aims to improve the evaluation of the code's performance at the specific blocklength under consideration.

The authors of [17] compared their new achievability and converse bounds with the major existing bounds. For the AWGN case, they found that Shannon's achievability bound stands out as the clear winner, which is very close to the converse bound. However, they showed that the shortcoming of Shannon's method is that it is more difficult to calculate and analyze than their derived bounds. By comparing their new bounds and the classical bounds, such as Feinstein's bound and Gallager's bound, they illustrated that their derived bounds are uniformly better than Feinstein's ones. In terms of small blocklength, Gallager's bound is slightly better than theirs due to two reasons which are the choice of the different suboptimal decoders and the different targeted range of the error probability.

Moreover, the more significant finding of their work is the normal approximation. They found that the channel dispersion quantifies the degree of random variation in a specific channel model, i.e., AWGN channel, compared to a deterministic channel model with the same channel capacity. In the finite blocklength regime, the channel dispersion, along with the channel capacity, presents a significantly accurate approximation.

1.4 History of Multiple-Input-Multiple-Output Wireless System

Multiple-input–multiple-output (MIMO) [18] has rapidly been of the utmost technical advancements in digital communication systems. This technology holds great promise for addressing the capacity constraints facing the future of internet-intensive wireless networks. It is astonishing to see that after its original introduction, MIMO

technology is poised to be widely adopted in industrial wireless devices and IoT networks. For instance, MIMO is widely used in wireless local area networks (WLAN) and orthogonal frequency-division multiple access (OFDMA).

In a wireless communication system, the MIMO technology is created by equipping both the transmitting and receiving ends with multiple antennas. The ultimate goal of MIMO is to receive the information signals from multiple transmit antennas at the transmitter side and mix these signals at the receive side to improve the signal quality, i.e., bit error rate (BER) or data rate of the communication for each user. This advantage has the potential to significantly enhance both the signal quality in the networks and alleviate the operator's costs. Speaking of the concept, it is space-time signal processing, which combines the time dimension and the spatial dimension into the whole communication system. MIMO systems are an extension of intelligent antenna technology, which has been used for several decades to improve wireless transmission using antenna arrays.

The most important part of the defining advantages of MIMO systems is their capability to transform multipath propagation, which has historically been a challenge in wireless communication systems, into a positive effect from the perspective of the receiver end. MIMO leverages random fading [19–21] and, when available, multipath delay spread [22] [23] to significantly increase transfer rates. The potential for vastly improved performance of the overall wireless communication system without additional occupation of the spectrum has been a major driving force behind the field of the research area. It has led to advancements in a wide range of fields, from totally different channel model settings to new mathematical challenges when analyzing the data rate, channel capacity, and new ways to process and filter the signal. Other different challenges occur in the implementation part, such as antenna design and cell coverage design.

1.5 Related Work and Motivation

In [24], a broad mathematical framework of the RIS-assisted wireless communication system over a Rayleigh fading channel was presented, and then a theoretical upper bound was derived. Moreover, the authors presented the relationship between the received SNR and the number of reflecting elements, indicating that the received SNR considerably grew as the number of reflecting elements increased. Thus the reliable transmission over a noisy channel could still be accomplished at low SNRs with the support of the RIS elements. The authors of [25] investigated the coverage expansion achieved by the RIS-assisted wireless communication system over quasi-static flat Rayleigh fading channels. Furthermore, compared with both direct link and relay-assisted wireless communication systems, the SNR gain and the delay outage rate of the RIS were investigated. In [26], the authors studied the RIS's placement optimization problem in a cellular network to maximize cell coverage. They developed a coverage maximization algorithm (CMA) to obtain the optimal RIS's orientation distance. The authors of [27–29] focused on the RIS-assisted multiple-input single-output (MISO) wireless communication system, for which efficient algorithms, such as Lagrangian dual transform, and active and passive beamforming, were studied to address the non-convex maximization problem of the weighted sum-rate that can be achieved by all groups. The authors of [30] statistically characterized the RIS-assisted wireless communication system under the premise that all cascaded fading channels between the transmitter, RIS and receiver follow the Rayleigh distribution. Furthermore, the closed-form expression of theoretical outage probability was derived, and the accuracy of their results was validated. In [31], the authors demonstrated and analyzed the performance of the intelligent reflecting surface-assisted ultra-reliability low-latency communications (URLLC) in a factory automation scenario. They also illustrated the achievable data rate and

the decoding error probability under finite blocklength for several channel models.

In [32], Liu *et al.* introduced a revolutionary communication system that enables different devices to transmit messages to each other by harvesting the energy from ambient RF source signals. This approach eliminates the need for wired communication and additional power, i.e., batteries, allowing for seamless communication on a massive scale and in previously inaccessible locations. By utilizing existing TV radio and cellular networks, the authors have created a new communication technology, which is defined as AmBC, where wireless communication between different devices can be achieved by reflecting ambient RF source signals. This avoids applying extra energy and power to create the RF waves resulting in a higher level of energy and power efficiency than conventional wireless communication systems. Furthermore, as it relies on ambient RF signals already present in the environment, there is no need for dedicated power infrastructure, unlike traditional AmBC. To demonstrate the viability of the design, the authors have built AmBC devices and achieved different information rates over a given distance. The authors proposed a hardware prototype that has been used to demonstrate two previously impossible applications of ubiquitous communication. Following on, Bharadia *et al.* [33] proposed the BackFi, a communication system that is similar to the AmBC, but it enables instant and long-range radio communication between IoT devices without sufficient power supply and the access points (APs) through ambient backscatter-assisted WiFi communication system. Our approach allows the APs to simultaneously transmit messages or information signals to the WiFi clients and decode the received signals from the IoT devices. The authors have shown that for a given data rate and a specific distance, there exists a reliable communication method. This performance is significantly better than the previous dominant ambient backscatter-assisted WiFi system by one to three orders of magnitude. BackFi is also highly energy-efficient, relying solely on

backscattering and requiring minimal power, resulting in low energy consumption per bit.

Valembois *et al.* [34] primarily focused on improving the performance of the 1967 sphere-packing bound (SPB67), derived by Shannon, Gallager, and Berlekamp. SPB67 was defined as a lower bound on the decoding error probability across a broad range of channels. Despite its potential value, SPB67 has not been utilized in practical telecommunication systems due to the fact that the main concentration on asymptotic analysis impedes it in moderate blocklengths, and the computational complexity involved in its derivation, which can be challenging and uninspiring to researchers. The aim of the authors is to rekindle interest in this topic by reviewing the 1959 sphere-packing bound (SPB59) derived by Shannon in 1959 and the following SPB67. The second aim is to broaden its scope of application to discrete input continuous output channels, specifically the modulated signals passing through the AWGN channel. The final aim is to improve its performance on the decoding error probability for moderate blocklengths. After numerical results and simulations analysis, the SPB67 can be proved as the lower bound with the best performance for most iteratively decodable codes, such as turbo codes and low-density parity-check (LDPC) codes. Apart from the AWGN channel, the symmetric memoryless channels have been discussed in [35]. Wiechman *et al.* derived a new, improved sphere-packing bound (ISPB) targeted at most error-correcting codes with a list decoder whose list size is given arbitrarily over symmetric memoryless channels. It started with a review of the classical results, the SPB59 of Shannon for the AWGN channel and the SPB67 for discrete memoryless channels, along with Valembois and Fossorier's improvement on the SPB67. The ISPB was then introduced as a uniformly tighter lower bound on the decoding error probability with a list decoder, whose list size is arbitrary, than the SPB67 and its improvement. The ISPB was ap-

plicable to the particular symmetric memoryless channels instead of general discrete memoryless channels, and its tightness under maximum likelihood (ML) decoding was evaluated through comparison with previous bounds. By simulation analysis, ISPB is proved that it can be applied in the turbo-family codes. The paper also presented a mathematical technique to make it possible to calculate the exact expression for moderate blocklengths without relying on asymptotic approximations.

In 2008, Telatar published his epic work. The paper [21] examined the benefits of using multiple transmitting antennas and multiple receiving antennas for a single-user communication system over the AWGN channel with Rayleigh fading or without Rayleigh fading. The author provided a general formula to compute the channel capacity and error exponent under the premise of the receiver knowing the channel distribution. The results demonstrated that the advantages of using MIMO systems over single-input-single-output (SISO) systems could be substantial, given the assumption of independent and identically distributed fading coefficient and noise at different receiving antennas.

The purpose of the paper [36] was to determine that the maximal achievable channel coding rate can be accomplished for a specific blocklength and a given decoding error probability over MIMO fading channels. Yang *et al.* considered scenarios in either or both the transmitter and the receiver have or do not have the knowledge of channel state information (CSI). The key finding was that the outage capacity, which is a long-term measure, accurately reflects the limitations of slow fading channels in finite blocklengths. It was demonstrated that the channel dispersion is insignificant, regardless of either or both the transmitter and the receiver knowing the CSI. By the numerical simulation results, the authors confirmed that the dispersion approaching zero leads to the convergence with a rapid speed to the outage capacity as the blocklength increases. Following on, Collins *et al.* [37] fo-

cused on a common channel model for mobile wireless communication at the finite blocklength regime. The channel model is multiple-antenna AWGN channels with random fading gains and full CSI at the receiver ends. The fading process was approximated by a piecewise-constant process, which was referred to as frequency non-selective fading. The objective of the paper was to derive a formula for channel dispersion, which determines the amount of delay required to reach capacity. However, one difficulty still remained that the converse bound was contingent on the relation between the transmit power and the blocklength. Another significant result of the paper was that the orthogonal Alamouti scheme is optimal for the MISO channel model.

1.6 Contributions

The main objective of this thesis is to analyze the performance of different systems, i.e., the RIS MIMO system and the AmBC MIMO system, by using the sphere-packing technique and the mutual information and the unconditional information variance along with the Berry Esseen theorem to present the simulation results.

1.6.1 Analytical Bounds for the Optimal Code over the Reconfigurable Intelligent Surface at a Short Blocklength

The first research work is to develop the sphere-packing bounds to assess the performance of an RIS-assisted wireless system at a short blocklength regime. Our approach builds upon the original work for sphere-packing bounds with an infinite blocklength over an AWGN channel [16], but we have derived new expressions for the lower and upper bounds specific to the RIS-assisted system. To achieve this, we employ the Wald sequential t-test lemma and the Riemann sum to derive a closed-

form expression for the bounds. In the short blocklength regime, the approximation of the angle used in the sphere-packing technique to calculate the code rate [16] [34] can have a margin of error. To address this issue, we have derived a new expression that provides an exact calculation of the angle.

1.6.2 Performance Analysis for Reconfigurable Intelligent Surface Assisted MIMO Systems

The second research work is to establish the achievability and converse bounds for the maximal achievable rate R in an RIS MIMO system, given a fixed maximal error probability and blocklength. The fundamental mathematical basis for our analysis includes the Berry-Esseen theorem, mutual information, and unconditional information variance.

To derive the achievability bound, we employ the Berry-Esseen theorem and additional inequalities to determine the exact probability density function (PDF) of the channel output. Our converse bound is derived by combining the maximum of the auxiliary channel's PDF, which is produced by m copies of the PDF of Gamma-distributed variables, with the Mellin transform and Meijer G-function, and the maximum of its output space by the Lebesgue measure.

We also use the saddle point approximation and Taylor series expansion to obtain closed-form expressions for both mutual information and unconditional information variance. To complete our analysis, we compare different modulation schemes in the RIS MIMO system, focusing on two key aspects: the required blocklength to achieve a given level of the maximal achievable rate and the impact of the unconditional information variance on the speed of convergence to the maximal achievable rate.

1.6.3 Performance Analysis of Multiple-Antenna Ambient Backscatter Systems at Finite Blocklengths

The last research work is to use the Berry-Esseen theorem as a fundamental basis to provide achievability and converse bounds on the achievable rate R for a legacy system with multiple transmit and receive antennas. For our achievability bound, we utilize the Berry-Esseen theorem, the mutual information, and the information variance under the condition of the probability of the tag symbol to get the bound. Furthermore, we exploit the Mellin transform and Meijer G-function to obtain a maximum on the auxiliary channel's PDF, a product of m copies of PDF of Gamma distributed variables. Then, we apply the Lebesgue measure to get the maximum of its output space. To complete our achievability and converse bounds, we utilize the different modulation schemes in our legacy system.

To reduce the complexity of multiple integrals for deriving the mutual information and the information variance, we use the saddle point approximation and the Taylor expansion to obtain closed-form expressions of the mutual information and the information variance.

We apply a low-complexity ML detection to compute the average error probability of the tag symbol based on the received signal and estimated RF source signal for a variety of transmitter and receiver antennas. We determine the relationship between the average error probability of the tag symbol and the maximal error probability of the RF source signal as a function of the blocklength n and the number of transmitter and receiver antennas t and r. We utilize different modulation schemes, i.e., BPSK and QPSK, and different coding methods, i.e., the EBCH code and the polar code, in our legacy system and AmBC system to validate the derived bounds and the error probability of the tag symbol.

Chapter 2

Background

This chapter briefly introduces the fundamental concepts of different systems that are discussed, including the RIS system, the AmBC system, and the MIMO system. Secondly, this chapter discusses the fundamental mathematical concepts and theories of several bounds, including the Polyanskiy-Poor-Verdú (PPV) bound and two sphere-packing bounds. Following on, this chapter briefly presents the fundamental concepts of error control coding, including BCH code and polar code.

2.1 Fundamentals of Different Systems

In this section, we discuss the mathematical basics of the RIS, AmBC, and MIMO systems.

2.1.1 Fundamentals of RIS System

In this subsection, we mainly focus on the fundamental of different cases of the RIS system. A traditional RIS system is comprised of a transmitter, a receiver, and a meta-surface. The transmitter equipped with a single antenna aims to establish

communication with a receiver that also has a single antenna. However, the LOS connection between the two is hindered by a wall. To enhance the signal quality, a reconfigurable meta-surface integrated with N_{ris} reflective elements, known as an RIS, has been placed between the transmitter and the receiver. The channels between the transmitter and the i-th RIS element, the i-th RIS element and the receiver are represented as $\mathbf{h}_i = [h_i(1), h_i(2), \ldots, h_i(n)]$, $1 \leq i \leq N_{ris}$, and $\mathbf{g}_i = [g_i(1), g_i(2), \ldots, g_i(n)]$ with $h_i(k) = |h_i(k)| \exp\{-j\psi_i(k)\}$, $1 \leq k \leq n$ and $g_i(k) = |g_i(k)| \exp\{-j\phi_i(k)\}$, respectively. $|h_i(k)|$ and $|g_i(k)|$ in the channel $\mathbf{h}_i$ and $\mathbf{g}_i$ denote the amplitude of the channel coefficient $h_i(k)$ and $g_i(k)$, respectively, while $\psi_i(k)$ and $\phi_i(k)$ represent the phase of the channel coefficient $h_i(k)$ and $g_i(k)$, respectively. The received signal at the receiver can be shown as

$$y(k) = \sum_{i=1}^{N_{ris}} \eta_i(k) h_i(k) g_i(k) x(k) + w(k), \tag{2.1}$$

where $w(k)$ denotes the AWGN with zero-mean and equal variance N_0 in both its real and imaginary components, i.e., $w(k) \sim \mathcal{CN}(0, N_0)$, and $\eta_i(k)$ denotes the reflection coefficient of the i-th RIS element with $\eta_i(k) = |\eta_i(k)| \exp\{-j\theta_i(k)\}$, $1 \leq k \leq n$, where $|\eta_i(k)|$ and $\theta_i(k)$ represent the coefficient gain and the phase shift controlled by the i-th RIS element. The coefficient gain $|\eta_i(k)|$ can be assumed as 1 for all i from 1 to N_{ris}. The assumption is made that the reflective elements of the RIS are fitted with varactor-tuned resonators, which can adjust each RIS element's phase by altering the bias voltage supplied to the varactor. We will discuss some of the most common cases of the channel model.

1. It is assumed that the RIS has perfect knowledge of the phases of the channels $h_i(k)$ and $g_i(k)$, and it selects the optimal phase shifting accordingly, i.e., $\theta_i(k) = -(\psi_i(k) + \phi_i(k))$. Furthermore, $|h_i(k)|$ and $|g_i(k)|$ are Rayleigh distribution random variables (RVs). Since the reflecting gain $|\eta_i(k)|$ are assumed

as 1 for all i from 1 to N_{ris}, the received signal can be rewritten as

$$y(k) = A(k)x(k) + w(k), \tag{2.2}$$

where $A(k) = \sum_{i=1}^{N_{ris}} |h_i(k)| \cdot |g_i(k)|$.

Since $|h_i(k)|$ and $|g_i(k)|$ are Rayleigh distributed RVs, their product is a double Rayleigh distributed RV. $A(k)$ is the sum of N_{ris} independent and identically distributed (i.i.d.) double Rayleigh distributed RV whose PDF can be tightly approximated as the first term of a Laguerre series expansion with the parameters $a = \frac{k_1^2}{k_2} - 1$ and $b = \frac{k_2}{k_1}$, where k_1 and k_2 denote the mean value and the variance of $A(k)$. Then, we have

$$k_1 = \mathbb{E}[A(k)] = \mathbb{E}[\sum_{i=1}^{N_{ris}} |h_i(k)g_i(k)|] = \sum_{i=1}^{N_{ris}} \mathbb{E}[|h_i(k)g_i(k)|]. \tag{2.3}$$

Since $|h_i(k)|$ and $|g_i(k)|$ are i.i.d. Rayleigh distributed RV, then we have

$$k_1 = \frac{N_{ris}\pi}{4}. \tag{2.4}$$

Following the same procedure as k_1, we obtain the value of k_2 as follows

$$k_2 = N_{ris}(1 - \frac{\pi^2}{16}). \tag{2.5}$$

Theorem 1. *The PDF of $A(k)$ can be expressed as*

$$f_{A(k)}(x) = \frac{x^a}{b^{a+1}\Gamma(a+1)} \exp\{-\frac{1}{b}x\}, \tag{2.6}$$

where $a = \frac{k_1^2}{k_2} - 1$ and $b = \frac{k_2}{k_1}$ with $k_1 = \frac{N_{ris}\pi}{4}$ and $k_2 = N_{ris}(1 - \frac{\pi^2}{16})$.

We validate the theoretical framework through respective Monte Carlo simulations and analyze the numerical results which is shown on Fig. 2.1.

2. It is assumed that the RIS has not the perfect knowledge of the phases of the channel $h_i(k)$ and $g_i(k)$. The phase shift $\theta_i(k)$ induced by the i-th RIS element

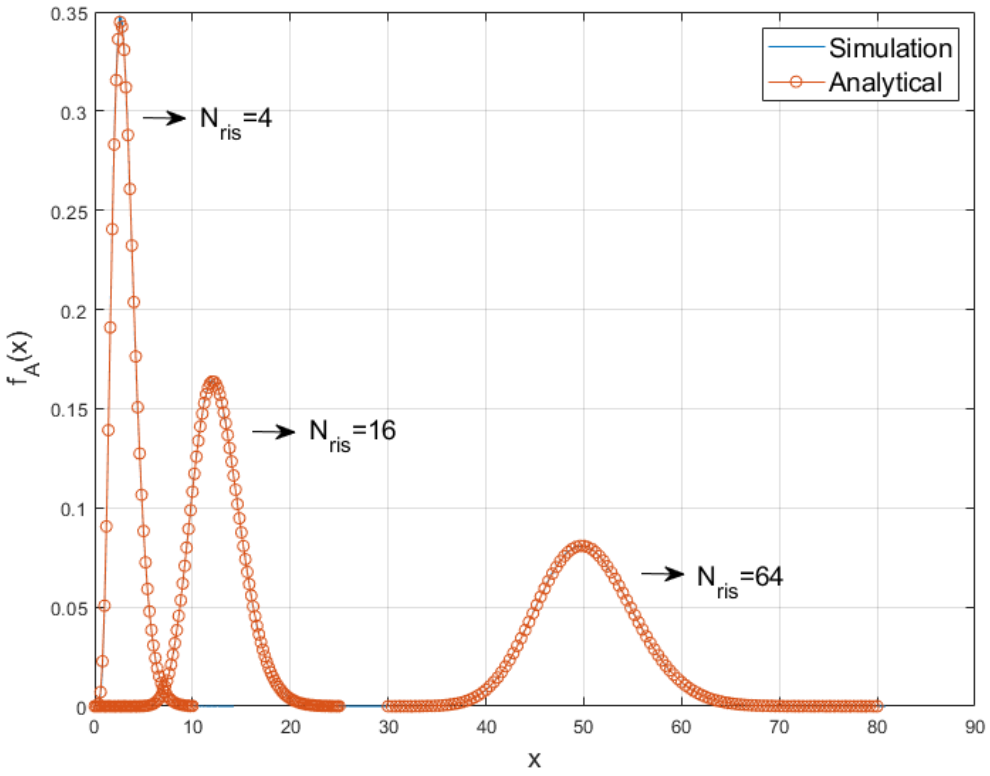

Figure 2.1: The PDF of $A(k)$ with the perfect knowledge of the phases of the channels $h_i(k)$ and $g_i(k)$ for different N_{ris}

follows the uniform distribution in $[0, 2\pi)$ and the reflecting gain $|\eta_i(k)|$ is 1 for all i from 1 to N_{ris}. Thus, $A(k)$ can be rewritten as

$$A(k) = |A(k)|e^{j\angle A(k)} = \sum_{i=1}^{N_{ris}} |h_i(k)|e^{-j\psi_i(k)} \times |g_i(k)|e^{j\phi_i(k)} \times e^{j\theta_i(k)}, \tag{2.7}$$

where $|h_i(k)|$ and $|g_i(k)|$ denote two Rayleigh distributed RV. Then the PDF of the product of two Rayleigh RVs is

$$f_{|h_i(k)||g_i(k)|}(x) = 4xK_0(2x), \quad i = 1, \ldots, N_{ris}. \tag{2.8}$$

The Fourier transform of $f_{|h_i(k)||g_i(k)|}(x)$ is

$$\begin{aligned} F_{|h_i(k)||g_i(k)|}(t) &= \int_{-\infty}^{\infty} f_{|h_i(k)||g_i(k)|}(x) \exp(-2\pi jtx)dx \\ &= \int_{-\infty}^{\infty} 4xK_0(2x) \exp(-2\pi jtx)dx. \end{aligned}$$

Then by using the inverse Fourier transform, we can obtain the distribution density of $|A(k)|$ as shown below

$$\begin{aligned} f_{|A(k)|}(x) &= \frac{1}{2\pi} \int_{-\infty}^{\infty} (F_{|h_i(k)||g_i(k)|}(t))^{N_{ris}} \exp(-jtx)dt \\ &= \frac{1}{2\pi} \int_{-\infty}^{\infty} \Big(\int_{-\infty}^{\infty} 4xK_0(2x) \exp(-2\pi jtx)dx \Big)^{N_{ris}} \exp(-jtx)dt \\ &= \frac{2x}{N_{ris}} \exp(-\frac{x^2}{N_{ris}}) \end{aligned}$$

and the angle of $A(k)$ also follows the uniform distribution in $[0, 2\pi)$. Therefore, we obtain the expression of the $A(k)$'s PDF. We validate the theoretical framework through respective Monte Carlo simulations and analyze the numerical results which is shown on Fig. 2.2.

2.1.2 Fundamental of AmBC System

In this subsection, we mainly focus on the fundamental of several decoding methods for the AmBC system. A conventional AmBC system is comprised of three components: a transmitter, an AmBC device (a tag), and a receiver (a reader). Each component is equipped with a single antenna. The AmBC device conveys the message symbols to the receiver through the modulation and reflection of transmitted signals, i.e., RF source signal. As a result, the receiver collects both the transmitted signals and the message symbols backscattered by the AmBC device. Its purpose is to extract the AmBC device symbols from the received signals. Consider an ambient RF source signal $x(k)$, where k ranges from 1 to n. The channel coefficient that represents the channel between the transmitter and the receiver is h, while g_1 represents

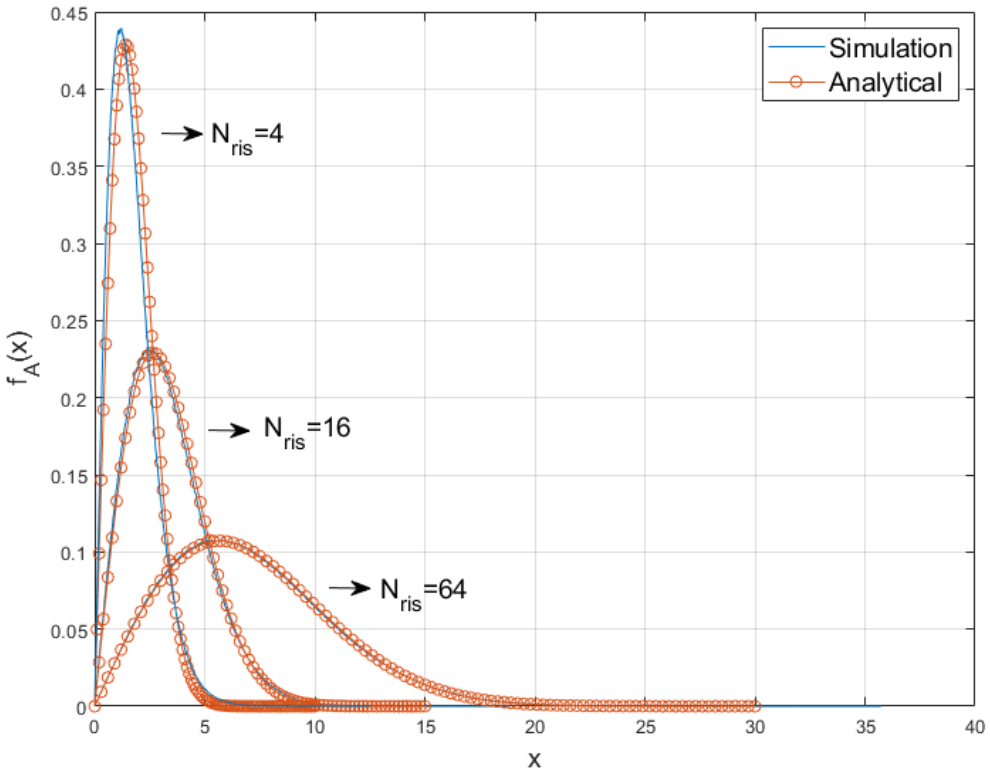

Figure 2.2: The PDF of $A(k)$ without the perfect knowledge of the phases of the channels $h_i(k)$ and $g_i(k)$ for different N_{ris}

the channel between the transmitter and the AmBC device, and g_2 represents the channel between the AmBC device and the receiver. The average transmitting power can be defined as $P = \mathbb{E}[\sum_{k=1}^{n} x^2(k)]$. It is assumed that the channel coefficients h, g_1, and g_2 experience slow fading and remain constant throughout n blocklength. The relative difference between the LOS link and the backscattered-link is defined as follows

$$\Delta = \frac{\mathbb{E}[(\eta g_1 g_2)^2]}{\mathbb{E}[h^2]}, \tag{2.9}$$

where η denotes the reflection coefficient of the AmBC device. Let d denote a message symbol transmitted by the AmBC device, where d can be either 0 or +1. The symbol of the AmBC device d is assumed to remain constant over n blocklength

of $x(k)$, which means that d_k is equal to d for all k ranging from 1 to n. The signal received and reflected by the AmBC device is shown below

$$y_2(k) = \eta g_1 g_2 d_k x(k). \tag{2.10}$$

Since the AmBC device is equipped with passive components, the electronic noise at the circuits of the AmBC device can be considered negligible. The receiver captures two signals, as mentioned before. The signal received by the receiver can be expressed as follows

$$y(k) = hx(k) + y_2(k) + w(k) = (h + \eta g_1 g_2 d_k)x(k) + w(k), \tag{2.11}$$

where $w(k)$ denotes the AWGN with zero-mean and equal variance σ^2 in both its real and imaginary components, i.e., $w(k) \sim \mathcal{CN}(0, \sigma^2)$. Then the received signal vector can be generated with one AmBC device symbol d as $\mathbf{y} = [y_1, y_2, \ldots, y_n]$. It is important to note that the time delay between the direct-link signal and the backscattered signal from the AmBC device is typically negligible, given that the distances between the transmitter and receiver and the transmitter and the AmBC device are significantly longer than the distance between the AmBC device and the receiver. Without time delay, there still exists a major challenge to recover the message symbol from the AmBC device in the AmBC system, as the signal reflected back by the AmBC device is much weaker than the direct-link signal. To address this challenge, we will discuss some of the most commonly employed detection methods for extracting the AmBC device symbols.

1. The ML detector is an optimal solution that explores all possible candidates to minimize the mean square error. The ML detector then estimates both the transmitted signal $x(k)$ and the AmBC device symbol d as follows

$$\hat{\mathbf{s}} = \arg \min_{\substack{x(k) \in \mathcal{A}_x, \\ d_k \in \mathcal{A}_d}} \Big| y(k) - hx(k) - \eta g_1 g_2 d_k x(k) \Big|, \tag{2.12}$$

where the set of modulation signals for $x(k)$ and d_k are represented by $\mathcal{A}_x$ and $\mathcal{A}_d$, respectively. The number of searches in the ML estimation described above is equal to the product of the size of the sets $\mathcal{A}_x$ and $\mathcal{A}_d$. However, as the size of $\mathcal{A}_x$ increases, the complexity of the ML detector grows exponentially, making it unfeasible to use the optimal ML detector for recovering both the transmitted signals and the symbols from the AmBC device in the AmBC system.

2. The SIC-based detector takes advantage of the fact that the LOS link signals are significantly better than the backscattered symbols. The SIC-based detector first estimates the transmitted signal $x(k)$, then subtracts it from the received signal $y(k)$. This allows for the AmBC device symbols d_k to be obtained. After estimating d_k, the transmitted signal $x(k)$ can be re-estimated by incorporating d_k back into $y(k)$. A step-by-step explanation of the SIC-based detector is provided below.

   The first step is to estimate the transmitted signal $x(k)$. The transmitted signal $x(k)$ can be estimated by treating the AmBC device symbols d_k as noise which is shown below

$$\hat{x}(k) = \arg \min_{x(k) \in \mathcal{A}_x} \left| x(k) - \frac{y(k)}{h + \eta g_1 g_2} \right|. \tag{2.13}$$

   The second step is to estimate the AmBC device symbols d_k. An intermediate signal $y_2(k)$ can be obtained by extracting $hx(k)$ from $y(k)$. Then the AmBC device symbols d_k can be estimated as

$$\hat{d}_k = \arg \min_{d_k \in \mathcal{A}_d} \sum_{k=1}^{n} \left|\left| d_k - \frac{y_2(k)}{\eta g_1 g_2} \right|\right|^2. \tag{2.14}$$

   The third step is to re-estimate the transmitted signal $x(k)$. Since the estimated AmBC device symbols $\hat{d}_k$ is obtained, the received signal can be ex-

pression as a different form

$$(y(k), \hat{d}_k) = (h + \eta g_1 g_2 \hat{d}_k)x(k) + w(k). \tag{2.15}$$

Thus, the re-estimated transmitted signal $x(k)$ can be obtained as

$$\hat{\hat{x}}(k) = \arg \min_{x(k)\in\mathcal{A}_x} \left| x(k) - \frac{(y(k), \hat{d}_k)}{h + \eta g_1 g_2} \right|. \tag{2.16}$$

2.1.3 Fundamental of MIMO System

In this subsection, we discuss the fundamental mathematical basics of MIMO system. In [21], a Gaussian channel model was considered that pertained to a single user, equipped with multiple transmitting antennas and multiple receiving antennas. The total number of antennas at the transmitter end was represented by t, while the total number of antennas at the receiver end was denoted by r. The author's focus would be solely on a linear model, where the output vector $\mathbf{y} \in \mathbb{C}^r$ was dependent on the input vector $\mathbf{x} \in \mathbb{C}^t$ as described by

$$\mathbf{y} = \mathbf{H}\mathbf{x} + \mathbf{n}, \tag{2.17}$$

where $\mathbf{H} \in \mathbb{C}^{r\times t}$ and $\mathbf{n}$ denotes the noise which is assumed to be a zero-mean complex Gaussian with independent and equal variance in both its real and imaginary components and $\mathbb{E}[\mathbf{n}\mathbf{n}^H] = I_r$. The transmitted power is constrained to P, i.e., $\mathbb{E}[\mathbf{x}^H\mathbf{x}] \leq P$. Consider a scenario where the channel matrix H is not determinate, but rather a channel matrix $\mathbf{H}$ with a random distribution that is independent of the distribution of $\mathbf{x}$ and $\mathbf{n}$. The distribution of channel matrix $\mathbf{H}$ is known at the receiver side, however, it is not available at the transmitter end. The channel model can be transformed to the input $\mathbf{x}$ and the output $(\mathbf{y}, \mathbf{H}) = (\mathbf{H}\mathbf{x} + \mathbf{n}, \mathbf{H})$. The assumption is made that the entries of $\mathbf{H}$ are independently distributed, each possessing a zero-mean Gaussian distribution, with both the real and imaginary

parts having independent variances of $\frac{1}{2}$. The aforementioned model is called as a Rayleigh fading channel where there is sufficient physical separation between the transmitting and receiving antennas to guarantee independence in the entries of $\mathbf{H}$.

Theorem 2. *The capacity of the channel is achieved when* $\mathbf{x}$ *is a circularly symmetric complex Gaussian with zero-mean and covariance* $(P/t)I_t$*. The capacity is given by*

$$C = \mathbb{E}\Big[\log\det(I_r + \frac{P}{t}\mathbf{H}\mathbf{H}^H)\Big]. \tag{2.18}$$

To evaluate $\det(I_r + \frac{P}{t}\mathbf{H}\mathbf{H}^H)$, a new matrix $\mathbf{M}$ is defined as follows

$$\mathbf{M} = \begin{cases} \mathbf{H}\mathbf{H}^H, & r < t, \\ \mathbf{H}^H\mathbf{H}, & r \geq t. \end{cases} \tag{2.19}$$

Then, $\mathbf{M}$ is an $m \times m$ random non-negative matrix with real, non-negative eigenvalues, where $m = \min\{r, t\}$. Thus, we can rewrite the capacity in terms of the eigenvalues $\lambda_1, \lambda_2, \ldots, \lambda_m$ of $\mathbf{M}$ as follows

$$C = \mathbb{E}\Big[\sum_{i=1}^{m}\log(1 + \frac{P}{t}\lambda_i)\Big]. \tag{2.20}$$

The joint PDF of the unordered eigenvalues is

$$f_{\lambda,unordered}(\lambda_1, \lambda_2, \ldots, \lambda_m) = (m!K_{m,n})^{-1}\exp\{-\sum_{i=1}^{m}\lambda_i\}\prod_{i=1}^{m}\lambda_i^{n-m}\prod_{i<j}(\lambda_i - \lambda_j)^2, \tag{2.21}$$

where $n = \max\{r, t\}$ and $K_{m,n}$ is a normalizing factor. The expectation the author aimed to calculate, $\mathbb{E}\Big[\sum_{i=1}^{m}\log(1 + \frac{P}{t}\lambda_i)\Big] = m\mathbb{E}[\log(1 + \frac{P}{t}\lambda_1)]$, is dependent solely on the distribution of one of the unordered eigenvalues. To determine the PDF of λ_1, it is necessary to perform an integration with respect to $\lambda_2, \ldots, \lambda_m$:

$$f_{\lambda_1}(\lambda_1) = \int\cdots\int f_{\lambda}(\lambda_1, \lambda_2, \ldots, \lambda_m)d\lambda_2\cdots d\lambda_m. \tag{2.22}$$

It is easy to observe that $\prod_{i<j}(\lambda_i - \lambda_j)$ is the determinant of a Vandermonde matrix which can be defined as below

$$V(\lambda_1, \lambda_2, \ldots, \lambda_m) = \begin{bmatrix} 1 & 1 & \ldots & 1 \\ \lambda_1 & \lambda_2 & \ldots & \lambda_m \\ \vdots & \vdots & & \vdots \\ \lambda_1^{m-1} & \lambda_2^{m-1} & \ldots & \lambda_m^{m-1} \end{bmatrix}. \tag{2.23}$$

Then, (2.21) can be rewritten as

$$f_{\lambda,unordered}(\lambda_1, \lambda_2, \ldots, \lambda_m) = (m! K_{m,n})^{-1} \det\left(V(\lambda_1, \lambda_2, \ldots, \lambda_m)\right)^2 \prod_{i=1}^{m} \lambda_i^{n-m} \exp\{-\sum_{i=1}^{m} \lambda_i\}. \tag{2.24}$$

With applying the elementary operation of matrix and the Gram-Schmidt orthogonalization procedure to the sequence $1, \lambda, \lambda^2, \ldots, \lambda^{m-1}$, $V(\lambda_1, \lambda_2, \ldots, \lambda_m)$ can be transformed to

$$\bar{V}(\lambda_1, \lambda_2, \ldots, \lambda_m) = \begin{bmatrix} \psi_1(\lambda_1) & \psi_1(\lambda_2) & \ldots & \psi_1(\lambda_m) \\ \psi_2(\lambda_1) & \psi_2(\lambda_2) & \ldots & \psi_2(\lambda_m) \\ \vdots & \vdots & & \vdots \\ \psi_m(\lambda_1) & \psi_m(\lambda_2) & \ldots & \psi_m(\lambda_m) \end{bmatrix}, \tag{2.25}$$

where $\psi_1, \psi_2, \ldots, \psi_m$ is the outcome after applying the Gram-Schmidt orthogonalization procedure in the space of the real valued functions with inner product

$$\int_0^\infty \psi_i(\lambda)\psi_i(\lambda)\lambda^{n-m} \exp\{-\lambda\} d\lambda = < \psi_i, \psi_i > = \delta_{ij}, \tag{2.26}$$

where δ_{ij} denotes Dirac delta function. Then,

$$\det V(\lambda_1, \lambda_2, \ldots, \lambda_m) = \det \bar{V}(\lambda_1, \lambda_2, \ldots, \lambda_m) = \sum_{\alpha} (-1)^{\mathsf{per}(\alpha)} \prod_i \psi_{\alpha_i}(\lambda_i), \tag{2.27}$$

where the sum is taken over all possible permutations of $\{1, 2, \ldots, m\}$, with $\mathsf{per}(\alpha)$ equal to 0 or 1 depending on whether the permutation α is even or odd. Thus, by

integrating over $\lambda_2, \ldots, \lambda_m$

$$f_{\lambda_1}(\lambda_1) = \frac{1}{m} \sum_{i=1}^{m} \psi_i(\lambda_1)^2 \lambda_1^{n-m} \exp\{-\lambda_1\}, \tag{2.28}$$

where the Gram-Schmidt orthonomalization $\psi_i(\lambda_1) = \sqrt{\frac{(i-1)!}{(i-1+n-m)!}} L_{i-1}^{n-m}(\lambda_1)$, and L_i^j denotes the associated Laguerre polynomial of order i. Therefore, the channel capacity, given t transmitters and r receivers with a power constraint of P, is equal to

$$\int_0^\infty \log(1 + \frac{P}{t}\lambda) \sum_{i=1}^{m} \frac{(i-1)!}{(i-1+n-m)!} \left[L_{i-1}^{n-m}(\lambda)\right]^2 \lambda^{n-m} \exp\{-\lambda\} d\lambda. \tag{2.29}$$

2.2 Fundamental of PPV and Sphere-Packing Bounds

In this section, we discuss the mathematical basics of PPV and sphere-packing bounds.

2.2.1 Fundamental of PPV Bound

In this subsection, we introduce the PPV bound [38, 39]. At first, we need to introduce an important tool for the PPV bound, that is the Berry-Esseen theorem.

Theorem 3. *[Berry-Esseen theorem [40]] Let $X_k, k = 1, \ldots, n$ be independent with*

$$\mu_k = \mathbb{E}[X_k], \quad \sigma_k^2 = Var[X_k], \quad t_k = \mathbb{E}[|X_k - \mu_k|^3], \quad \sigma^2 = \sum_{k=1}^{n} \sigma_k^2 \quad \textit{and} \quad T = \sum_{k=1}^{n} t_k.$$

Then for any $-\infty < \tau < \infty$

$$\left| \mathbb{P}\Big[\sum_{k=1}^{n} (X_k - \mu_k) \geq \tau\sigma \Big] - Q(\tau) \right| \leq \frac{6T}{\sigma^3}, \tag{2.30}$$

where $Q(\cdot)$ is the Q function, $Q(x) = \frac{1}{\sqrt{2\pi}} \int_x^\infty \exp(-\frac{1}{2}t^2) dt$.

In order to use Theorem 3 into the PPV bound, we first need to define the information density $i(X;Y)$ as follows

$$i(X;Y) = \log \frac{dP_{XY}}{d(P_X \times P_Y)}(X,Y). \tag{2.31}$$

Moreover, we need to prove the second moment of $i(X;Y)$ is nonzero and its third moment is always less than infinite.

$$\begin{aligned} U(X;Y) &= \mathbb{E}[|i(X;Y) - I(X;Y)|^2] \\ &= \int_0^\infty \int_{-\infty}^\infty \sum_{\mathbf{X}\in\mathcal{A}^t} \Big(P(\mathbf{X})p(\mathbf{Y},\mathbf{H}|\mathbf{X})(1-p(\mathbf{Y},\mathbf{H}|\mathbf{X}))\cdot \\ &\quad \log^2 \big\{ \frac{p(\mathbf{Y},\mathbf{H}|\mathbf{X})}{\sum_{\mathbf{X}'\in\mathcal{A}^t} P(\mathbf{X}')p(\mathbf{Y},\mathbf{H}|\mathbf{X}')} \big\} \Big) d\mathbf{Y} d\mathbf{H} \qquad (2.32) \\ &> 0, \qquad (2.33) \end{aligned}$$

where (2.32) follows from $2\binom{|\mathcal{A}|^t}{2}/|\mathcal{A}|^t = |\mathcal{A}|^t - 1$ and $P(\mathbf{X}) = 1/|\mathcal{A}|^t$ and (2.33) follows from $1 - p(\mathbf{Y},\mathbf{H}|\mathbf{X}) > 0$.

Then, we need to present the third moment of $i(X;Y)$ is less than infinite.

$$\begin{aligned} T(X;Y) &= \mathbb{E}[|i(X;Y) - I(X;Y)|^3] \\ &\le \mathbb{E}[|p(\mathbf{Y},\mathbf{H}|\mathbf{X})|^3] + \mathbb{E}[|\frac{1}{\sum_{\mathbf{X}'\in\mathcal{A}^t} P(\mathbf{X}')p(\mathbf{Y},\mathbf{H}|\mathbf{X}')}|^3] + 2I(X;Y)^3 \qquad (2.34) \\ &\le |\mathcal{B}|(3e^{-1}\log e)^3 + 2I(X;Y)^3, \qquad (2.35) \end{aligned}$$

where (2.34) follows from Holder's inequality and (2.35) follows from $\max_{0<x<1}\{x\log^3 x\} = 0$ at $x = 1$ and $\max_{0<x<1}\{x\log^3 \frac{1}{x}\} = (3e^{-1}\log e)^3$ at $x = e^{-3}$. We denote $i(X^n;Y^n) = \sum_n i(X;Y)$, and let its second moment $\sum_n U(X;Y)$ be nonzero and its third moment $\sum_n \mathbb{E}[|i(X;Y) - I(X;Y)|^3] < \infty$. Thus, Theorem 3 is still applicable to $i(X^n;Y^n)$.

Theorem 4. *[DT Bound] For any input distribution, there exists a code with M codewords and an error probability ϵ not exceeding*

$$\epsilon \le \mathbb{E}\Big[\exp\Big\{ -\big[i(X;Y) - \log\frac{M-1}{2} \big]^+ \Big\} \Big], \tag{2.36}$$

where $[\cdot]^+$ *denotes* $\max\{\cdot, 0\}$.

According to the DT bound, we have $\epsilon \leq \mathbb{E}\big[\exp\big\{-[i(X^n;Y^n) - \log\frac{M-1}{2})]^+\big\}\big]$. In the sequel, we prove that there exist some λ values, so that

$$\begin{aligned}\epsilon &\geq \mathbb{E}\Big[\exp\{0\}1_{\{i(X^n;Y^n)-\log\lambda\leq 0\}}\Big] + \mathbb{E}\Big[\exp\big\{-i(X^n;Y^n)+\log\lambda\big\}1_{\{i(X^n;Y^n)-\log\lambda>0\}}\Big] \\ &= \mathbb{P}\Big[i(X^n;Y^n)\leq \log\lambda\Big] + \lambda\mathbb{E}\Big[\exp\big\{-i(X^n;Y^n)\big\}1_{\{i(X^n;Y^n)>\log\lambda\}}\Big]. \qquad (2.37)\end{aligned}$$

The first step is to obtain the maximum of the first part of the right-hand side of (2.37). After applying Theorem 3, we have

$$\mathbb{P}\Big[i(X^n;Y^n)\leq nI(X;Y)-\tau\sqrt{nU(X;Y)}\Big] \leq \frac{6T(X;Y)}{\sqrt{n}U(X;Y)^{\frac{3}{2}}} + Q(\tau). \qquad (2.38)$$

We assume

$$\log\lambda = nI(X;Y) - \tau\sqrt{nU(X;Y)}, \qquad (2.39)$$

and

$$\mathbb{P}\Big[i(X^n;Y^n)\leq \log\lambda\Big] \leq \frac{6T(X;Y)}{\sqrt{n}U(X;Y)^{\frac{3}{2}}} + Q(\tau). \qquad (2.40)$$

The maximum of the second part of the right-hand side of (2.37) is given below. For $0 \leq i < \infty$ and any $\Delta > 0$,

$$\begin{aligned}&\mathbb{P}\Big[-\sqrt{nU(X;Y)}(\tau - \frac{i\Delta}{\sqrt{nU(X;Y)}}) \leq i(X^n;Y^n) \qquad (2.41)\\ &\qquad\qquad - nI(X;Y) \leq -\sqrt{nU(X;Y)}(\tau - \frac{(i+1)\Delta}{\sqrt{nU(X;Y)}})\Big] \\ &= \mathbb{P}\Big[\log\lambda + i\Delta \leq i(X^n;Y^n) \leq \log\lambda + (i+1)\Delta\Big] \qquad (2.42)\\ &\leq \frac{12T(X;Y)}{\sqrt{n}U(X;Y)^{\frac{3}{2}}} + Q(\tau + \frac{i\Delta}{\sqrt{nU(X;Y)}}) - Q(\tau + \frac{(i+1)\Delta}{\sqrt{nU(X;Y)}}), \qquad (2.43)\end{aligned}$$

where (2.42) is obtained by applying Theorem 3 twice. Then, we have

$$\mathbb{E}\Big[\exp\big\{-i(X^n;Y^n)\big\}1_{\{i(X^n;Y^n)>\log\lambda\}}\Big]$$
$$=\sum_{i=0}^{\infty}\exp\{-(\log\lambda+i\Delta)\}\mathbb{P}\Big[\log\lambda+i\Delta\le i(X^n;Y^n)\le\log\lambda+(i+1)\Delta\Big] \quad (2.44)$$
$$\le\left(\frac{\Delta}{\sqrt{2\pi}\sqrt{nU(X;Y)}}+\frac{12T(X;Y)}{\sqrt{n}U(X;Y)^{\frac{3}{2}}}\right)\sum_{i=0}^{\infty}\exp\{-(\log\lambda+i\Delta)\}, \quad (2.45)$$

where (2.44) is a result of the Riemann integral and (2.45) follows from the fact that for any σ, $Q(\frac{x}{\sigma})-Q(\frac{x+\Delta}{\sigma})\le\frac{\Delta}{\sqrt{2\pi}\sigma}$. Thus, we have

$$\lambda\mathbb{E}\Big[\exp\big\{-i(X^n;Y^n)\big\}1_{\{i(X^n;Y^n)>\log\lambda\}}\Big]$$
$$\le\left(\frac{\Delta}{\sqrt{2\pi}\sqrt{nU(X;Y)}}+\frac{12T(X;Y)}{\sqrt{n}U(X;Y)^{\frac{3}{2}}}\right)\frac{\exp\{\Delta\}}{\exp\{\Delta\}-1}, \quad (2.46)$$

where (2.46) follows for any $\exp\{x\}>1$, $\sum_{i=0}^{\infty}\exp\{-ix\}=\frac{\exp\{x\}}{\exp\{x\}-1}$. Substituting (2.40) and (2.46) into (2.37), we have

$$\mathbb{P}\Big[i(X^n;Y^n)\le\log\lambda\Big]+\lambda\mathbb{E}\Big[\exp\big\{-i(X^n;Y^n)\big\}1_{\{i(X^n;Y^n)>\log\lambda\}}\Big]$$
$$\le Q(\tau)+\frac{1}{\sqrt{n}}\frac{6T(X;Y)}{U(X;Y)^{\frac{3}{2}}}\Big(1+2\frac{\exp\{\Delta\}}{\exp\{\Delta\}-1}+\frac{U(X;Y)\Delta\exp\{\Delta\}}{\sqrt{2\pi}6T(X;Y)(\exp\{\Delta\}-1)}\Big). \quad (2.47)$$

Based on (2.37), we can assume that the right hand side of (2.47) equals to ϵ, then we obtain the value of τ

$$\tau=Q^{-1}\Big(\epsilon-\frac{1}{\sqrt{n}}\frac{6T(X;Y)}{U(X;Y)^{\frac{3}{2}}}\Big(1+2\frac{\exp\{\Delta\}}{\exp\{\Delta\}-1}+\frac{U(X;Y)\Delta\exp\{\Delta\}}{\sqrt{2\pi}6T(X;Y)(\exp\{\Delta\}-1)}\Big)\Big). \quad (2.48)$$

For large n, the second item inside the Q function of (2.48) vanishes. Therefore, we can obtain $\tau=Q^{-1}(\epsilon)+\mathcal{O}(\frac{1}{\sqrt{n}})$. Then, we have $\log\lambda=nI(X;Y)-Q^{-1}(\epsilon)\sqrt{nU(X;Y)}+\mathcal{O}(\frac{1}{\sqrt{n}})$.

Thus, we finally obtain

$$R\ge I(X;Y)-Q^{-1}(\epsilon)\sqrt{\frac{U(X;Y)}{n}}+\frac{1}{n}+\mathcal{O}(n^{-\frac{3}{2}}). \quad (2.49)$$

After we complete the achievability part, we move to the proof of the converse part. The important theorem is shown below

Theorem 5 (Converse)**.** *Every* (M, ϵ) *code with codewords belonging to* F *satisfies*

$$M \leq \inf_{Q_Y} \sup_{x \in \mathsf{F}} \frac{1}{\beta_{1-\epsilon}(x, Q_Y)}, \tag{2.50}$$

where the infimum is over all distributions Q_Y *on* B*, and* A *and* B *denote as the n-fold Cartesian products of alphabets* $\mathcal{A}$ *and* $\mathcal{B}$*. If* $\mathsf{A} = \mathcal{A}^n$*,* $M = |\mathcal{A}|^k$*, and* $\mathcal{A}$ *is a finite field, a random linear code with its input distribution being equiprobable on* A *can be constructed by a random* $n \times k$ *matrix whose entries are independent and equiprobable on* $\mathcal{A}$*. The* M *codewords of this random linear code can be generated by the products of the aforementioned matrix and every vector in* $\mathcal{A}^k$*.*

The cost constraint on each codeword can be defined by a subset $\mathsf{F} \subset \mathsf{A}$ *of permissible inputs. And we have*

$$\beta_\alpha(x, Q_Y) \geq \sup_{\gamma > 0} \frac{1}{\gamma} \Big(\alpha - P_{Y|X=x} \big[\frac{dP_{Y|X=x}}{dQ_Y} \geq \gamma \big] \Big), \tag{2.51}$$

where $\frac{dP_{Y|X=x}}{dQ_Y}$ *denotes the Radon-Nikodym derivative between two distributions* $P_{Y|X=x}$ *and* Q_Y*.*

Then we have

$$\log M \leq -\log \beta^n_{1-\epsilon}(x^n, P_{Y^n}). \tag{2.52}$$

By applying the following lemma which is shown below,

Lemma 1. *Define two measures on* $\mathcal{A}^n$*:* $Q = \prod_{i=1}^n Q_i$ *and* $P = \prod_{i=1}^n P_i$*, where two measures* Q_i *and* P_i *belong to the measurable space* $\mathcal{A}$*. And define* $D_n = \frac{1}{n} \sum_{i=1}^n D(Q_i || P_i)$ *and* $V_n = \frac{1}{n} \sum_{i=1}^n \int (\log \frac{dQ_i}{dP_i})^2 dQ_i - D(Q_i||P_i)^2$*.*

Assuming that all quantities are finite and $V_n > 0$*. Then, we have*

$$\log \beta_\alpha \geq -nD_n - \sqrt{\frac{2nV_n}{\alpha}} + \log \frac{\alpha}{2}. \tag{2.53}$$

Then we utilize the same procedure as the achievability part, we have

$$\log M \leq nI(X;Y) + \sqrt{nU(X;Y)}Q^{-1}(1-\epsilon) + \frac{1}{2}\log n. \tag{2.54}$$

$$R \leq I(X;Y) - Q^{-1}(\epsilon)\sqrt{\frac{U(X;Y)}{n}} + \frac{1}{2n}\log n + \mathcal{O}(n^{-\frac{3}{2}}). \tag{2.55}$$

2.2.2 Fundamentals of SPB59

In this subsection, we briefly introduce the fundamentals of SPB59. Shannon [16] explored various scenarios and presented formulas with varying levels of simplicity and accuracy for computing them. His focus was on the scenario where all codewords require equal energy for transmission, which was a characteristic of Phase-Shift Keying (PSK) modulation. He aimed to find the most precise formula for this specific case. The equal energy requirement for transmitting codewords implies that the transmitted signals $(x_1, x_2, \ldots, x_n)$ occupy positions on a sphere, S with radius $\sqrt{nE_s}$, where E_s denotes the average energy of the transmitted signal. There are the total number of 2^{Rn} codewords, where R represents the coding rate, each corresponding to a distinct point on S. These points can be used to define Voronoi cells, which are the convex regions in $\mathbb{R}^n$ comprising of 2^{Rn} points whose distance to the given point are smaller than that to any of the remaining $2^{Rn} - 1$ points.

As all points reside on the surface of the sphere, each Voronoi cell takes the form of a polyhedral cone, whose solid angle is the angle at a vertex subtended by the face of the cone, bounded by at most $2^{Rn} - 1$ hyperplanes that intersect at the origin. Since 2^{Rn} cones collectively cut the entire $\mathbb{R}^n$ space, i.e., the whole sphere, the summation of the solid angles of 2^{Rn} cones equals that of $\mathbb{R}^n$, which in the specific case the summation is equivalent to the total surface area of the unit sphere. The additive white Gaussian noise (AWGN) modifies the area of the polygon base, i.e., more noise means larger size of the area. The error probability of

maximum likelihood (ML) decoder occurs when the AWGN causes the area of the polygon base of one codeword to overlap that of another codeword. The PDF of the noise moving the code point a distance d is shown as follows

$$\frac{1}{(2\pi)^{n/2}} \exp\{-\frac{1}{2}d^2\}dV, \tag{2.56}$$

where dV denotes the element of the volume. Thus, the differential probability for a circular cone of the half angle θ is

$$\frac{1}{(\sqrt{2\pi})^n} \exp\big[\frac{-(r^2 + A^2 n - 2rA\sqrt{n}\cos\theta)}{2}\big]\big[\frac{(n-1)\pi^{(n-1)/2}(r\sin\theta)^{n-2}}{\Gamma(\frac{n+1}{2})}\big] r dr d\theta, \tag{2.57}$$

where r denotes the radius, θ represents the solid angle, and A denotes the SNR of $\sqrt{2E_s/N_0}$.

For any angle θ, the probability $P_{e,SPB59}$ that the noise makes the area of the polygon base overlap another point is

$$P_{e,SPB59} = \frac{(n-1)e^{-nA^2/2}}{\sqrt{2\pi}2^{(n-1)/2}\Gamma(\frac{n+1}{2})} \int_\theta^{\pi/2} (\sin\theta)^{n-2} \int_0^\infty r^{n-1} \exp\{-\frac{1}{2}r^2 + \sqrt{n}rA\cos\theta\} dr d\theta + \int_{\sqrt{n}A}^\infty \frac{1}{\sqrt{2\pi}} \exp\{-\frac{1}{2}t^2\} dt. \tag{2.58}$$

To complete the SPB59, we need to obtain the relation between θ and R. The total area of the circular cone of half angle θ is

$$\Omega(\theta) = \frac{2\pi^{(n-1)/2}}{\Gamma(\frac{n-1}{2})} \int_0^\theta (\sin\phi)^{n-2} d\phi. \tag{2.59}$$

And the surface of the n-dimensional sphere of unit radius is

$$\Omega(\pi) = \frac{2\pi^{(n-1)/2}}{\Gamma(\frac{n-1}{2})} \int_0^\pi (\sin\phi)^{n-2} d\phi. \tag{2.60}$$

By solving the equation $\frac{\Omega(\theta)}{\Omega(\pi)} = 2^{-nR}$, for all $\theta < \pi/2$, we have the approximation as follows

$$\frac{\Gamma(n/2)(\sin\theta)^{n-1}}{2\Gamma(\frac{n+1}{2})\pi^{1/2}\cos\theta}(1 - \frac{\tan^2\theta}{n}) \le 2^{-nR} \le \frac{\Gamma(n/2)(\sin\theta)^{n-1}}{2\Gamma(\frac{n+1}{2})\pi^{1/2}\cos\theta}. \tag{2.61}$$

2.2.3 Fundamental of SPB67

This subsection briefly demonstrates the fundamentals of SPB67. In [41], the authors considers a discrete memoryless channel with the finite input alphabet $\{1, 2, \ldots, K\}$ whose input distribution is $\mathbf{q} = (q_1, q_2, \ldots, q_k)$, and the finite output alphabet $\{1, 2, \ldots, J\}$. The transition probabilities were defined as $P(j|k)$, $1 \leq k \leq K$, $1 \leq j \leq J$. They get the lower bound for the fixed composition codes which the numbers of occurrences of the input letter k, $1 \leq k \leq K$ were exactly $q_k n$. For any $0 < \rho < 1$, we have

$$P_{e,SPB67} > \frac{1}{4} \exp\left\{ n \sum_{k=1}^{K} q_k \Big[\mu_k(\rho) - \rho \mu_k'(\rho) \Big] - \rho \sqrt{\frac{2 \sum_{k=1}^{K} q_k \mu_k''(\rho)}{n}} \right\}, \tag{2.62}$$

where $\mu_k(\rho) = \ln \sum_{j=1}^{J} P(j|k)^{1-\rho} f(j)^{\rho}$, and $f(j)$ is any function as long as the summation of all $f(j)$ equals to 1, and $\mu_k'(\rho)$ and $\mu_k''(\rho)$ are the first and second derivative of $\mu_k(\rho)$ with respect to ρ.

To attain the most optimal result from this starting point, the authors have employed a combination of convex optimization and variational calculus, which led them to select the function $f(j)$ as follows

$$f(j) = \frac{\left(\sum_{k=1}^{K} q_{k,\rho} P(j|k)^{1-\rho} \right)^{1/(1-\rho)}}{\sum_{j'=1}^{J} \left(\sum_{k=1}^{K} q_{k,\rho} P(j'|k)^{1-\rho} \right)^{1/(1-\rho)}}, \tag{2.63}$$

where the input distribution $q_{k,\rho}$ is chose to maximize $E_0(\rho)$ which is defined below

$$E_0(\rho) = -\ln \sum_{j=1}^{J} \Big[\sum_{k=1}^{K} q_k P(j|k)^{1-\rho} \Big]^{1/(1-\rho)}. \tag{2.64}$$

It is easy to prove that the quantity

$$\sum_{k=1}^{K} q_k \Big[\mu_k(\rho) + (1-\rho) \mu_k'(\rho) \Big] - (1-\rho) \sqrt{\frac{2 \sum_{k=1}^{K} q_k \mu_k''(\rho)}{n}} \tag{2.65}$$

is monotonic increase starting from $\rho = 0$ to 1 and always negative. Thus, there exists $\bar{\rho} \in [0, 1]$ that satisfies the following equation

$$2^{-nR} = \frac{1}{4} \exp\left\{ n \sum_{k=1}^{K} q_k \Big[\mu_k(\rho) + (1-\rho)\mu_k'(\rho) \Big] - (1-\rho)\sqrt{\frac{2\sum_{k=1}^{K} q_k \mu_k''(\rho)}{n}} \right\}, \quad (2.66)$$

where $R \in [\frac{2}{n}, C + \frac{2}{n} + \frac{\sqrt{2/n \sum_{k=1}^{K} q_k \mu_k''(\rho)}}{\ln 2}]$ and $C = \frac{dE_0(\rho)}{d\rho}(0)$ denotes the channel capacity. For sufficiently large n, it is still easy to prove that the quantity

$$\sum_{k=1}^{K} q_k \Big[\mu_k(\rho) - \rho\mu_k'(\rho) \Big] - \rho\sqrt{\frac{2\sum_{k=1}^{K} q_k \mu_k''(\rho)}{n}} \quad (2.67)$$

is monotonic decrease as a function of ρ. Thus, by selecting $\rho = \bar{\rho}$, we have

$$\sum_{k=1}^{K} q_k \mu_k'(\rho) = \frac{\ln 2}{1-\bar{\rho}}(-R + \frac{2}{n}) - \frac{1}{1-\bar{\rho}} \sum_{k=1}^{K} q_k \mu_k(\bar{\rho}) + \sqrt{\frac{2\sum_{k=1}^{K} q_k \mu_k''(\bar{\rho})}{n}}. \quad (2.68)$$

By eliminating $\sum_{k=1}^{K} q_k \mu_k'(\rho)$ in (2.62), the optimal lower bound is achieved as follows

$$\begin{aligned} P_{e,SPB67} &> \frac{1}{4} \exp\left\{ n \Big[\frac{\sum_{k=1}^{K} q_k \mu_k(\bar{\rho})}{1-\bar{\rho}} + \frac{\bar{\rho}}{1-\bar{\rho}}(R - \frac{2}{n}) \ln 2 + 2\bar{\rho}\sqrt{\frac{2\sum_{k=1}^{K} q_k \mu_k''(\bar{\rho})}{n}} \Big] \right\} \\ &= \frac{1}{4} \exp\left\{ - n \Big[E_0(\frac{\bar{\rho}}{1-\bar{\rho}}) - \frac{\bar{\rho}}{1-\bar{\rho}}(R - \frac{2}{n}) \log 2 + 2\bar{\rho}\sqrt{\frac{2\sum_{k=1}^{K} q_k \mu_k''(\bar{\rho})}{n}} \Big] \right\}. \end{aligned}$$

2.3 Forward Error Control Coding

In this section, we give a brief discussion on the Forward error control coding (FECC), commonly referred to as channel coding, which is a widely used error detection and correction technique that enhances the reliability of transmission in existing communication networks. The fundamental concept behind error control coding is to append code bits to the information bits, thus reducing the BER of the received signal when it is transmitted through a noisy channel. The earliest error control code, known as the Hamming code, was developed by Richard Hamming [42]

in 1950. In the ensuing decades, various error control codes were invented for use in different applications and situations. There are two primary categories of error control codes, including BCH code and polar code.

1. BCH codes comprise a vast and robust category of cyclic codes capable of correcting random number of errors. This category represents a notable extension of the Hamming code with the capability of correcting multiple errors. Only binary BCH codes are considered. For any positive integers $m \geq 3$ and $t < 2m - 1$, there exists a binary BCH code with blocklength $n = 2^m - 1$, the total number of the parity check digits in a single codeword less than mt, and the minimum distance of the BCH code d larger than $2t + 1$. We refer to this code as an BCH code capable of correcting t errors.

   Let α denote a primitive element in the Galois field of order 2^m, $GF(2^m)$. In order to encode the BCH code, the generator polynomial is required. This polynomial of the BCH code with blocklength $2^m - 1$ is defined as $g(x)$. If $g(x)$ has roots $\alpha, \alpha^2, \ldots, \alpha^{2t}$, it can be seen as the lowest degree polynomial over Galois field of order 2, $GF(2)$. Since its roots $\alpha, \alpha^2, \ldots, \alpha^{2t}$ and $\beta, \beta^2, \ldots, \beta^{2t}$ are mutual conjugate with each other, where β is selected from $(\alpha^2, \alpha^3, \ldots, \alpha^{n-1})$. Therefore, $\beta, \beta^2, \ldots, \beta^{2t}$ are $g(x)$'s roots as well. Due to the fact that the generator polynomial is the least common multiple of $2t$ minimal polynomial, we denote the minimal polynomial of α^i as $\phi_i(x)$. From the above argument, the generator polynomial can be rewritten as $g(x) = LCM\{\phi_1(x), \phi_2(x), \ldots, \phi_{2t}(x)\}$, where $LCM\{\cdot\}$ represents the least common multiple of $\cdot$. If i is even, it can be rewritten as an odd number multiplied by an even number, i.e., $i = 2^l i'$, where i' is odd and l is larger than 1. Then α to the even power of i α^i can be transformed to $(\alpha^{i'})^{2l}$. We can define α to the even power of i α^i is a conjugate of α to the odd power of i' $\alpha^{i'}$. Then we have the minimal poly-

nomials of α^i $\phi_i(x)$ which is equal to the minimal polynomial of $\alpha^{i'}$ $\phi_{i'}(x)$. Thus, by eliminating all the even number i and keeping all the odd number i', it is easy to obtain that $g(x)$ is the least common multiple of the minimal polynomial of all odd number i', i.e., $\phi_1(x), \phi_3(x), \ldots, \phi_{2t-1}(x)$. The degree of the generator polynomial $g(x)$ is not larger than mt, which implies the above mentioned feature of the binary BCH code, i.e., the total number of the parity check bits cannot exceed mt. When t is relatively small, mt precisely equals the total number of parity-check bits. BCH codes that are defined using α as a primitive element are typically referred to as primitive (or narrow-sense) BCH codes.

For the decoding BCH code, An BCH code capable of correcting t errors with blocklength $n = 2^m - 1$ can be defined as follows: An n-bit binary vector $\mathbf{r} = (r_0, r_1, \ldots, r_{n-1})$ is considered a codeword if and only if the polynomial $\mathbf{r}(x) = r_0 + r_1 x + \cdots + r_{n-1}x_{n-1}$ has the roots $\alpha, \alpha^2, \ldots, \alpha^{2t}$. As α^i is a root of $\mathbf{r}(x)$ for $1 \leq i \leq 2t$, it follows that $\mathbf{r}(\alpha^i) = r_0 + r_1\alpha^i + r_2\alpha^{2i} + \cdots + r_{n-1}\alpha^{(n-1)i} = 0$. We can represent this equality as a matrix product, as shown below

$$(r_0, r_1, \ldots, r_{n-1}) \begin{bmatrix} 1 \\ \alpha^i \\ \alpha^{2i} \\ \vdots \\ \alpha^{(n-1)i} \end{bmatrix} = 0, \tag{2.69}$$

for $1 \leq i \leq 2t$. Let

$$\mathbf{H} = \begin{bmatrix} 1 & \alpha & \alpha^2 & \ldots & \alpha^{n-1} \\ 1 & (\alpha^2) & (\alpha^2)^2 & \ldots & (\alpha^2)^{n-1} \\ \vdots & \vdots & \vdots & \ddots & \vdots \\ 1 & (\alpha^{2t}) & (\alpha^{2t})^2 & \ldots & (\alpha^{2t})^{n-1} \end{bmatrix}. \tag{2.70}$$

For the BCH code capable of correcting t errors, if $\mathbf{r} = (r_0, r_1, \ldots, r_{n-1})$ is a codeword, then $\mathbf{r}\mathbf{H}^H = 0$. If an n-bit vector $\mathbf{r}$ satisfies the aforementioned condition, then α^i is a root of $\mathbf{r}(x)$. Consequently, $\mathbf{r}$ is a codeword in the BCH code capable of correcting t errors. The parity-check matrix $\mathbf{H}$ is used to check for errors in the code. If α^j is a conjugate of α^i for some i and j, then $\mathbf{r}(\alpha^j) = 0 \Leftrightarrow \mathbf{r}(\alpha^i) = 0$. $\mathbf{H}$ can be reduced to

$$\mathbf{H} = \begin{bmatrix} 1 & \alpha & \alpha^2 & \ldots & \alpha^{n-1} \\ 1 & (\alpha^3) & (\alpha^3)^2 & \ldots & (\alpha^3)^{n-1} \\ \vdots & \vdots & \vdots & \ddots & \vdots \\ 1 & (\alpha^{2t-1}) & (\alpha^{2t-1})^2 & \ldots & (\alpha^{2t-1})^{n-1} \end{bmatrix}. \tag{2.71}$$

By replacing each entry of $\mathbf{H}$ with its corresponding m-bit binary vector in column form over $GF(2)$, we can generate the parity-check matrix to decode the BCH code.

2. Polar codes, invented by Erdal Arikan [43] in 2009, are the first type of error control codes capable of achieving channel capacity for binary-input, discrete, memoryless symmetric (B-DMS) channels. Polar codes offer the benefit of efficient encoding and decoding, with complexity $\mathcal{O}(N \log N)$. The concept of polar codes stems from channel polarization, which transforms N branches of a symmetric channel, whose capacity is defined as the mutual information of the channel W $I(W)$, into nearly perfect or entirely noisy channels. Out of N channels, the channels with the capacity of $I(W)$ tend to be the perfect channels, while the channels with the capacity of $1 - I(W)$ tend to be the fully noisy channels. Consequently, the total number K of the information bits in the N blocklength are only sent to pass the perfect channels, while the rest $N - K$ bits to other fully noisy channels are set as the frozen bits

which is zero. As the number N approaches infinity, the fraction of perfect channels approaches the channel capacity of $I(W)$. To encode the information vector $\mathbf{b} = (b_1, b_2, \ldots, b_K)$, the encoder constructs an intermediate vector $\mathbf{x} = (x_1, x_2, \ldots, x_N)$ of length N. The elements x_i, $i \in \mathcal{I} \subset \{1, 2, \ldots, N\}$ contain the information bits, while the other elements x_j, $j \in \mathcal{F}_c \subset \{1, 2, \ldots, N\}$ contain frozen bits (e.g., zeros) that are pre-determined which means that the positions of the frozen bits are fully known at the transmitter and receiver ends. The intermediate sequence $\mathbf{x}$ can then be encoded into a codeword vector $\mathbf{u} = (u_1, u_2, \ldots, u_N)$ as $\mathbf{u} = \mathbf{x}\mathbf{G}_N = \mathbf{x}(\mathbf{G}_2)^{\otimes n}$, where $n = \log N$. Here, $(\mathbf{G}_2)^{\otimes n}$ denotes the n-th Kronecker power of matrix $\mathbf{G}_2$, where

$$\mathbf{G}_2 = \begin{bmatrix} 1 & 0 \\ 1 & 1 \end{bmatrix}. \tag{2.72}$$

Thus, the $\mathbf{G}_N$ is the generator matrix of the polar code.

For the SCL decoding, the algorithm, introduced in [44], transforms the original SC decoding into a list-first search while satisfying complexity constraints. At each level $s \in \mathcal{S}$, the decoder duplicates into two parallel decoding threads whose countable set is defined as $\mathcal{T}$, allowing decoding in either direction. However, to prevent an exponential increase in decoding threads, at each step, only the L most probable threads (out of $2L$ possibilities) are retained once the number of parallel decoding threads reaches L. The decoder produces a list of L candidates $\hat{x}(l)$, $l \in \{0, 1, \ldots, L-1\}$, corresponding to L (out of 2^{NR}) paths on the binary tree. The most probable path is selected as the final estimate. This procedure is described in Algorithm 1, where c_s denotes the s-th element

of a vector $\mathbf{x}$, $\mathbf{x}_0^{s-1}$ represents the sub-vector $[x_0, x_1, \ldots, x_{s-1}]^T$. Additionally,

$$\begin{aligned} W_n^s(\mathbf{y}, \mathbf{x}_0^{s-1} \,|\, x_s) &= \sum_{\mathbf{x}_{s+1}^{N-1} \in \mathcal{X}^{N-s-1}} \frac{1}{2^{N-1}} W_n(\mathbf{y}|\mathbf{x}) \\ &= \sum_{\mathbf{x}_{s+1}^{N-1} \in \mathcal{X}^{N-s-1}} \frac{1}{2^{N-1}} \prod_{s=0}^{N-1} W(y_s|u_s), \end{aligned}$$

where u_s denotes the s-th element of vector $\mathbf{u} = \mathbf{x}\mathbf{G}_N$.

Algorithm 1: SCL Decoding [44]

$\mathcal{T} \leftarrow \{0\}$;
for $s = 0, 1, \ldots, N-1$ **do**
  if $s \notin \mathcal{S}$ **then**
    $\hat{x}_s(l) \leftarrow x_s$ for $\forall l \in \mathcal{T}$;
  else
    if $|\mathcal{T}| < L$ **then**
      foreach $l \in \mathcal{T}$ **do**
        Duplicate_Path(l);
    else
      Calculate $P_{l,\hat{x}} = W_n^{(s)}(\mathbf{y}, \hat{\mathbf{x}}_0^{s-1}(l) \,|\, x)$ for $\forall l \in \mathcal{T}$ and $\forall x \in \{0, 1\}$;
      $\delta \leftarrow$ the mean value of $2L$ tentative $P_{l,x}$;
      foreach $l \in \mathcal{L}$ *which satisfies* $P_{l,0} < \delta$ *and* $P_{l,1} < \delta$ **do**
        Eliminate the thread l and set $\mathcal{T} \leftarrow \mathcal{T} \setminus \{l\}$;
      for $l \in \mathcal{T}$ **do**
        if $P_{l,x} > \delta$ *while* $P_{l,x \otimes 1} < \delta$ **then**
          $\hat{x}_s(l) \leftarrow x$;
        else
          Duplicate_Path(l);
$l^* \leftarrow \arg\max_{l \in \mathcal{T}} W_n^{(N-1)}(\mathbf{y}, \hat{\mathbf{x}}_0^{N-1}(l) \,|\, \hat{x}_N(l))$;
return $\hat{\mathbf{x}}_{\mathcal{S}}[l^*]$;
subroutine Duplicate_Path(l)
  Copy the thread l into a new thread $l' \notin \mathcal{T}$;
  $\mathcal{T} \leftarrow \mathcal{T} \cup \{l'\}$;
  $\hat{x}_s[l] \leftarrow 0$;
  $\hat{x}_s[l'] \leftarrow 1$;

Chapter 3

Analytical Bounds for the Optimal Code over the Reconfigurable Intelligent Surface at a Short Blocklength

3.1 Introdution

In this chapter, we derives the sphere-packing bounds to evaluate the performance of an RIS-assisted wireless system at a short blocklength regime. Compared with the original work for sphere-packing bound with an infinite blocklength over an AWGN channel in [16], we derive the expression for the lower and upper bounds over the RIS-assisted system in order to utilize our mathematical framework at a short blocklength regime. Then, we use Wald sequential t-test lemma and the Riemann sum to obtain the closed-form expression for the bounds. At a short blocklength regime, the approximation of the angle in the sphere-packing theory, which is used

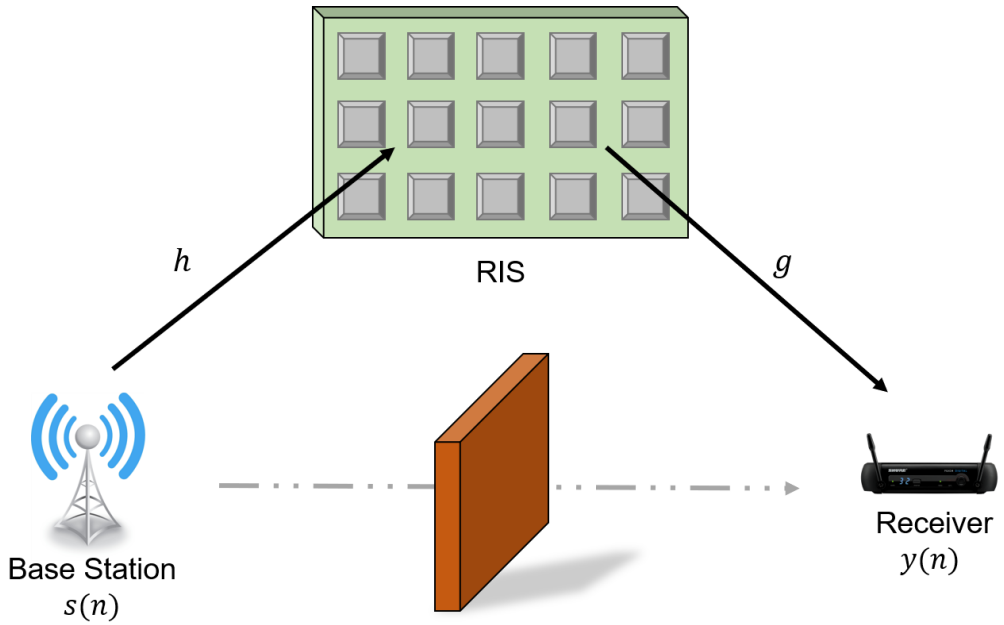

Figure 3.1: System model for the RIS-assisted wireless system

to determine the code rate in [16] [34], will have a margin of error. To overcome it, we derive the expression to calculate the exact value of the angle.

3.2 System Model

We consider an RIS-assisted wireless communication system with the direct link which is blocked by an obstacle (i.e. a wall or building) between the transmit and receive antenna shown in Fig. 3.1. A rectangular RIS of N_{ris} elements is utilized to improve the whole system performance, and only reflection-type RIS is considered in this letter. We assume that all the RIS elements are ideal which means that each of them can independently influence the phase and the reflection angle of the impinging wave.

The signal vector at the receive antenna is given by

$$y(i) = \sqrt{P_r}A(i)s(i) + w(i), \quad i = 1, \ldots, n, \tag{3.1}$$

where $w(i)$ is the equivalent baseband AWGN with a zero mean and variance N, i.e., $w(i) \sim \mathcal{CN}(0, N_0)$, and $A(i)$ is the channel coefficient, P_r is the average power at the receiver which can be obtained from the path-loss model [45] as $P_r = \frac{PG_tG_r\lambda^2}{16\pi^2(d_1^2+d_2^2)}$, where P is signal power at the transmitter, and λ is the wavelength in meters, and G_t and G_r are the transmitter and receiver antenna gains. d_1 and d_2 denote the distance between the transmitter and the RIS, the RIS and the receiver, respectively. We assume that the binary phase shift keying (BPSK) modulation is adopted in the air interface. The transmitted signal $s(i) \in \mathcal{A}$, $i = 1, \ldots, n$, where $\mathcal{A} = \{-1, +1\}$.

We denote the baseband equivalent channels between the transmitter and the m-th reflecting element of the RIS by $\mathbf{h}_m = [h_m(1), \ldots, h_m(n)], \quad \forall m = 1, \ldots, N_{ris}$ with $h_m(i) = |h_m(i)|e^{j\phi_m(i)}$, where $|h_m(i)|$ and $\phi_m(i)$ represent the amplitude and phase of the channel coefficient $h_m(i)$, respectively. The reflecting channels between the m-th reflecting element and the receiver are $\mathbf{g}_m = [g_m(1), \ldots, g_m(n)]$ with $g_m(i) = |g_m(i)|e^{j\varphi_m(i)}$, where $|g_m(i)|$ and $\varphi_m(i)$ represent the amplitude and phase of the channel coefficient $g_m(i)$, respectively. The channels are assumed to be i.i.d., and their envelops follow the Rayleigh distribution, i.e., we have $h_m(i)$, $g_m(i) \sim \mathcal{CN}(0, 1)$. Then, the channel coefficient $A(i)$ of our RIS-assisted system can be expressed as

$$A(i) = \sum_{m=1}^{N_{ris}} \eta_m(i) h_m(i) g_m(i), \tag{3.2}$$

where $\eta_m(i)$ denotes the reflecting coefficient of the m-th reflecting element with $\eta_m(i) = |\eta_m(i)|e^{j\theta_m(i)}$, where $|\eta_m(i)|$ represents the reflecting gain and $\theta_m(i)$ is the phase shift configured by the m-th reflecting element. Without loss of generality, we assume the reflecting gain $|\eta_m(i)| = 1$. In addition, we assume that the phases of the channels $h_m(i)$ and $g_m(i)$ are perfectly known to the transmitter, and that the transmitter can choose the optimal phase shifting. Hence, (3.2) can be re-written

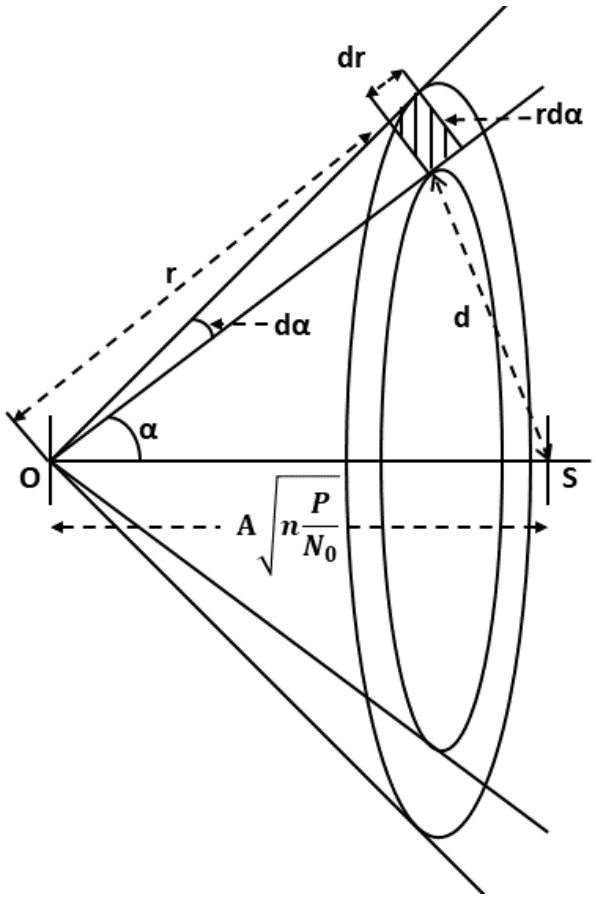

Figure 3.2: Plane of cone of angle α

as

$$A(i) = \sum_{m=1}^{N_{ris}} |h_m(i)| \cdot |g_m(i)| \tag{3.3}$$

In Fig. 3.2, we assume that O is the origin of a n dimensional sphere and S is a signal point which situates on the surface of the n dimensional sphere. α denotes the angle of the cone intersected by the two outer lines and the angle $\alpha + d\alpha$ is the slightly larger angle which represents a larger cone. The radius of outer cone is $r + dr$ and that of the inner cone is r. Therefore, the two sides of the ring shaped plane is $rd\alpha$ and dr, respectively. d presents the distance between the signal point S and the above ring. We consider that there is a channel code with the number of codewords M. For notation simplicity, in the following we use A instead of $A(i)$, the

code can place its M points arbitrarily on the surface of the n dimensional sphere whose radius is $A\sqrt{n\frac{P}{N_0}}$.

3.3 Performance Analysis

Theorem 6. *For any $\alpha_1 < \frac{\pi}{2}$, given the channel coefficient A, the conditional probability of error $P_{e,\ opt}(n, R|A)$ for the optimal code with the length n, and code rate R can be bounded by*

$$\Phi(\alpha, n, A) \leq P_{e,\ opt}(n, R|A) \leq \Phi(\alpha, n, A) + \frac{M}{\Lambda(\pi, n)} \int_0^{\alpha_1} \Lambda(\alpha, n) d\Phi(\alpha, n, A), \quad (3.4)$$

where $\Phi(\alpha, n, A)$ denotes the probability of a signal point S in the n dimensional sphere that n also represents the code length, which has the $A\sqrt{n\frac{P}{N_0}}$ distance between the origin point O, being moved outside the cone whose angle is α. And $\Lambda(\alpha, n)$ denotes the $n-1$ dimensional area of the cap which is cut out by the cone on the $n-1$ dimensional unit sphere. And α_1 is the angle which can evenly cut the sphere into M parts, equivalently $M\Lambda(\alpha_1, n) = \Lambda(\pi, n)$.

Then by taking the expectation over the channel coefficient A, both upper and lower bounds of the error probability $P_{e,\ opt}(n, R)$ for the optimal code with the length n, and code rate R can be finally obtained as

$$\mathbb{E}_A\Big[\Phi(\alpha, n, A)\Big] \leq P_{e,\ opt}(n, R) \leq \mathbb{E}_A\Big[\Phi(\alpha, n, A) + \frac{M}{\Lambda(\pi, n)} \int_0^{\alpha_1} \Lambda(\alpha, n) d\Phi(\alpha, n, A)\Big], \quad (3.5)$$

where the parameter α_1 is determined by solving the equation

$$2^{nR}\Lambda(\alpha_1, n) = \Lambda(\pi, n). \quad (3.6)$$

The proof of Theorem 6 can be found in [16] [34].

According to Theorem 6, at first, we need to calculate $\Lambda(\alpha_1, n)$. The surface of a n dimensional sphere with r radius can be given as

$$S_n(r) = \frac{n\pi^{n/2} r^{n-1}}{\Gamma(\frac{n+2}{2})}. \tag{3.7}$$

According to the cosine law, and the fact of the $n-1$ dimensional unit sphere, we obtain that the radius of the cap is $\sin\alpha$. Thus, we get

$$\Lambda(\alpha_1, n) = \frac{(n-1)\pi^{\frac{n-1}{2}}}{\Gamma(\frac{n+1}{2})} \int_0^{\alpha_1} \sin^{n-2}\alpha d\alpha. \tag{3.8}$$

From (3.8), we can easily get

$$\Lambda(\pi, n) = S_n(1) = \frac{n\pi^{n/2}}{\Gamma(\frac{n+2}{2})}. \tag{3.9}$$

And in order to decrease the margin of error at the short blocklength regime and get the exact expression for $\Lambda(\alpha, n)$, we need to calculate $\int_0^{\alpha}(\sin\alpha)^{n-2}d\alpha$ which is defined by the recursive relationship for all $n > 3$

$$\begin{aligned} I_n &= \int_0^{\alpha} (\sin\alpha)^{n-2} d\alpha = -\sin^{n-3}\alpha\cos\alpha + (n-3)\int_0^{\alpha} \cos^2\alpha \sin^{n-4}\alpha d\alpha \\ &= -\sin^{n-3}\alpha\cos\alpha + (n-3)\Big(\int_0^{\alpha} \sin^{n-4}\alpha d\alpha - \int_0^{\alpha} \sin^{n-2}\alpha d\alpha\Big) \\ &= -\frac{\sin^{n-3}\alpha\cos\alpha}{n-2} + \frac{n-3}{n-2} I_{n-2} \end{aligned}$$

and by the initial conditions

$$I_2 \triangleq \alpha; \qquad I_3 \triangleq -\cos\alpha. \tag{3.10}$$

For numerical accuracy purpose, we use this recursive relationship to compute the value of I_n, then times the coefficient which is $(n-1)\pi^{\frac{n-1}{2}}/\Gamma(\frac{n+1}{2})$. We can therefore get the expression for $\Lambda(\alpha, n)$, if n is even, then

$$\begin{aligned} \Lambda(\alpha, n) = \frac{(n-1)\pi^{\frac{n-1}{2}}}{\Gamma(\frac{n+1}{2})}\Big(&\frac{(n-3)!!}{(n-2)!!}\alpha - \frac{\sin^{n-3}\alpha\cos\alpha}{n-2} \\ &- \sum_{i=0} \sin^{n-5-2i}\alpha\cos\alpha \frac{\prod_{j=\frac{n}{2}-i}^{\frac{n}{2}}(2j-3)}{\prod_{k=\frac{n}{2}-(i+1)}^{\frac{n}{2}}(2k-2)}\Big) \end{aligned} \tag{3.11}$$

and if n is odd, then

$$\Lambda(\alpha,n)=-\frac{(n-1)\pi^{\frac{n-1}{2}}}{\Gamma(\frac{n+1}{2})}\Big(\frac{(n-3)!!}{(n-2)!!}\cos\alpha+\frac{\sin^{n-3}\alpha\cos\alpha}{n-2}+\sum_{i=0}\sin^{n-5-2i}\alpha\cos\alpha\cdot \frac{\prod_{j=\frac{n}{2}-i}^{\frac{n}{2}}(2j-3)}{\prod_{k=\frac{n}{2}-(i+1)}^{\frac{n}{2}}(2k-2)}\Big). \quad (3.12)$$

Then we need to calculate $\Phi(\alpha,n)$ which corresponds to the probability of signal point S being carried outside the cone by the noise. The noise, of which the mean value and variance are zero and one, respectively, is generated by a n dimensional Gaussian distribution function

$$f(d)=\frac{1}{(2\pi)^{n/2}}e^{-d^2/2}. \quad (3.13)$$

Based on the cosine law, from Fig. 3.2, we have the expression for d

$$d^2=r^2+A^2n\frac{P}{N_0}-2rA\sqrt{n\frac{P}{N_0}}\cos\alpha. \quad (3.14)$$

The differential volume of the ring shaped region equals to the shaded area which is $rdrd\alpha$ times the surface of a $n-1$ dimensional sphere whose radius is $r\sin\theta$

$$dV=rdrd\alpha S_{n-1}(r\sin\alpha)=rdrd\alpha\frac{(n-1)\pi^{\frac{n-1}{2}}(r\sin\alpha)^{n-2}}{\Gamma(\frac{n+1}{2})}. \quad (3.15)$$

We multiply the probability density in (3.13) and the differential volume in (3.15) and then substitute d from (3.14), we can get the expression for $\Phi(\alpha)$,

$$\Phi(\alpha,n,A)=\frac{(n-1)\exp(-\frac{1}{2}A^2n\frac{P}{N_0})}{2^{n/2}\pi^{1/2}\Gamma(\frac{n+1}{2})}\int_{\alpha_1}^{\pi/2}\sin^{n-2}\alpha\cdot \int_0^{\infty}r^{n-1}\exp(-\frac{1}{2}r^2+rA\sqrt{n\frac{P}{N_0}}\cos\alpha)drd\alpha+Q(A\sqrt{n\frac{P}{N_0}}). \quad (3.16)$$

Now, to reduce the complexity of (3.16), we want to obtain the closed form of $\Phi(\alpha,n,A)$ by eliminating integrals with respect to r and α, respectively. At first,

by applying Wald sequential t-test lemma in [46], we can eliminate the integral with respect to r as follows

$$\int_0^\infty r^{n-1}\exp(-\frac{1}{2}r^2 + rA\sqrt{n\frac{P}{N_0}}\cos\alpha)dr \approx \sqrt{2\pi}\Delta(\alpha,n)(\frac{\bar{r}(\alpha,n)}{e})^{n-1}\exp\big(\frac{1}{2}\bar{r}^2(\alpha,n,A)\big), \quad (3.17)$$

where

$$\bar{r}(\alpha,n,A) = A\bar{r}(\alpha,n) = \sqrt{n}A\Big(\frac{1}{2}\sqrt{\frac{P}{N_0}}\cos\alpha + \sqrt{\frac{P\cos^2\alpha}{4N_0}+\frac{1}{n}}\Big)$$

and

$$\Delta(\alpha,n) = \frac{1}{2}\Bigg(\Big(1+\frac{1}{4}\big(\sqrt{\cos^2\alpha\frac{P}{N_0}+\frac{1}{4}}-\cos\alpha\sqrt{\frac{P}{N_0}}\big)^2\Big)^{-1/2} + \sqrt{\frac{\bar{r}^2(\alpha,n)}{\bar{r}^2(\alpha,n)+\frac{1}{n-1}}}\Bigg)$$

Then, we have

$$\Phi(\alpha,n,A) \approx Q(A\sqrt{n\frac{P}{N_0}}) + \frac{(n-1)}{e^{n-1}2^{(n-1)/2}\Gamma(\frac{n+1}{2})} \int_{\alpha_1}^{\pi/2}\frac{\Delta(\alpha,n)}{\bar{r}(\alpha,n,A)\sin^2\alpha}\exp\Big(-n\big(\frac{1}{2}\frac{A^2P}{N_0}-\frac{1}{2n}\bar{r}^2(\alpha,n,A)-\log(\bar{r}(\alpha,n,A)\sin\alpha)\big)\Big)d\alpha. \quad (3.18)$$

Then, to eliminate the integral with respect to α, we utilize the Riemann sum. A partition of the interval $[\alpha_1, \pi/2]$ is a finite sequence of numbers of the form $\alpha_1 = \alpha_1 < \alpha_2 < \cdots < \alpha_\infty = \pi/2$ with the subinterval $[\alpha_i, \alpha_{i+1}]$. Due to the fact that the exponential part in (3.18) has its maximum at α_1 in the interval $[\alpha_1, \pi/2]$, the whole function of (3.18) will go down exponentially. Therefore, we assume that the first K subintervals dominate the integral and the length of each subinterval is the same and $\alpha_{i+1} - \alpha_i = n^{-1}$. Then, we have the closed-form expression for

$\Phi(\alpha, n, A)$ as follows

$$\Phi(\alpha, n, A) \approx Q(A\sqrt{n\frac{P}{N_0}}) + \frac{1}{e^{n-1}2^{(n-1)/2}\Gamma(\frac{n+1}{2})} \sum_{i=1}^{K} \frac{\Delta(\alpha_i + \frac{1}{2n}, n)}{\bar{r}(\alpha_i + \frac{1}{2n}, n, A)\sin^2(\alpha_i + \frac{1}{2n})} \cdot \exp\Big(- n\big(\frac{1}{2}\frac{A^2P}{N_0} - \frac{1}{2n}\bar{r}^2(\alpha_i + \frac{1}{2n}, n, A) - \log\big(\bar{r}(\alpha_i + \frac{1}{2n}, n, A)\sin(\alpha_i + \frac{1}{2n})\big)\big)\Big) \tag{3.19}$$

Additionally, we focus on our upper bound. From (3.18), We have

$$d\Phi(\alpha, n, A) = \frac{(n-1)}{2^{(n-1)/2}\Gamma(\frac{n+1}{2})}\big(\Delta(\alpha, n)(\frac{\bar{r}(\alpha, n, A)}{e})^{n-1}\sin^{n-2}\alpha\big) \cdot \exp\big(- \frac{1}{2}A^2 n\frac{P}{N_0} + \frac{1}{2}\bar{r}^2(\alpha, n, A)\big)d\alpha \tag{3.20}$$

Then, we can also use the Riemann sum to obtain the closed form of $\Lambda(\alpha, n)d\Phi(\alpha, n, A)$. A partition of the interval $[0, \alpha_1]$ is a finite sequence of numbers of the form $0 = \alpha_{-\infty} < \cdots < \alpha_0 < \alpha_1 = \alpha_1$ with the subinterval $[\alpha_i, \alpha_{i+1}]$. We utilize the last K subintervals to the Riemann sum.

$$\int_0^{\alpha_1} \Lambda(\alpha, n)d\Phi(\alpha, n, A) \approx \frac{1}{2^{(n-1)/2}\Gamma(\frac{n+1}{2})} \sum_{i=-K+1}^{1} \big(\Lambda(\alpha_i, n) \cdot \Delta(\alpha_i, n)(\frac{\bar{r}(\alpha_i, n, A)}{e})^{n-1}\sin^{n-2}\alpha_i\big) \exp\big(- \frac{1}{2}A^2 n\frac{P}{N_0} + \frac{1}{2}\bar{r}^2(\alpha_i, n, A)\big). \tag{3.21}$$

Moreover, we need to get the probability density of the channel coefficient A to calculate the expectation over A. The PDF of A in (3.3) can be statistically evaluated as [30]

$$f_A(x) = \frac{x^a}{b^{a+1}\Gamma(a+1)} \exp\big(- \frac{x}{b}\big), \tag{3.22}$$

where

$$a = \frac{k_1^2}{k_2} - 1 \quad \text{and} \quad b = \frac{k_2}{k_1}, \tag{3.23}$$

where $k_1 = \frac{N_{ris}\pi}{4}$ and $k_2 = N_{ris}(1 - \frac{\pi^2}{16})$.

Finally, we combine (3.22) and (3.19) together to obtain the closed-form expression for the lower bound denoted as $P^L_{e,\ opt}(n, R)$ in (3.24) which is shown as

follows.

$$P^{L}_{e,\ opt}(n,R)=\frac{1}{e^{n-1}2^{(n-1)/2}\Gamma(\frac{n+1}{2})}\sum_{i=1}^{K}\frac{\Delta(\alpha_i+\frac{1}{2n},n)}{\bar{r}^2(\alpha_i+\frac{1}{2n},n)\sin^3(\alpha_i+\frac{1}{2n})}\cdot$$
$$X^{-\frac{a}{2}}(\alpha_i+\frac{1}{2n},n)\Big(\sqrt{X(\alpha_i+\frac{1}{2n},n)}\Gamma(\frac{a-1}{2})_1F_1(\frac{a-1}{2},\frac{1}{2},\frac{1}{4b^2X(\alpha_i+\frac{1}{2n},n)})$$
$$-\Gamma(\frac{a}{2})_1F_1(\frac{a}{2},\frac{1}{2},\frac{1}{4b^2X(\alpha_i+\frac{1}{2n},n)})\Big). \quad (3.24)$$

Then we combine (3.22) and (3.21) together to obtain the upper bound as $P^{U}_{e,\ opt}(n,R)$ for the case that only n is even in (3.25), which is shown as follows.

$$P^{U}_{e,\ opt}(n,R)=P^{L}_{e,\ opt}(n,R)+\frac{2^{nR}\Gamma((n+2)/2)}{n\pi^{n/2}2^{(n-1)/2}\Gamma(\frac{n+1}{2})}\sum_{i=-K+1}^{1}\frac{\Lambda(\alpha_i,n)\Delta(\alpha_i,n)}{\bar{r}^2(\alpha_i,n)\sin^3(\alpha_i)}\cdot$$
$$\Big(\sqrt{X(\alpha_i,n)}\Gamma(\frac{a-1}{2})_1F_1(\frac{a-1}{2},\frac{1}{2},\frac{1}{4b^2X(\alpha_i,n)})-\Gamma(\frac{a}{2})_1F_1(\frac{a}{2},\frac{1}{2},\frac{1}{4b^2X(\alpha_i,n)})\Big), \quad (3.25)$$

where $X(\alpha,n)=\frac{nP}{2N_0}-\frac{\bar{r}^2(\alpha,n)}{2}$ and a, b are given in (3.23).

Compared with the approximation of α_1 in [16] [34] which is tightly suitable when R and n grow relatively large. To compute the exact value of α_1 in (3.6) at a short blocklength regime, in the case of an even n, we use (3.11) divided by (3.9) to obtain the exact value of α_1. Otherwise, we use (3.12) divided by (3.9) to calculate α_1.

3.4 Simulation Results

In this section, we compare the lower and upper bounds for different blocklength and numbers of the RIS elements. Figs. 3.3 and 3.4 illustrate the comparison between the lower and upper bounds on the ML decoding error probability for the codes with the code length $n=128$ bits and $n=64$ bits and with the same code rate $R=0.5$ bits per channel use over the perfect Rayleigh fading channel in Section 3.3 for different

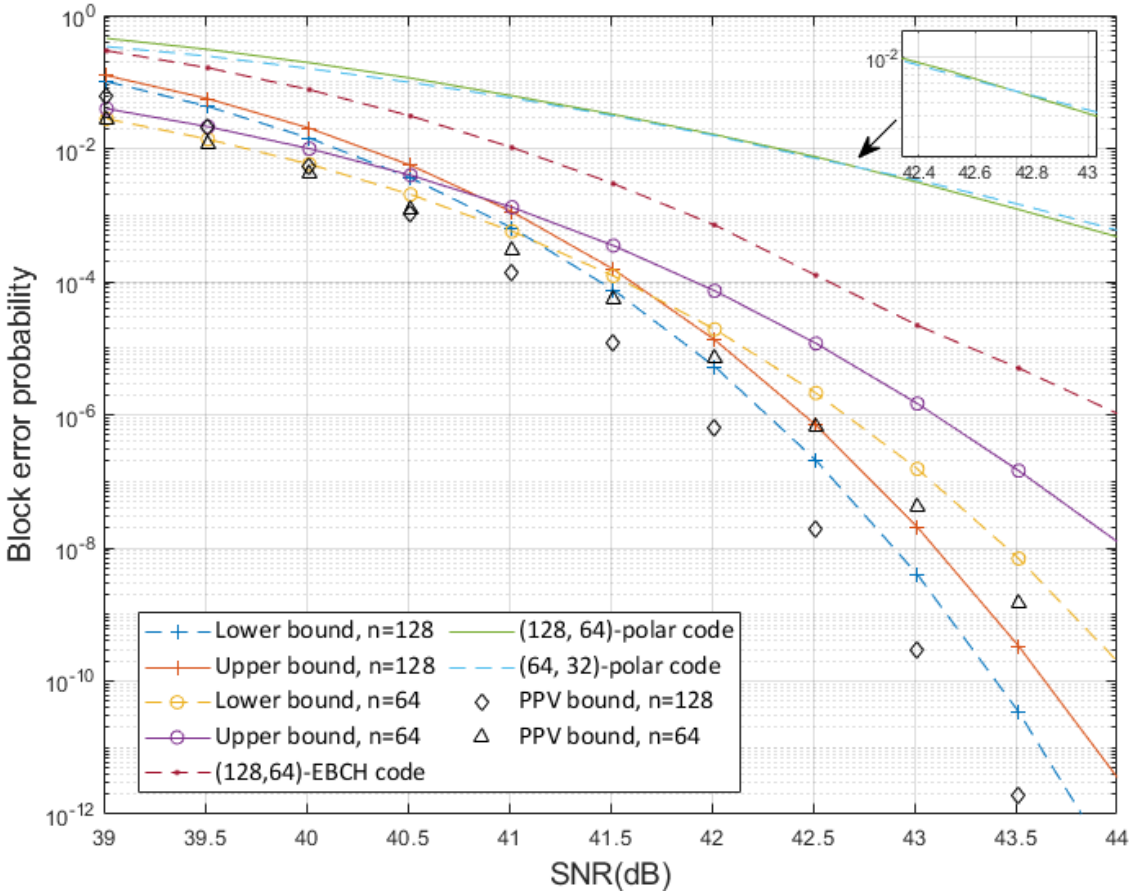

Figure 3.3: A comparison between the lower and upper bounds on the ML decoding error probability for the codes of code length $n = 64$ bits and $n = 128$ bits with the same code rate $R = 0.5$ bits per channel use over the perfect Rayleigh fading channel in Section 3.3 for $N_{ris} = 4$.

numbers of RIS elements 4 and 64, respectively. We define the transmit SNR as $\frac{P}{N_0}$ in decibels (dB) and set $P_r = 0$dB, the wavelength $\lambda = 0.125m$ (the operating frequency $f_c = 2.4$ GHz), $G_t = G_r = 8$ (9.03 dBi) and $d_1 = d_2 = 10m$. We utilize the Polar code with SCL decoder and the EBCH code with OSD decoder to validate our bounds. All the simulations are averaged by 10^6 Monte Carlo realization. We set the PPV bound in [17] as a reference. From Fig. 3.3, we observe that at the low SNR regime, the performance of the code with the short blocklength, i.e., $n = 64$, is slightly better than the one with the long blocklength, i.e., $n = 128$,. When

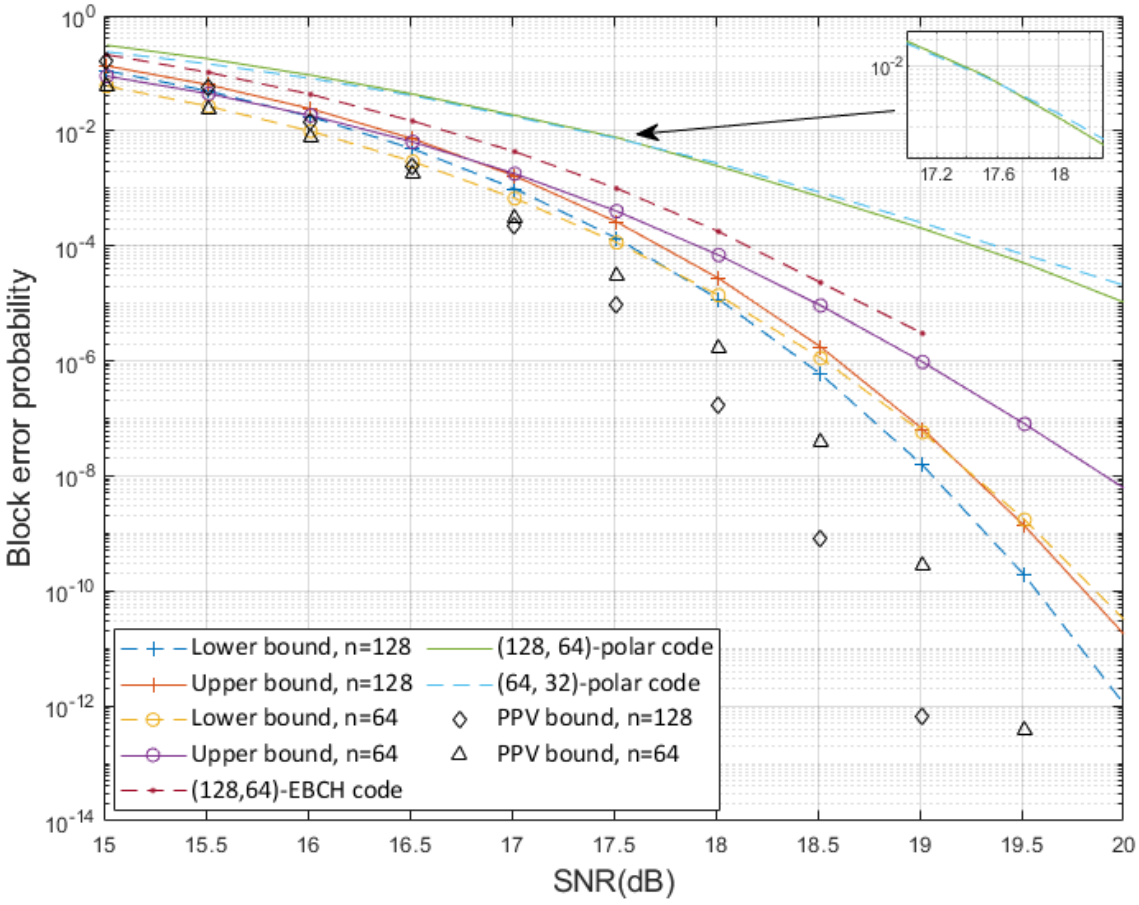

Figure 3.4: A comparison between the lower and upper bounds on the ML decoding error probability for the codes of code length $n = 64$ bits and $n = 128$ bits with the same code rate $R = 0.5$ bits per channel use over the perfect Rayleigh fading channel in Section 3.3 for $N_{ris} = 64$.

we increase the SNR, the long code will finally outperform the short code. The SNR's value of the intersection on the lower bounds is approximately 40.25 dB. It indicates that the short code is preferred when the targeted SNR is less than 40.25 dB. Otherwise, we can choose the long code to accomplish better transmission. In Fig. 3.3, in terms of the code length of 128 bits, for a decoding error probability of 10^{-2}, the gap between the lower and upper bounds is 0.10 dB. When the decoding error probability level is low i.e., 10^{-4}, the gap decreases to 0.15 dB. This margin means that if the performance of the actual code is in this area, the correspondingly

actual code can be seen as the optimal code. Moreover, the SNR's value of the intersection on the upper bounds is basically the same as the lower bounds, which is around 40.25 dB.

Fig. 3.4 shows, as N_{ris} increase from 4 to 64, the comparison between the performances of both the lower and upper bounds of the different code length with the same code rate. When it comes to $n = 64$ bits, for the same decoding error probability of 10^{-4}, the gap between its lower and upper bounds decreases from 0.85 dB to 0.25 dB. Thus, this result indicates that when the number of RIS elements increases, the gap between the lower and upper bounds narrows. Furthermore, the SNR's value of the intersection on the lower bounds is approximately 15.50 dB. Compared with Fig. 3.3, it indicates that with the increase of the RIS elements, the short code outperforms the long code over a more extensive range of SNR.

In this section, we derive the lower and upper bounds for the optimal code over the RIS system. If the BLER performance of the practical code falls within the region bounded by the lower and upper bounds, it is the optimal code for that particular channel. Obviously, the investigated EBCH code and the polar code are not the optimal code for the investigated RIS channel, that is the reason why their BLER are outside the derived bounds. To further illustrate this, we also reproduced the lower and upper bounds over the AWGN channel from the original study [15] and simulated the investigated EBCH code over the AWGN channel. We set the code rate $R = 0.5$, and the blocklength $n = 128$. The simulation result for the $(128, 64)$-EBCH code with OSD decoder (the order is chosen to 3) is also shown in Fig. 3.5. All the simulations are averaged over 10^5 Monte Carlo realizations. It can be seen that the BLER falls outside the bounds as well.

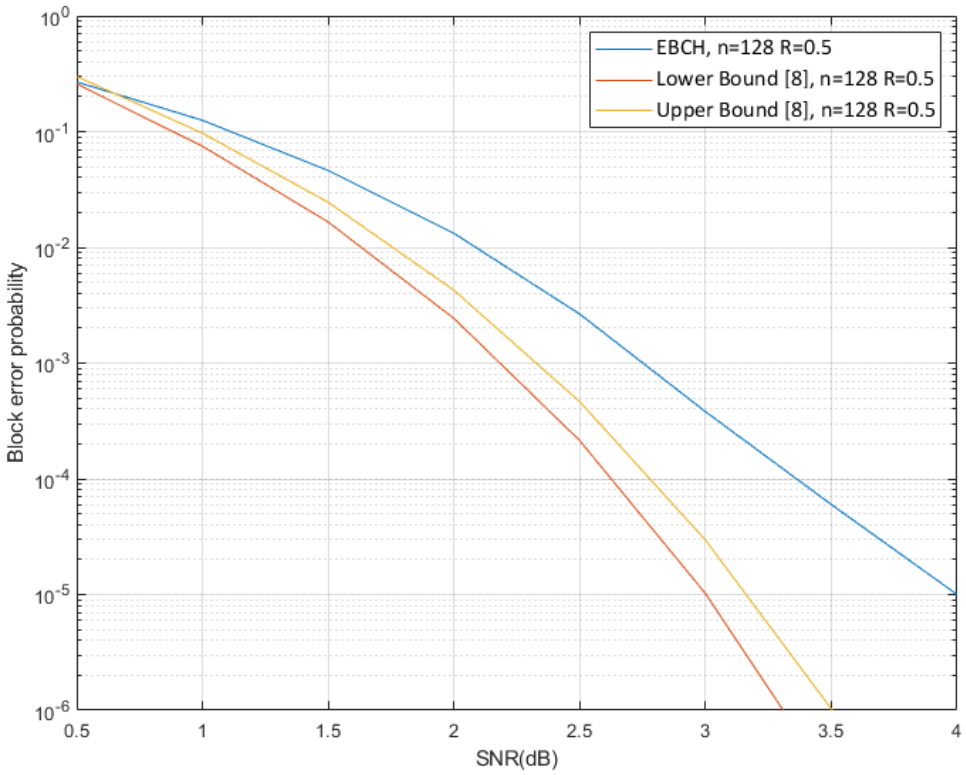

Figure 3.5: A comparison between the $(128, 64)$-EBCH code with OSD decoder whose order is 3 and the bounds on the ML decoding error probability for the codes of code length $n = 64$ bits and $n = 128$ bits over the AWGN channel.

3.5 Summary

In this chapter, we investigated the lower and upper bounds of the decoding error probability for the optimal code of the specific length, SNR and code rate over the RIS assisted communication system at a short blocklength regime. The sphere-packing technique is mainly used to derive our bounds with the closed-form expression for both the lower and upper bounds. The numerical findings demonstrate how different blocklength performs over the RIS-assisted wireless system for a given code rate and how exactly the number of RIS elements improves the signal quality at the receiver side.

Chapter 4

Performance Analysis for Reconfigurable Intelligent Surface Assisted MIMO Systems

4.1 Introduction

In this chapter, we use the Berry-Esseen theorem, mutual information and unconditional information variance as the fundamental mathematical basis to obtain the achievability and converse bounds for the maximal achievable rate R given a fixed maximal error probability ϵ and blocklength n for an RIS MIMO system. To derive the achievability bound, we use the Berry-Esseen theorem and some other inequalities and show the channel output's exact PDF. To derive our converse bound, we combine the maximum of the auxiliary channel's PDF, which is a product of m copies of the PDF of Gamma distributed variables by the Mellin transform and Meijer G-function, and the maximum of its output space by the Lebesgue measure. Furthermore, we utilize the saddle point approximation and the Taylor series expan-

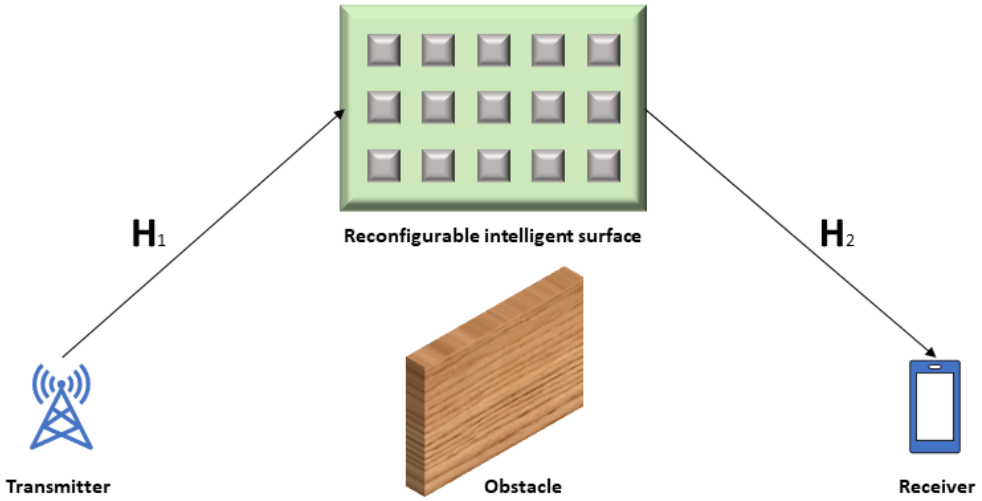

Figure 4.1: System Model.

sion to find the closed forms for both the mutual information and the unconditional information variance. In order to complete our achievability and converse bounds, we utilize different modulation schemes in our RIS MIMO system, and compare the performance of each modulation scheme mainly in two aspects. One is the required blocklength to achieve a certain level of the maximal achievable rate, and the other is how the unconditional information variance affects the convergence's speed to the maximal achievable rate.

4.2 System Model

We consider an RIS-assisted wireless communication system with t transmit and r receive antennas shown in Fig. 4.1. Both of the transmitter and receiver have multiple antennas which are placed as uniform linear arrays (ULAs). The direct link is blocked by an obstacle (i.e. a wall or building) which is situated between the transmit and receive antennas. A rectangular RIS of N_{ris} elements is utilized to

improve the whole system performance, and only reflection-type RIS is considered in this paper. We assume that all the RIS elements are ideal which means that each of them can independently influence the phase and the reflection angle of the impinging wave.

We let $m = \min\{t, r\}$. The signal vector at the receive antenna array is given by

$$\mathbf{Y} = \mathbf{H}\mathbf{X} + \mathbf{W}, \tag{4.1}$$

where $\mathbf{H} \in \mathbb{C}^{r\times t}$ is the channel matrix, $\mathbf{X} \in \mathbb{C}^{t\times n}$ is the transmit signal over n channel uses, $\mathbf{Y} \in \mathbb{C}^{r\times n}$ is the corresponding received signal, and $\mathbf{W} \in \mathbb{C}^{r\times n}$ is the additive noise at the receiver, which is independent of $\mathbf{H}$ and has i.i.d. $\mathcal{CN}(0, 1)$ entries.

The channel matrix $\mathbf{H}$ of our RIS-assisted system can be expressed as

$$\mathbf{H} = \mathbf{H}_2\mathbf{\Sigma}(\boldsymbol{\theta})\mathbf{H}_1, \tag{4.2}$$

where $\mathbf{H}_1 \in \mathbb{C}^{N_{ris}\times t}$ represents the channel between the transmitter and the RIS, $\mathbf{H}_2 \in \mathbb{C}^{r\times N_{ris}}$ represents the channel between the RIS and the receiver, and $\mathbf{\Sigma}(\boldsymbol{\theta}) = diag(\boldsymbol{\theta}) \in \mathbb{C}^{N_{ris}\times N_{ris}}$, where $\boldsymbol{\theta} = [\theta_1, \ldots, \theta_{N_{ris}}]^T \in \mathbb{C}^{N_{ris}\times 1}$ represents the signal reflecting coefficient from the RIS. In this paper, similar to the related works [47–49], we assume that the signal reflection from any RIS element is ideal, i.e., without any power loss. In other words, we may write $\theta_i = \exp\{j\phi_i\}$ for $i = 1, \ldots, N_{ris}$, where ϕ_i is the phase shift induced by the i-th RIS element, which can be flexibly adjusted in $[0, 2\pi)$[1]. Equivalently, we may write $|\theta_i| = 1$, $i = 1, \ldots, N_{ris}$.

Let us consider input and output sets $\mathcal{A}$ and $\mathcal{B}$ and a conditional probability measure $P_{\mathbf{Y}|\mathbf{X}} : \mathcal{A}^{t\times n} \mapsto \mathcal{B}^{r\times n}$. We denote a codebook with M codewords by

[1]To characterize the achievable rate limit of RIS-assisted MIMO systems without perfect phase shifting, we assume that the phase shift by each RIS element can be continuously adjusted, i.e., we assume that the phase shift of the RIS elements obeys the continuous uniform distribution over the interval $[0, 2\pi)$.

$(\mathbf{C}_1, \ldots, \mathbf{C}_M)$. A decoder is defined as a random transformation $P_{Z|\mathbf{Y}} : \mathcal{B}^{r\times n} \mapsto \{1, \ldots, M\}$ which satisfies $P_{Z|\mathbf{X}}(j|\mathbf{C}_j) \geq 1-\epsilon$, $j = 1, \ldots, M$ where ϵ is the maximal error probability. We also consider that each codeword $\mathbf{C}_j$ satisfies the equal power constraint $||\mathbf{C}_j||^2 = nP$, where P is the transmit power. Then, a codebook and a decoder whose maximal error probability is smaller than ϵ are termed as an (n, M, ϵ) code and its coding rate is defined as $R = \frac{\log M}{n}$. In this paper, the information density also plays an essential role, which is defined as [50]

$$i(X;Y) \triangleq \log \frac{P_{\mathbf{Y}|\mathbf{X}}(\mathbf{y}|\mathbf{x})}{P_{\mathbf{Y}}(\mathbf{y})}, \tag{4.3}$$

where $P_{\mathbf{Y}|\mathbf{X}}(\mathbf{y}|\mathbf{x})$ denotes the conditional distribution on $\mathcal{B}^{r\times 1}$ for all $\mathbf{x} \in \mathcal{A}^{t\times 1}$, and $P_{\mathbf{Y}}(\mathbf{y})$ represents the output distribution.

4.3 Achievability and Converse Bounds

In this section, we provide the definitions of achievability and converse bounds. The achievability and converse bounds are important to the proof of the channel coding theorem. The achievability bound is a lower bound on the size of a code that can be guaranteed to exist with a given arbitrary blocklength and error probability. The converse bound is an upper bound on the size of any code with a given arbitrary blocklength and error probability. The mutual information is defined as $I(X;Y) \triangleq \mathbb{E}[i(X;Y)]$. Additionally, the unconditional information variance is defined as $U(X;Y) \triangleq Var[i(X;Y)]$, where $Var[\cdot]$ denotes the variance of $(\cdot)$. Moreover, our achievability and converse bounds for the examined RIS MIMO system are presented below.

Theorem 7. *We consider a communication system with finite input alphabet $\mathcal{A}$, and the continuous output alphabet $\mathcal{B}$. Let $p(\mathbf{Y}, \mathbf{H}|\mathbf{X})$ be the corresponding conditional*

PDF on $\mathcal{B}$ for all $\mathbf{X} \in \mathcal{A}^n$, where $\mathbf{H}$ is a channel matrix. The input distribution $P(\mathbf{X}) \triangleq [\mathbf{q}_1, \ldots, \mathbf{q}_t]^T$, where $\mathbf{q}_i = [q_{i,0}, \ldots, q_{i,n}]$, $i = 1, \ldots, t$ with $q_{i,j}$ being equiprobable, i.e., $q_{i,j} = \frac{1}{|\mathcal{A}|}$. Then we define the mutual information and the unconditional information variance as $I(X;Y)$ and $U(X;Y)$, respectively.

Thus for the RIS MIMO channel and arbitrary $0 < \epsilon < 1$, we have the achievability and converse bounds

$$I(X;Y) - \sqrt{\frac{U(X;Y)}{n}}Q^{-1}(\epsilon) + \frac{1}{n} + \mathcal{O}(n^{-\frac{3}{2}}) \leq R \leq I(X;Y) - \sqrt{\frac{U(X;Y)}{n}}Q^{-1}(\epsilon + \frac{\epsilon}{\sqrt{n}}) + \frac{(m+1)\log n}{2n} + \mathcal{O}(n^{-\frac{3}{2}}), \quad (4.4)$$

where Q is the complementary Gaussian cumulative distribution function $Q(x) = \int_x^\infty \frac{1}{\sqrt{2\pi}} \exp(-\frac{u^2}{2})du$.

Proof. We give the key proof steps. At first, we prove that the second moment of $i(X;Y)$ is nonzero and the third moment is always less than infinity. According to the DT bound in [17], we have $\epsilon \geq \mathbb{P}[i(X^n;Y^n) \leq \log\lambda] + \lambda\mathbb{E}[\exp\{-i(X^n;Y^n)\}1_{\{i(X^n;Y^n)>\log\lambda\}}]$. After applying the Berry-Esseen theorem several times, we have $\mathbb{P}[i(X^n;Y^n) \leq \log\lambda] + \lambda\mathbb{E}[\exp\{-i(X^n;Y^n)\}1_{\{i(X^n;Y^n)>\log\lambda\}}] \leq Q(\tau) + \frac{1}{\sqrt{n}}\frac{6T(X;Y)}{U(X;Y)^{\frac{3}{2}}}(1 + 2\frac{\exp\{\Delta\}}{\exp\{\Delta\}-1} + \frac{U(X;Y)\Delta\exp\{\Delta\}}{\sqrt{2\pi}6T(X;Y)(\exp\{\Delta\}-1)})$. Then, we can select a particular value of τ to eliminate the right hand of the above equation. Thus, we have the achievability bound. For the converse part, we denote the auxiliary channel as $Q_{\mathbf{Y}|\mathbf{X},\mathbf{H}}$. After applying the Meijer G function and the Lebesgue measure, we have the converse bound of the maximal error probability of the auxiliary channel. According to the binary hypothesis testing in [17], we finally obtain the converse part. The detailed proof of Th. 7 can be found in Section 2.2.1 and Appendix A. □

To accomplish the achievability bound by applying Th. 7, we need to obtain the exact expression of both the mutual information and the unconditional variance. At

first, for our system model, the input distribution $P(\mathbf{X}) = [\mathbf{q}_1, \ldots, \mathbf{q}_t]^T$, where $\mathbf{q}_i = [\underbrace{\frac{1}{2}, \ldots, \frac{1}{2}}_{n}]$ and $\mathbf{q}_i = [\underbrace{\frac{1}{4}, \ldots, \frac{1}{4}}_{n}]$, for BPSK and QPSK, respectively[2]. Additionally the conditional PDF of a MIMO Rayleigh fading channel, $p(\mathbf{Y}, \mathbf{H}|\mathbf{X})$, is given by [35, 51, 52]

$$p(\mathbf{Y}, \mathbf{H}|\mathbf{X}) = p(\mathbf{H})p(\mathbf{Y}|\mathbf{X}, \mathbf{H}) = \frac{p(\mathbf{H})}{det(\pi \mathbf{I}_r)} \exp\big(-(\mathbf{Y} - \mathbf{H}\mathbf{X})(\mathbf{Y} - \mathbf{H}\mathbf{X})^H\big), \quad (4.5)$$

where $\mathbf{I}_r$ designates the $r \times r$ identity matrix and $det(\cdot)$ denotes the determinant.

Then

$$I(X;Y) = \quad (4.6)$$

$$\int_0^\infty \int_{-\infty}^\infty \sum_{\mathbf{X} \in \mathcal{A}^t} \left(P(\mathbf{X}) p(\mathbf{Y}, \mathbf{H}|\mathbf{X}) \log \big\{ \frac{p(\mathbf{Y}, \mathbf{H}|\mathbf{X})}{\sum_{\mathbf{X}' \in \mathcal{A}^t} P(\mathbf{X}') p(\mathbf{Y}, \mathbf{H}|\mathbf{X}')} \big\} \right) d\mathbf{Y} d\mathbf{H}$$

$$= \sum_{i=1}^{|\mathcal{A}|^t} \frac{P(\mathbf{x}_i)^t}{det(\pi \mathbf{I}_r)} \underbrace{\int_0^\infty \cdots \int_0^\infty}_{\substack{\text{m-dimensions} \\ \text{(w.r.t. } \mathbf{h})}} \underbrace{\int_{-\infty}^\infty \cdots \int_{-\infty}^\infty}_{\substack{\text{m-dimensions} \\ \text{(w.r.t. } \mathbf{y})}} p(\mathbf{h}) \exp\{-\frac{1}{2}||\mathbf{y} - \mathbf{h}\mathbf{x}_i||^2\} \cdot \quad (4.7)$$

$$\left(-\frac{\log e}{2} ||\mathbf{y} - \mathbf{h}\mathbf{x}_i||^2 - \log \big\{ \sum_{i'=1}^{|\mathcal{A}|^t} P(\mathbf{x}_{i'})^t \exp\{-\frac{1}{2}||\mathbf{y} - \mathbf{h}\mathbf{x}_{i'}||^2\} \big\} \right) d\mathbf{y} d\mathbf{h}$$

[2] As long as we have the conditional distribution of different modulation scheme, we can obtain the derivations in Section 4.3. The conditional distributions for PSK and QAM modulations are given below. Therefore, the derivations in Section 4.3 are applicable for both PSK and QAM signalings.For PSK modulation, let $M = 2^p$ be the size of the constellation of the PSK modulation, and denote the input to the channel by $\mathbf{x} = (x_1, x_2)$ where the possible input values are given by $\mathbf{x}_k = (cos\theta_k, sin\theta_k)$, where $\theta_k = \frac{(2k+1)\pi}{M}, k = 0, 1, \ldots, M-1$. Therefore, the conditional probability density function of the channel output is given by $p(\mathbf{Y}, \mathbf{H}|\mathbf{X}) = \frac{p(\mathbf{h})}{2\pi\sigma^2} \exp\left(-\frac{||\mathbf{y}-\mathbf{h}\mathbf{x}_k||^2}{2\sigma^2}\right)$. For QAM modulation, let $M = 2^p$, where p is even, be the size of the constellation for the QAM modulation, and denote the input to the channel by $\mathbf{x} = (x_1, x_2)$ where the possible input values are given by $\mathbf{x}_k = (\frac{I_k}{T}, \frac{J_k}{T})$, where $I_k = J_k = (2k + 1 - \sqrt{M}), k = 0, 1, \ldots, \sqrt{M} - 1$ and T is a normalization factor which $T = \sqrt{\frac{1}{2}\sum_k (2k + 1 - \sqrt{M})^2}$. Therefore, the conditional probability density function of the channel output is given by $p(\mathbf{Y}, \mathbf{H}|\mathbf{X}) = \frac{p(\mathbf{h})}{2\pi\sigma^2} \exp\left(-\frac{||\mathbf{y}-\mathbf{h}\mathbf{x}_k||^2}{2\sigma^2}\right)$.

and

$$U(X;Y) = \tag{4.8}$$
$$\int_0^\infty \int_{-\infty}^\infty \sum_{\mathbf{X}\in\mathcal{A}^t} \Big(P(\mathbf{X}) p(\mathbf{Y},\mathbf{H}|\mathbf{X}) \log^2 \{ \frac{p(\mathbf{Y},\mathbf{H}|\mathbf{X})}{\sum_{\mathbf{X}'\in\mathcal{A}^t} P(\mathbf{X}') p(\mathbf{Y},\mathbf{H}|\mathbf{X}')} \} \Big) d\mathbf{Y} d\mathbf{H}$$
$$= \sum_{i=1}^{|\mathcal{A}|^t} \frac{P(\mathbf{x}_i)^t}{det(\pi \mathbf{I}_r)} \underbrace{\int_0^\infty \cdots \int_0^\infty}_{\substack{\text{r-dimensions} \\ \text{(w.r.t. } \mathbf{h}\text{)}}} \underbrace{\int_{-\infty}^\infty \cdots \int_{-\infty}^\infty}_{\substack{\text{r-dimensions} \\ \text{(w.r.t. } \mathbf{y}\text{)}}} p(\mathbf{h}) \exp\{-\frac{1}{2}||\mathbf{y}-\mathbf{h}\mathbf{x}_i||^2\} \cdot \tag{4.9}$$
$$\Big(-\frac{\log e}{2}||\mathbf{y}-\mathbf{h}\mathbf{x}_i||^2 - \log\Big\{ \sum_{i'=1}^{|\mathcal{A}|^t} P(\mathbf{x}_{i'})^t \exp\{-\frac{1}{2}||\mathbf{y}-\mathbf{h}\mathbf{x}_{i'}||^2\} \Big\} \Big)^2 d\mathbf{y} d\mathbf{h}$$
$$- [I(X;Y)]^2,$$

where $\mathbf{x}$ is selected equiprobably from t-dimension constellation consisted of $|\mathcal{A}|^t$ vectors and $\mathbf{x}_i$ and $\mathbf{x}_{i'}$ are the i-th and i'-th points in the constellation of $\mathbf{x}$. In order to reduce the complexity of the mutual information and the unconditional variance, we give the approximation of (4.7) and (4.9). At first, we deal with the mutual information $I(X;Y)$,

$$I(X;Y) = t\log|\mathcal{A}| + \frac{1}{|\mathcal{A}|^t} \sum_{i=1}^{|\mathcal{A}|^t} \int_0^\infty \int_{-\infty}^\infty \frac{1}{det(\pi \mathbf{I}_r)} p(\mathbf{h}) \exp\{-\frac{1}{2}\|\mathbf{y}-\mathbf{h}\mathbf{x}_i\|^2\} \cdot \tag{4.10}$$
$$\log\{ \frac{\exp\{-\frac{1}{2}\|\mathbf{y}-\mathbf{h}\mathbf{x}_i\|^2\}}{\sum_{i'=1}^{|\mathcal{A}|^t} \exp\{-\frac{1}{2}\|\mathbf{y}-\mathbf{h}\mathbf{x}_{i'}\|^2\}} \} d\mathbf{y} d\mathbf{h}$$
$$= t\log|\mathcal{A}| - \frac{1}{|\mathcal{A}|^t \ln 2} \sum_{i=1}^{|\mathcal{A}|^t} \sum_{p=1}^{\infty} \frac{1}{p} \sum_{q=0}^{p} \frac{p!(-1)^q}{q!(p-q)!} \frac{1}{det(\pi \mathbf{I}_r)} \int_0^\infty \int_{-\infty}^\infty p(\mathbf{h}) \cdot \tag{4.11}$$
$$\Big(\mathbf{\Pi}(\mathbf{y},\mathbf{h}) \Big)^{-q} + \mathcal{O}(\frac{1}{(\mathbf{\Pi}(\mathbf{y},\mathbf{h}))^{q+1}}) d\mathbf{y} d\mathbf{h},$$

where (4.11) comes from Taylor series expansion of (4.10) and

$$\mathbf{\Pi}(\mathbf{y},\mathbf{h}) = \sum_{i'=1}^{|\mathcal{A}|^t} \exp\Big\{ \frac{\big\|\mathbf{y} - q\mathbf{h}(\mathbf{x}_i - \mathbf{x}_{i'})\big\|^2}{2q} - \frac{(q+1)\big\|\mathbf{h}(\mathbf{x}_i - \mathbf{x}_{i'})\big\|^2}{2} \Big\}. \tag{4.12}$$

Before utilizing the saddle point approximation, we need to guarantee the existence of the saddle point. For convenience of notation, we use vector $\mathbf{c}_{i,i'}$ to represent

$\mathbf{h}(\mathbf{x}_i - \mathbf{x}_{i'})$. Since q is positive integers, it is easy for us to validate that

$$\mathbf{\Pi}^{-q}(\mathbf{y}) = \Big[\sum_{i'}^{|\mathcal{A}|^t} \exp\{\frac{\big\|\mathbf{y} - q\mathbf{c}_{i,i'}\big\|^2}{2q} - \frac{(q+1)\big\|\mathbf{c}_{i,i'}\big\|}{2}\}\Big]^{-q} > 0$$

$$\lim_{\mathbf{y}\to\infty}\{\mathbf{\Pi}^{-q}(\mathbf{y})\} = \lim_{\mathbf{y}\to\infty}\Big[\sum_{i'}^{|\mathcal{A}|^t} \exp\{\frac{\big\|\mathbf{y} - q\mathbf{c}_{i,i'}\big\|^2}{2q} - \frac{(q+1)\big\|\mathbf{c}_{i,i'}\big\|}{2}\}\Big]^{-q} \to 0$$

$$\lim_{\mathbf{y}\to-\infty}\{\mathbf{\Pi}^{-q}(\mathbf{y})\} = \lim_{\mathbf{y}\to-\infty}\Big[\sum_{i'}^{|\mathcal{A}|^t} \exp\{\frac{\big\|\mathbf{y} - q\mathbf{c}_{i,i'}\big\|^2}{2q} - \frac{(q+1)\big\|\mathbf{c}_{i,i'}\big\|}{2}\}\Big]^{-q} \to 0$$

Thus there exists a maximum value of $\mathbf{\Pi}^{-q}(\mathbf{y})$, which satisfies the condition of the saddle point approximation. Then we can assume that $\mathbf{\Pi}^{-q}(\mathbf{y})$ achieves its maximum at $\mathbf{y} = \mathbf{y}_0$, which $\mathbf{y}_0$ satisfies $\frac{\partial}{\partial \mathbf{y}}\mathbf{\Pi}^{-q}(\mathbf{y})|_{\mathbf{y}=\mathbf{y}_0} = 0$

$$\sum_{i'=1}^{|\mathcal{A}|^t} \frac{2(\mathbf{y}_0 - q\mathbf{c}_{i,i'})}{2q} \exp\{\frac{\big\|\mathbf{y}_0 - q\mathbf{c}_{i,i'}\big\|^2}{2q} - \frac{(q+1)\big\|\mathbf{c}_{i,i'}\big\|}{2}\} = 0. \tag{4.13}$$

After solving (4.13), we have $\mathbf{y}_0 = \sum_{i'=1}^{|\mathcal{A}|^t} q\rho_{i,i'}\mathbf{c}_{i,i'}$, where $\rho_{i,i'} = \mathbf{\Pi}(\mathbf{y}_0)/\sum_{i'=1}^{|\mathcal{A}|^t}\mathbf{\Pi}(\mathbf{y}_0)$ is a positive number from $(0,1)$ and satisfies that $\sum_{i'=1}^{|\mathcal{A}|^t}\rho_{i,i'} = 1$. Therefore, we have for a non-zero number q, the multiple integrals over the complex number vector $\mathbf{y}$ can be approximated by the saddle point approximation

$$\int_{-\infty}^{\infty} \frac{1}{det(\pi\mathbf{I}_r)}\Big(\mathbf{\Pi}(\mathbf{y},\mathbf{h})\Big)^{-q} d\mathbf{y} \approx \Big[\sum_{i'=1}^{|\mathcal{A}|^t} \exp\{-\frac{\big\|\mathbf{h}(\mathbf{x}_i - \mathbf{x}_{i'})\big\|^2}{3 - \exp\{-\big\|\mathbf{h}(\mathbf{x}_i - \mathbf{x}_{i'})\big\|^2/4\}}\}\Big]^{-q}. \tag{4.14}$$

Combining (4.11) and (4.14), we eliminate the multiple integrals over the complex vector $\mathbf{y}$ as

$$I(X;Y) \approx t\log|\mathcal{A}| - \frac{1}{|\mathcal{A}|^t \ln 2}\sum_{i=1}^{|\mathcal{A}|^t}\sum_{p=1}^{\infty}\frac{1}{p}\sum_{q=0}^{p}\frac{p!(-1)^q}{q!(p-q)!}\int_0^{\infty} p(\mathbf{h})\cdot \Big[\sum_{i'=1}^{|\mathcal{A}|^t} \exp\Big\{-\frac{\big\|\mathbf{h}(\mathbf{x}_i - \mathbf{x}_{i'})\big\|^2}{3 - \exp\{-\big\|\mathbf{h}(\mathbf{x}_i - \mathbf{x}_{i'})\big\|^2/4\}}\Big\}\Big]^{-q} d\mathbf{h}. \tag{4.15}$$

Then by observing (4.15), we take advantage of inverse Taylor series expansion, leading to the following result.

Lemma 2. *Let t represent the number of transmitter antennas, and $\mathcal{A}$ denotes the input alphabet, and $p(\mathbf{h})$ represents the channel distribution, and $\mathbf{x}_i$ denotes the transmitted vector in the i-th transmitter antenna. The mutual information can be approximated as*

$$I(X;Y) \approx t\log|\mathcal{A}| - \int_0^\infty p(\mathbf{h})\frac{1}{|\mathcal{A}|^t}\sum_{i=1}^{|\mathcal{A}|^t}\log\Big[\sum_{i'=1}^{|\mathcal{A}|^t}\exp\Big\{-\frac{\big\|\mathbf{h}(\mathbf{x}_i-\mathbf{x}_{i'})\big\|^2}{3-\exp\{-\big\|\mathbf{h}(\mathbf{x}_i-\mathbf{x}_{i'})\big\|^2/4\}}\Big\}\Big]d\mathbf{h}. \quad (4.16)$$

Moreover, we need to obtain the approximation of the unconditional variance $U(X;Y)$. The first step is similar with the process of the approximation of $I(X;Y)$, we utilize the Taylor series expansion as follows

$$U(X;Y) = \frac{1}{|\mathcal{A}|^t}\sum_{i=1}^{|\mathcal{A}|^t}\int_0^\infty\int_{-\infty}^\infty \frac{1}{det(\pi\mathbf{I}_r)}p(\mathbf{h})\exp\{-\frac{1}{2}\|\mathbf{y}-\mathbf{h}\mathbf{x}_i\|^2\}\cdot \quad (4.17)$$
$$\log^2\{\frac{\exp\{-\frac{1}{2}\|\mathbf{y}-\mathbf{h}\mathbf{x}_i\|^2\}}{\frac{1}{|\mathcal{A}|^t}\sum_{i'=1}^{|\mathcal{A}|^t}\exp\{-\frac{1}{2}\|\mathbf{y}-\mathbf{h}\mathbf{x}_{i'}\|^2\}}\}d\mathbf{y}d\mathbf{h} - I(X;Y)^2$$

$$= -[I(X;Y)-(t\log|\mathcal{A}|)]^2 + \frac{1}{det(\pi\mathbf{I}_r)|\mathcal{A}|^t\ln 2}\cdot \quad (4.18)$$
$$\sum_{i=1}^{|\mathcal{A}|^t}\int_0^\infty\int_{-\infty}^\infty p(\mathbf{h})\Big(\sum_{p=1}^\infty\frac{1}{p}\sum_{q=0}^p\frac{p!(-1)^q}{q!(p-q)!}\big(\mathbf{\Pi}_2(\mathbf{y},\mathbf{h})\big)^{-q} + \mathcal{O}(\frac{1}{\mathbf{\Pi}_2(\mathbf{y},\mathbf{h})\big)^{q+1}})\Big)^2 d\mathbf{y}d\mathbf{h},$$

where

$$\mathbf{\Pi}_2(\mathbf{y},\mathbf{h}) = \sum_{i'=1}^{|\mathcal{A}|^t}\exp\Big\{\frac{\big\|\mathbf{y}-2q\mathbf{h}(\mathbf{x}_i-\mathbf{x}_{i'})\big\|^2}{4q} - \frac{(2q+1)\big\|\mathbf{h}(\mathbf{x}_i-\mathbf{x}_{i'})\big\|^2}{2}\Big\}. \quad (4.19)$$

Then we use the same techniques as the approximation of $I(X;Y)$, i.e., the saddle point approximation, we have for a non-zero number q, the multiple integrals over the

complex number vector $\mathbf{y}$ can be approximated by the saddle point approximation

$$\int_{-\infty}^{\infty} \frac{1}{det(\pi \mathbf{I}_r)} \Big(\mathbf{\Pi}_2(\mathbf{y}, \mathbf{h}) \Big)^{-2q} d\mathbf{y} = \Big(\int_{-\infty}^{\infty} \frac{1}{det(\pi \mathbf{I}_r)} \big(\mathbf{\Pi}_2(\mathbf{y}, \mathbf{h}) \big)^{-q} d\mathbf{y} \Big)^2 \tag{4.20}$$

$$\approx \Big[\sum_{i'=1}^{|\mathcal{A}|^t} \exp\{ - \frac{\big\| \mathbf{h}(\mathbf{x}_i - \mathbf{x}_{i'}) \big\|^2}{6 - \exp\{ - \big\| \mathbf{h}(\mathbf{x}_i - \mathbf{x}_{i'}) \big\|^2 / 16 \}} \} \Big]^{-2q}. \tag{4.21}$$

By using the inverse Taylor series expansion, leading to the following result.

Lemma 3. *Keeping parameters the same as Lemma 2, the unconditional variance can be approximated as*

$$U(X;Y) \approx -[I(X;Y) - (t \log |\mathcal{A}|)]^2 + \int_0^{\infty} p(\mathbf{h}) \frac{1}{|\mathcal{A}|^t} \sum_{i=1}^{|\mathcal{A}|^t} \log^2 \Big[\sum_{i'=1}^{|\mathcal{A}|^t} \exp \Big\{ - \frac{\big\| \mathbf{h}(\mathbf{x}_i - \mathbf{x}_{i'}) \big\|^2}{6 - \exp\{ - \big\| \mathbf{h}(\mathbf{x}_i - \mathbf{x}_{i'}) \big\|^2 / 16 \}} \Big\} \Big] d\mathbf{h}. \tag{4.22}$$

Moreover, we need to get the probability density of the channel coefficient $\mathbf{h}$ to calculate the expectation over $\mathbf{h}$. From (4.2), we let $h_{i,j}$, $h_{1,i,j}$ and $h_{2,i,j}$ denote the element of the i-th row and the j-th column of $\mathbf{H}$, $\mathbf{H}_1$ and $\mathbf{H}_2$, respectively. For notational convenience, we denote $h_{i,j}$ as h, $h_{1,i,j}$ as h_1 and $h_{2,i,j}$ as h_2, respectively, then we have

$$h = |h| e^{j \angle h} = \sum_{i=1}^{N_{ris}} |h_{2,i}| e^{j \angle h_{2,i}} \times |h_{1,i}| e^{j \angle h_{1,i}} \times e^{j \theta_i}, \tag{4.23}$$

where $|h_{1,i}|$ and $|h_{2,i}|$ denotes two Rayleigh RVs. Then the PDF of the product of two Rayleigh RVs is

$$p_{|h_{1,i}||h_{2,i}|}(x) = 4 x K_0(2x), \quad i = 1, \ldots, N_{ris}. \tag{4.24}$$

The Fourier transform of $p_{|h_{1,i}||h_{2,i}|}(x)$ is

$$F_{|h_{1,i}||h_{2,i}|}(k) = \int_{-\infty}^{\infty} p_{|h_{1,i}||h_{2,i}|}(x) \exp(-2\pi j k x) dx = \int_{-\infty}^{\infty} 4 x K_0(2x) \exp(-2\pi j k x) dx. \tag{4.25}$$

Then by using the inverse Fourier transform, we can obtain the distribution density of $|h|$ as shown below

$$\begin{aligned} p_{|h|}(x) &= \frac{1}{2\pi}\int_{-\infty}^{\infty}(F_{|h_i||g_i|}(k))^{N_{ris}}\exp(-jkx)dk \\ &= \frac{1}{2\pi}\int_{-\infty}^{\infty}\Big(\int_{-\infty}^{\infty}4xK_0(2x)\exp(-2\pi jkx)dx\Big)^{N_{ris}}\exp(-jkx)dk \\ &= \frac{2x}{N_{ris}}\exp(-\frac{x^2}{N_{ris}}) \end{aligned} \tag{4.26}$$

and the angle of h also follows the uniform distribution in $[0, 2\pi)$. Therefore, we obtain the expression of the h's PDF.

Substituting (4.26) into the mutual information and the unconditional variance (4.16) and (4.22), respectively. Then applying the right Riemann sum to eliminate the multiple integrals over the complex vector $\mathbf{h}$, we obtain the closed-form expression of $I(X;Y)$ and $U(X;Y)$ as follows

$$I(X;Y) \approx t\log|\mathcal{A}| - \sum_{k=1}\Delta h_k\cdot \tag{4.27}$$
$$\frac{2h_k}{N_{ris}}\exp(-\frac{h_k^2}{N_{ris}})\frac{1}{|\mathcal{A}|^t}\sum_{i=1}^{|\mathcal{A}|^t}\log\Big[\sum_{i'=1}^{|\mathcal{A}|^t}\exp\Big\{-\frac{\big\|h_k(\mathbf{x}_i-\mathbf{x}_{i'})\big\|^2}{2(3-\exp\{-\big\|h_k(\mathbf{x}_i-\mathbf{x}_{i'})\big\|^2/8\})}\Big\}\Big]$$

$$U(X;Y) \approx -[I(X;Y)-(t\log|\mathcal{A}|)]^2 + \sum_{k=1}\Delta h_k\cdot \tag{4.28}$$
$$\frac{2h_k}{N_{ris}}\exp(-\frac{h_k^2}{N_{ris}})\frac{1}{|\mathcal{A}|^t}\sum_{i=1}^{|\mathcal{A}|^t}\log^2\Big[\sum_{i'=1}^{|\mathcal{A}|^t}\exp\Big\{-\frac{\big\|h_k(\mathbf{x}_i-\mathbf{x}_{i'})\big\|^2}{2(6-\exp\{-\big\|h_k(\mathbf{x}_i-\mathbf{x}_{i'})\big\|^2/8\})}\Big\}\Big],$$

where $\Delta_{h_k} = h_k - h_{k-1}$. Finally, we substitute (4.27) and (4.28) into (4.4) to obtain our achievability and converse bounds for the Rayleigh fading channel.

To compare with our result, we calculate the capacity of the channel whose input is a circularly symmetric complex Gaussian with zero mean and covariance $\frac{P}{t}\mathbf{I}_t$. The Theorem is shown below.

Theorem 8. *[21] Under the power constraint P, we assume the same channel with the same number of transmitting and receiving antennas as our system model. Its*

capacity, as determined by the complex Gaussian input, is equal to

$$\mathbb{E}_{\mathbf{g}}[\log(1+\frac{P}{t}g)] = \int_0^\infty \log(1+\frac{P}{t}g)dg, \tag{4.29}$$

where g denotes the eigenvalues of the matrix $\mathbf{H}^H\mathbf{H}$, where $\mathbf{H}$ is from (4.2), and its PDF is given by

$$p_g(x) = \sum_{i=0}^{m} \frac{i!}{2(i+\max\{r,t\}-m)!}(L_i^{\max\{r,t\}-m}(x/N_{ris}))^2 \cdot (x/N_{ris})^{\max\{r,t\}-m}\exp(-x/N_{ris}). \tag{4.30}$$

Thus we have

$$C_{Gaussian} = \sum_{k=1}\Delta_{g_k}\log(1+\frac{P}{t}g_k)\sum_{i=0}^{m} \frac{i!}{2(i+\max\{r,t\}-m)!}(L_i^{\max\{r,t\}-m}(g_k/N_{ris}))^2 \cdot (g_k/N_{ris})^{\max\{r,t\}-m}\exp(-g_k/N_{ris}), \tag{4.31}$$

where $\Delta_{g_k} = g_k - g_{k-1}$.

4.4 Extension To More General Cases

In this chapter, we apply our achievability and converse bounds to several possible cases. We assume perfect channel estimation in Sections 4.4.1 and 4.4.3. When the channel is not known to the receiver, there exists mismatched decoding, i.e., scaled nearest neighbor (SNN) decoding [53]. We briefly introduce the general notion of mismatched decoding. Consider a conditional probability measure $P_{\mathbf{Y}|\mathbf{X}}$ with input $\mathbf{X} \in \mathcal{A}^{t\times n}$ and output $\mathbf{Y} \in \mathcal{B}^{r\times n}$. At coding rate R and blocklength n, a codebook with M codewords by $(C_1, \ldots, C_M)$. For mismatched decoding, we let a function $d : \mathcal{A}^{t\times n} \times \mathcal{B}^{r\times n} \to \mathbb{R}$ be a decoding metric, which hence induces the following decoding rule: $\hat{j} = \arg\min_{j\in M} d(\mathbf{X}, \mathbf{Y})$, with ties broken arbitrarily. A coding rate R is achievable if there exists a sequence of codebook such that the maximal error

probability asymptotically vanishes as $n \to \infty$, and the supremum of the achievable rate is called the mismatched capacity.

Furthermore, to analyze the effect of the CSI estimation in finite blocklength, there is a received pilot overhead provided to the receiver. For the RIS MIMO system, if the receiver antenna is 1, the overall pilot overhead is $N_{ris}+1$ [54]. When the pilot overhead is inserted in every channel use, then the resulting achievable rate should be discounted by a factor of $(1-\frac{N_{ris}+1}{n})$.

4.4.1 Perfect Phase Alignment-Rayleigh fading channel

In this subsection, we consider the case when the phase shift can be perfectly aligned with the channel phases due to the perfect channel estimation. Generally, the perfect phase shift is unknown for capacity maximization over the MIMO channel. However, according to [55,56], the discrete-Fourier transform (DFT)-based phase-shifting configuration along with an additional steering direction $\boldsymbol{\vartheta} \in \mathbb{C}^{N_{ris}\times 1}$could be adopted to obtain a proper design on $\boldsymbol{\Phi} = [\boldsymbol{\theta}_1, \ldots, \boldsymbol{\theta}_{N_{ris}}]$, where $\boldsymbol{\Phi} = diag(\boldsymbol{\vartheta})\mathbf{F}$ and $\mathbf{F}$ is the DFT matrix, which guarantees that the whole channel information in all directions can be estimated. Therefore, to compare with the imperfect phase shift, we assume that there exists a perfect phase shift that can be achieved in the MIMO system. In this case, the channel coefficient h in (4.23) is modified to

$$h = \sum_{i=1}^{N_{ris}} |h_{2,i}| \cdot |h_{1,i}|. \tag{4.32}$$

Note that the closed-form approximation of the h's PDF can be evaluated as

$$p_h(x) = \frac{x^a}{b^{a+1}\Gamma(a+1)} \exp\big(-\frac{x}{b}\big), \tag{4.33}$$

where $a = \frac{z_1^2}{z_2} - 1$ and $b = \frac{z_2}{z_1}$ with $z_1 = \frac{N_{ris}\pi}{4}$ and $z_2 = N_{ris}(1-\frac{\pi^2}{16})$. Substituting (4.33) into the closed forms of the mutual information and the unconditional variance

(4.27) and (4.28), we have

$$I(X;Y) \approx t\log|\mathcal{A}| - \sum_{k=1}\Delta_{h_k}\frac{1}{b^{a+1}\Gamma(a+1)}h_k^a\exp\big(-\frac{h_k}{b}\big)\cdot \tag{4.34}$$
$$\frac{1}{|\mathcal{A}|^t}\sum_{i=1}^{|\mathcal{A}|^t}\log\Big[\sum_{i'=1}^{|\mathcal{A}|^t}\exp\Big\{-\frac{\big\|h_k(\mathbf{x}_i-\mathbf{x}_{i'})\big\|^2}{2(3-\exp\{-\big\|h_k(\mathbf{x}_i-\mathbf{x}_{i'})\big\|^2/8\})}\Big\}\Big]$$
$$U(X;Y) \approx -[I(X;Y)-(t\log|\mathcal{A}|)]^2 + \sum_{k=1}\Delta_{h_k}\frac{1}{b^{a+1}\Gamma(a+1)}h_k^a\exp\big(-\frac{h_k}{b}\big)\cdot \tag{4.35}$$
$$\frac{1}{|\mathcal{A}|^t}\sum_{i=1}^{|\mathcal{A}|^t}\log^2\Big[\sum_{i'=1}^{|\mathcal{A}|^t}\exp\Big\{-\frac{\big\|h_k(\mathbf{x}_i-\mathbf{x}_{i'})\big\|^2}{2(6-\exp\{-\big\|h_k(\mathbf{x}_i-\mathbf{x}_{i'})\big\|^2/8\})}\Big\}\Big].$$

Therefore, we substitute (4.34) and (4.35) into (4.4) to obtain our achievability and converse bounds for the perfect phase alignment-Rayleigh fading channel.

4.4.2 Rician Fading Channel

In this subsection, we consider the Rician fading channel. Specially, we assume the channel coefficient $|h_1|$ in (4.23) follows the Rician distribution which is $|h_1| \sim$ Rician(α_1, β_1). The PDF of which is given by

$$p_{|h_1|}(x) = \frac{x}{\alpha_1^2}\exp\big(-\frac{x^2+\beta_1^2}{2\alpha_1^2}\big)I_0(\frac{\beta_1 x}{\alpha_1^2}), \tag{4.36}$$

where the shape parameter of the Rician fading $K_1 = \frac{\beta_1^2}{2\alpha_1^2}$ denotes the ratio of the power contributions by line-of-sight path to the remaining multipaths, and the scale parameter of the Rician fading $\Omega = 2\alpha_1^2 + \beta_1^2$ is the total power received in all paths. We assume that the PDF of $|h_2|$ in (4.23) is also Rician distribution which is $|h_2| \sim$ Rician(α_2, β_2).

Note that we change the distribution of entries in (4.2) from the Rayleigh distribution to the Rician distribution, then the process is similar to the Rayleigh part which is omitted for simplicity. We have the PDF of $|h|$ as

$$p_{|h|}(x) = \frac{2x}{N_{ris}(1+K_1)(1+K_2)}\exp\big(-\frac{x^2}{N_{ris}(1+K_1)(1+K_2)}\big). \tag{4.37}$$

Substituting (4.37) into the closed forms of the mutual information and the unconditional variance (4.27) and (4.28), we have

$$I(X;Y) \approx t\log|\mathcal{A}| - \sum_{k=1}\Delta_{h_k}\frac{2h_k}{N_{ris}(1+K_1)(1+K_2)}\exp\big(-\frac{h_k^2}{N_{ris}(1+K_1)(1+K_2)}\big)\cdot \frac{1}{|\mathcal{A}|^t}\sum_{i=1}^{|\mathcal{A}|^t}\log\Big[\sum_{i'=1}^{|\mathcal{A}|^t}\exp\Big\{-\frac{\big\|h_k(\mathbf{x}_i-\mathbf{x}_{i'})\big\|^2}{2(3-\exp\{-\big\|h_k(\mathbf{x}_i-\mathbf{x}_{i'})\big\|^2/8\})}\Big\}\Big] \quad (4.38)$$

$$U(X;Y) \approx -[I(X;Y)-(t\log|\mathcal{A}|)]^2 + \sum_{k=1}\Delta_{h_k}\frac{2h_k}{N_{ris}(1+K_1)(1+K_2)}\cdot \exp\big(-\frac{h_k^2}{N_{ris}(1+K_1)(1+K_2)}\big)\frac{1}{|\mathcal{A}|^t}\sum_{i=1}^{|\mathcal{A}|^t}\log^2\Big[\sum_{i'=1}^{|\mathcal{A}|^t} \exp\Big\{-\frac{\big\|h_k(\mathbf{x}_i-\mathbf{x}_{i'})\big\|^2}{2(6-\exp\{-\big\|h_k(\mathbf{x}_i-\mathbf{x}_{i'})\big\|^2/8\})}\Big\}\Big]. \quad (4.39)$$

Therefore, we substitute (4.38) and (4.39) into (4.4) to obtain our achievability and converse bounds for the Rician fading channel.

4.4.3 Perfect Phase Alignment-Rician Fading Channel

In this subsection, we consider perfect phase alignment case with the Rician fading channel. In this case, the channel coefficient h in (4.32) is given by

$$h = \sum_{i=1}^{N_{ris}}|h_{2,i}|\cdot|h_{1,i}|. \quad (4.40)$$

where $|h_1| \sim \text{Rician}(\alpha_1,\beta_1)$ and $|h_2| \sim \text{Rician}(\alpha_2,\beta_2)$, respectively. Note that the closed form approximation of PDF of the channel coefficient h can be evaluated as

$$p_h(x) = \frac{x^a}{b^{a+1}\Gamma(a+1)}\exp\big(-\frac{x}{b}\big), \quad (4.41)$$

where $a = \frac{z_1^2}{z_2} - 1$ and $b = \frac{z_2}{z_1}$ with $z_1 = N_{ris}(\frac{\pi}{4}L_{1/2}(-K_1)L_{1/2}(-K_2))$ and $z_2 = N_{ris}((1+K_1)(1+K_2) - \frac{\pi^2}{16}L_{1/2}^2(-K_1)L_{1/2}^2(-K_2))$, where $L_q(\cdot)$ denotes a Laguerre

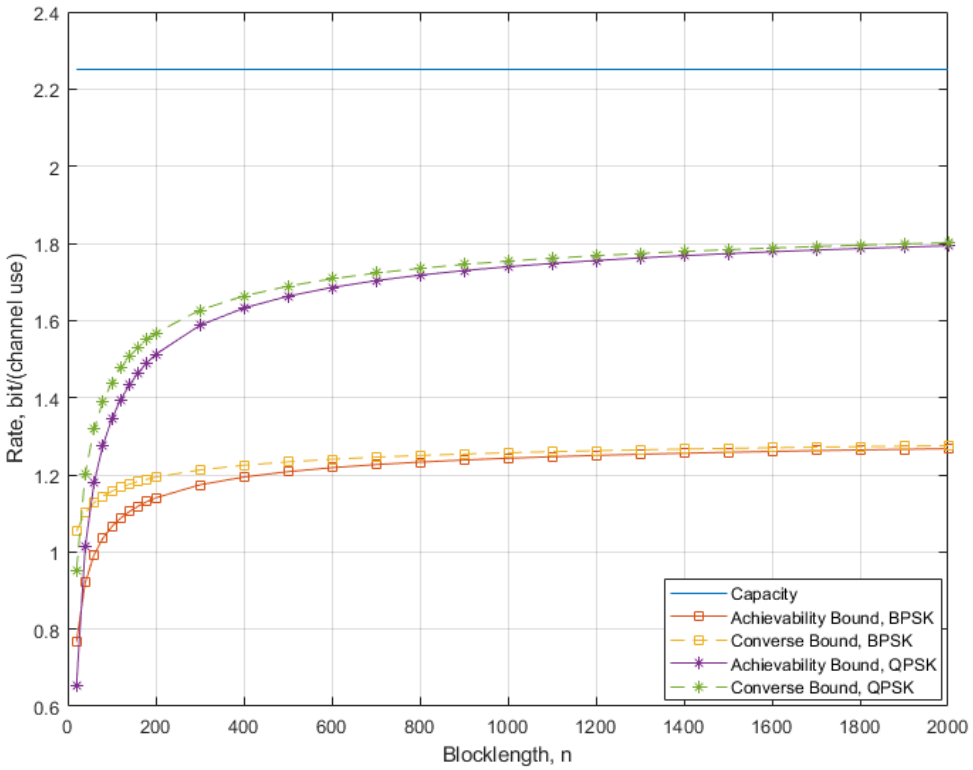

Figure 4.2: Achievability and converse bounds for (n, M, ϵ) codes for an RIS MIMO system over a Rayleigh fading channel and transmit antennas $t = 2$ and receive antennas $r = 2$, $N_{ris} = 16$ and SNR=$-$10dB for $\epsilon = 10^{-3}$ and with BPSK and QPSK modulation, repectively.

polynomial. Substituting (4.33) into the closed forms of the mutual information and the unconditional variance (4.27) and (4.28), we have the same equations as (4.34) and (4.35) with different values of z_1 and z_2. Therefore, we substitute the above mutual information and unconditional variance into (4.4) to obtain our achievability and converse bounds for the perfect phase alignment-Rician fading channel.

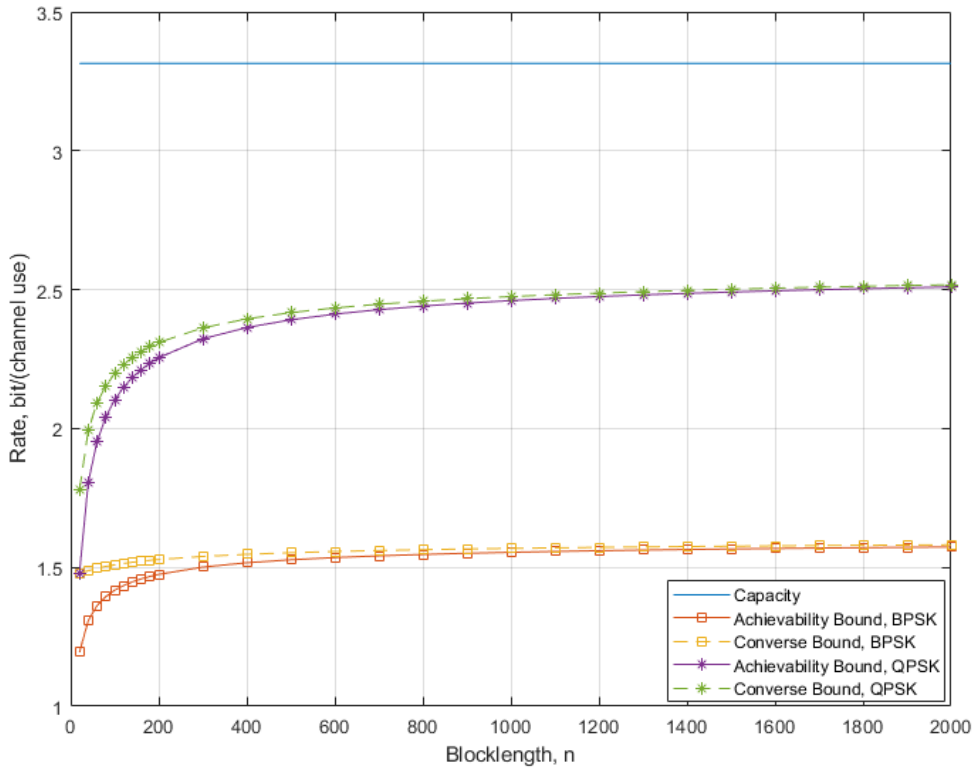

Figure 4.3: Achievability and converse bounds for (n, M, ϵ) codes for an RIS MIMO system over a Rayleigh fading channel and transmit antennas $t = 2$ and receive antennas $r = 2$, $N_{ris} = 32$ and SNR=$-$10dB for $\epsilon = 10^{-3}$ and with BPSK and QPSK modulation, repectively.

4.5 Simulation Results

4.5.1 Evaluation of the Derived Bounds

In this section, we consider an RIS MIMO system consisting of multiple transmitter antennas, a rectangular RIS of N_{ris} elements and multiple receive antennas. We assume all the channels, i.e., the channels between the transmitter and the RIS, the RIS and the receiver, and the transmitter and the receiver, are independent with the maximal error probability $\epsilon = 10^{-3}$. Assuming that all the channels are Rayleigh fading channels, the number of the transmit and receive antennas are

$t = 2$ and $r = 2$, respectively, and the SNR is -10 dB, Figs. 4.2 and 4.3 show the numerical results of the derived bounds with BPSK and QPSK modulated signals and the capacity for $N_{ris} = 16$ and 32, respectively. From Fig. 4.2, we can see that $C_{Gaussian} = 2.2509$ bit/(channel use), which is calculated based on Theorem 8, and the maximal achievable rate for the BPSK modulated signal is 1.3283 bit/(channel use) from (4.27). The required blocklength n to achieve above 80% and 90% of its maximal achievable rate starts at $n = 100$ and $n = 400$, respectively. With the QPSK modulation, the required blocklengths are $n = 240$ and $n = 940$, respectively. In Fig. 4.3, we only change the RIS element from $N_{ris} = 16$ to 32. The capacity is 3.3145 bit/(channel use), and the required blocklengths decrease dramatically to 40 and 160, respectively. For QPSK modulation, the required blocklengths are $n = 100$, and $n = 400$, respectively.

The channel variance can be treated as the unconditional information variance $U(X;Y)$ in (4.28). It shows how quickly the performance converges to the maximal achievable rate as blocklength n grows. When $\epsilon > Q(\frac{(m+1)\log n}{2n\sqrt{(\frac{U(X;Y)}{n})}})$, the converse bound will first decrease and then converge to its achievability part, while $0 < \epsilon < Q(\frac{(m+1)\log n}{2n\sqrt{(\frac{U(X;Y)}{n})}})$, the converse bound will be monotonic increasing along with the increase of the blocklength. Additionally, if the target is to transmit at a fraction of the maximal achievable rate $0 < \eta < 1$ with a maximal error probability ϵ, the relationship between the required blocklength n and the channel variance is $n \approx \frac{U(X;Y)}{(I(X;Y))^2}\left(\frac{Q^{-1}(\epsilon)}{1-\eta}\right)^2$.

The performance of the 2×2 MIMO case over different channels, i.e., perfect phase alignment Rayleigh fading channel in Section 4.4.1, Rician fading channel in Section 4.4.2 and perfect phase alignment Rician fading channel in Section 4.4.3, in terms of the required blocklength, with the different number of RIS elements and different SNR level are summarized in Table 4.1. Moreover, the gap between the

Table 4.1: Required blocklengths to achieve 80% and 90% of the maximal achievable rate for an RIS MIMO system over different channels and transmit antennas $t = 2$ and receive antennas $r = 2$, $\epsilon = 10^{-3}$.

	80%				90%			
	$N_{ris} = 16$		$N_{ris} = 32$		$N_{ris} = 16$		$N_{ris} = 32$	
	BPSK	QPSK	BPSK	QPSK	BPSK	QPSK	BPSK	QPSK
Perfect phase alignment-Rayleigh fading channel[1]	80	220	20	40	360	860	80	140
Rician fading channel[2]	180	380	80	180	720	1560	300	720
Perfect phase alignment-Rician fading channel[3]	100	220	20	40	400	920	10	140

[1] The SNR=−20 dB. [2] The SNR=−30 dB. [3] The SNR=−40 dB.

two bounds and the maximal achievable rate of the 2×2 MIMO case over different channels with a specific number of RIS elements $N_{ris} = 16$, a given maximal error probability $\epsilon = 10^{-3}$, and the blocklength $n = 256$ are summarized in Table 4.2. From Figs. 4.2 and 4.3 and Tables 4.1 and 4.2, we can conclude that: 1) as N_{ris} increases, the overall channel between the transmitter and the receiver becomes better. That means that the gap between the maximal achievable rate for different modulation schemes and the capacity increases and vice versa at the same SNR level; 2) the required blocklength n falls significantly to achieve a given fraction of the maximal achievable rate as the number of RIS elements increases.

In Figs. 4.4-4.7, we demonstrate the performance of the 3×3 MIMO case over the four different channels. From these figures, we observe that: 1) the Rician fading channel is much better than the Rayleigh fading channel regardless of whether it is perfect phase alignment or not; 2) when N_{ris} increases, the RIS element's effect on the QPSK modulated signal is more significant than that on the BPSK modulated

Table 4.2: The gap between the achievability and converse bounds and the maximal achievable rate for an RIS MIMO system over different channels and the number of RIS elements $N_{ris} = 16$, transmit antennas $t = 2$ and receive antennas $r = 2$, $\epsilon = 10^{-3}$, and the blocklength $n = 256$.

	Maximal achievable rate		Gap to the achievability bound		Gap to the converse bound	
	BPSK	QPSK	BPSK	QPSK	BPSK	QPSK
Rayleigh fading channel[1]	1.3283	1.9254	0.3042	0.5204	0.2613	0.4774
Perfect phase alignment-Rayleigh fading channel[2]	1.3435	1.9843	0.3028	0.5246	0.2599	0.4816
Rician fading channel[3]	1.0945	1.4743	0.2774	0.4598	0.2345	0.4169
Perfect phase alignment-Rician fading channel[4]	1.2865	1.8978	0.2942	0.5122	0.2513	0.4693

[1] The SNR=−10 dB. [2] The SNR=−20 dB. [3] The SNR=−30 dB. [4] The SNR=−40 dB.

signal; 3) to achieve the same performance, the required SNR for the channel with perfect phase alignment is approximately 20 dB smaller than the one without perfect phase alignment.

To validate our results, we transform the achievability and converse bounds in Theorem 7 to the lower and upper bounds on the average error probability. From Theorem 7, We have the achievability and converse bounds on maximal error probability. Since there always exists an (n, M, ϵ)-code in the maximal error probability ϵ that guarantees the existence of an (n, M', ϵ')-code in the average error probability ϵ', for any $\epsilon' < \epsilon < 1$ and $0 < \xi < 1$, where $M' = 2^{nR/(1-\xi)}$ and $\epsilon' = \xi\epsilon$. From (4.4), we have $I(X;Y) - \sqrt{U(X;Y)/n}Q^{-1}(\epsilon) + \mathcal{O}(n^{-3/2}) \leq R \leq I(X;Y) - \sqrt{U(X;Y)/n}Q^{-1}(\epsilon) + (m+1)\log n/(2n) + \mathcal{O}(n^{-3/2})$. Therefore, we obtain the lower and upper bounds on the average error probability, i.e., ϵ', which is shown below.

$$\xi Q\Big(\frac{I(X;Y) + \frac{m+1}{2}\frac{\log n}{n} - R(1-\xi)}{\sqrt{\frac{U(X;Y)}{n}}}\Big) \leq \epsilon' \leq \xi Q\Big(\frac{I(X;Y) - R(1-\xi)}{\sqrt{\frac{U(X;Y)}{n}}}\Big).$$

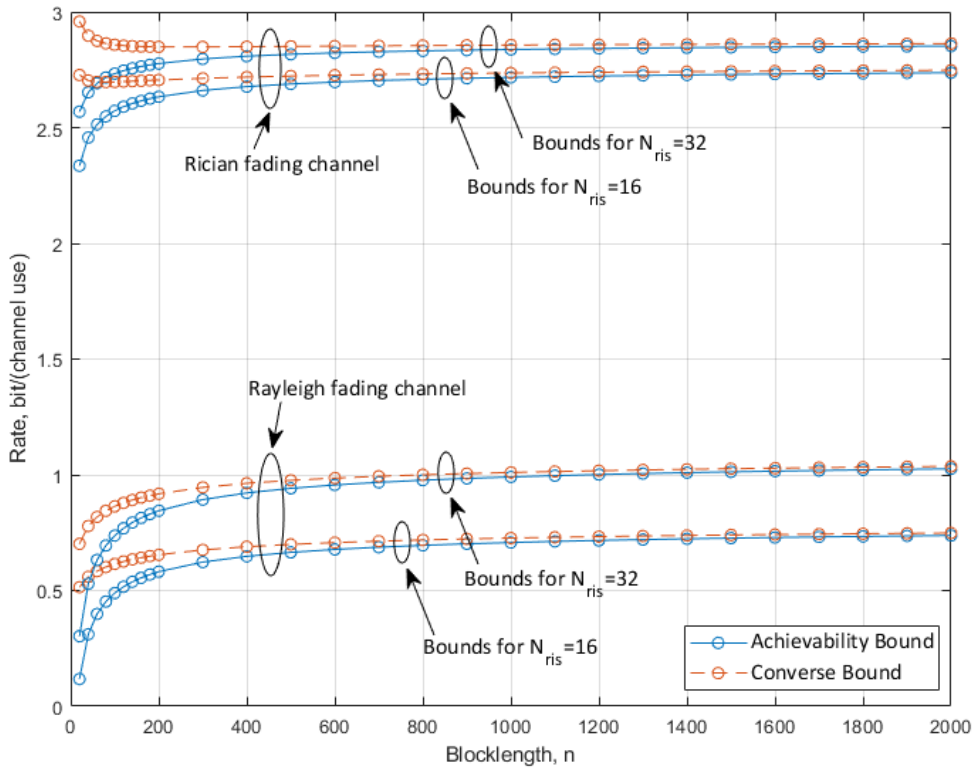

Figure 4.4: The comparison of achievability and converse bounds between Rayleigh fading channel, Rician fading channel whose two shape parameters are $K_1 = 10$ and $K_2 = 5$ respectively and transmit antennas $t = 3$ and receive antennas $r = 3$ for $\epsilon = 10^{-3}$ and SNR$= -20$ dB with BPSK modulation and $N_{ris} = 16$ and $N_{ris} = 32$, respectively.

By utilizing the polar code with a successive cancellation list (SCL) decoder and the extended BCH code with an ordered statistic decoder (OSD), we validate our derived results. In Fig. 4.8, we set the number of RIS elements $N_{ris} = 16$, the number of the transmitter and receiver antennas to 2, the modulation scheme to BPSK, the coding rate $R = 0.5$, and the blocklength $n = 128$. All the simulations are averaged over 10^6 Monte Carlo realizations. We choose two coding methods: one is the $(128, 2^{64}, \epsilon')$-polar code with SCL decoder (the list size is $L = 32$), and the other is the $(128, 2^{64}, \epsilon')$-EBCH code with OSD decoder (the order is chosen

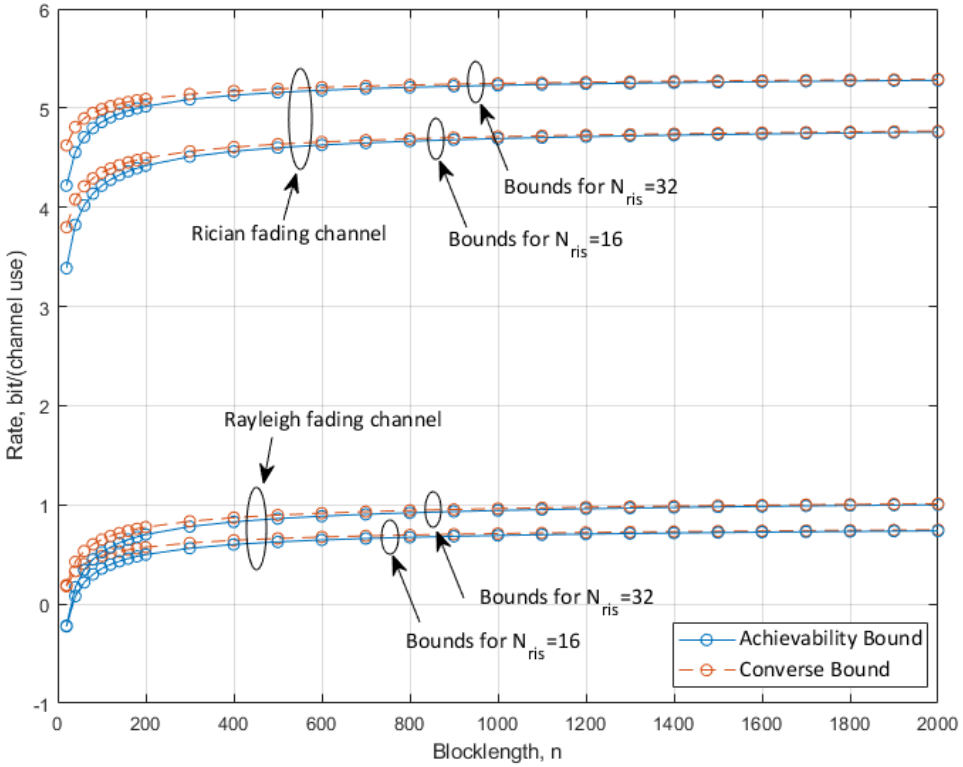

Figure 4.5: The comparison of achievability and converse bounds between Rayleigh fading channel, Rician fading channel whose two shape parameters are $K_1 = 10$ and $K_2 = 5$ respectively and transmit antennas $t = 3$ and receive antennas $r = 3$ for $\epsilon = 10^{-3}$ and SNR$= -20$ dB with QPSK modulation and $N_{ris} = 16$ and $N_{ris} = 32$, respectively.

to 4). We observe that the simulation result of the EBCH code is slightly better than the one of the polar code at the blocklength $n = 128$. Furthermore, as long as the simulation results are below the upper bound, they would validate our derived results. In Fig. 4.9, we change the number of the transmitter and receiver antennas to 3, and the rest parameters remain the same as in Fig. 4.8. At first, we compare the performance of two codes in different MIMO systems, i.e., 2×2 MIMO and 3×3 MIMO systems. At the same EbNo level of -14 dB, the average error probability drops from 0.3248 to 0.0607 for the EBCH code and from 0.4441 to 0.0754 for the

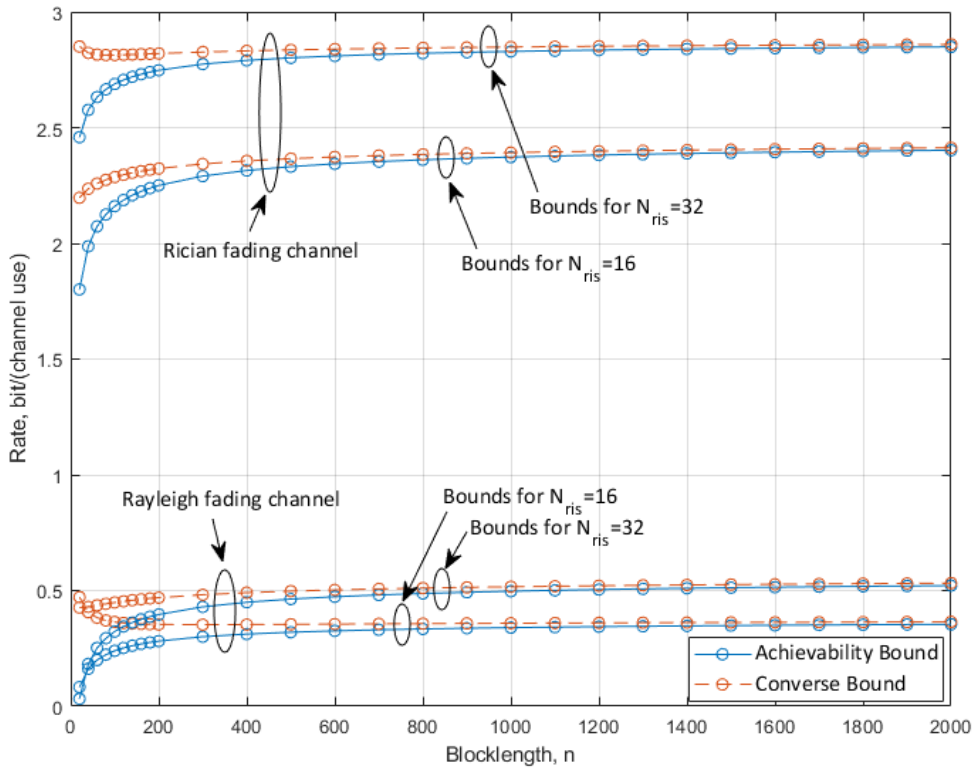

Figure 4.6: The comparison of achievability and converse bounds between Rayleigh fading channel with perfect phase alignment, Rician fading channel with perfect phase alignment whose two shape parameters are $K_1 = 10$ and $K_2 = 5$ and transmit antennas $t = 3$ and receive antennas $r = 3$ for $\epsilon = 10^{-3}$ and SNR$= -40$ dB with BPSK modulation and $N_{ris} = 16$ and $N_{ris} = 32$, respectively.

polar code. At the same average error probability level of 10^{-2}, the gaps between the simulation result and the lower bound are 2 dB and 2.5 dB for the EBCH code and polar code, respectively. We observe that the gaps increase to 2.5 dB and 3 dB for the EBCH code and the polar code. The performance of bounds over the 3×3 MIMO system is better than that over the 2×2 MIMO system.

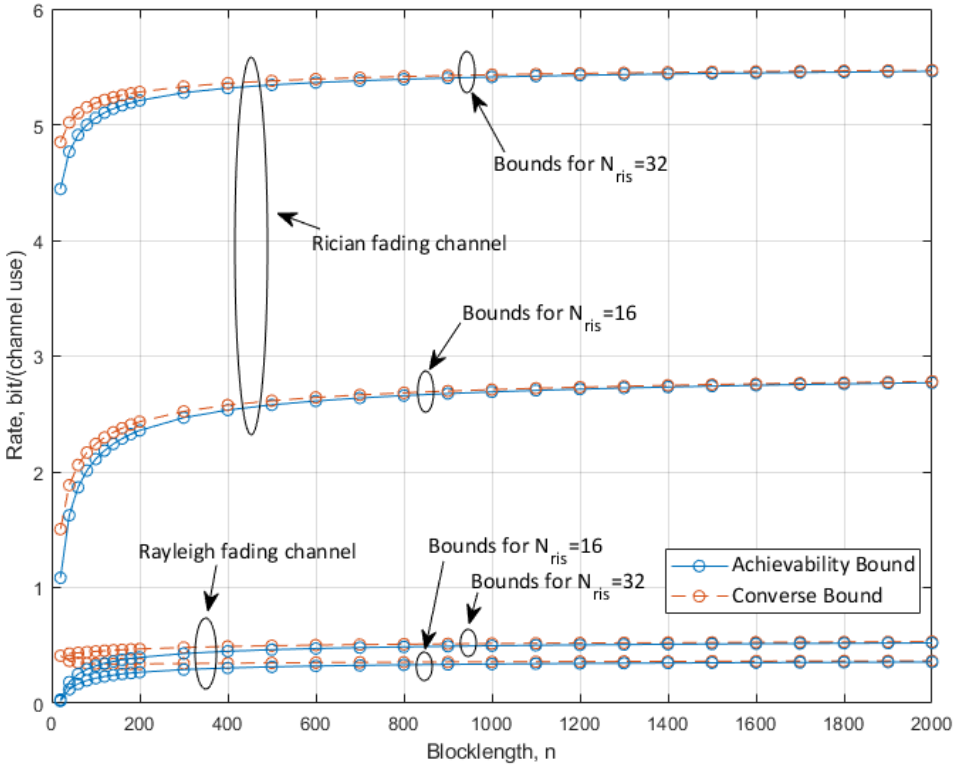

Figure 4.7: The comparison of achievability and converse bounds between Rayleigh fading channel with perfect phase alignment, Rician fading channel with perfect phase alignment whose two shape parameters are $K_1 = 10$ and $K_2 = 5$ and transmit antennas $t = 3$ and receive antennas $r = 3$ for $\epsilon = 10^{-3}$ and SNR$= -40$ dB with QPSK modulation and $N_{ris} = 16$ and $N_{ris} = 32$, respectively.

4.5.2 Rate vs SNR

In Figs. 4.10 and 4.11, we illustrate the capacity, the maximal achievable rate of QPSK and BPSK modulated signals over Rayleigh fading channel with the different number of RIS elements $N_{ris} = 4$ and 32 and different transmit antennas $t = 2$ and 3, respectively. Fig. 4.10 shows the tightness of the mutual information in Lemma 2. Moreover, it shows that the capacity achieved by circularly symmetric complex Gaussian inputs increases without any boundary as the SNR increases, and the gaps between the Gaussian input and the different modulated signals increase as the SNR

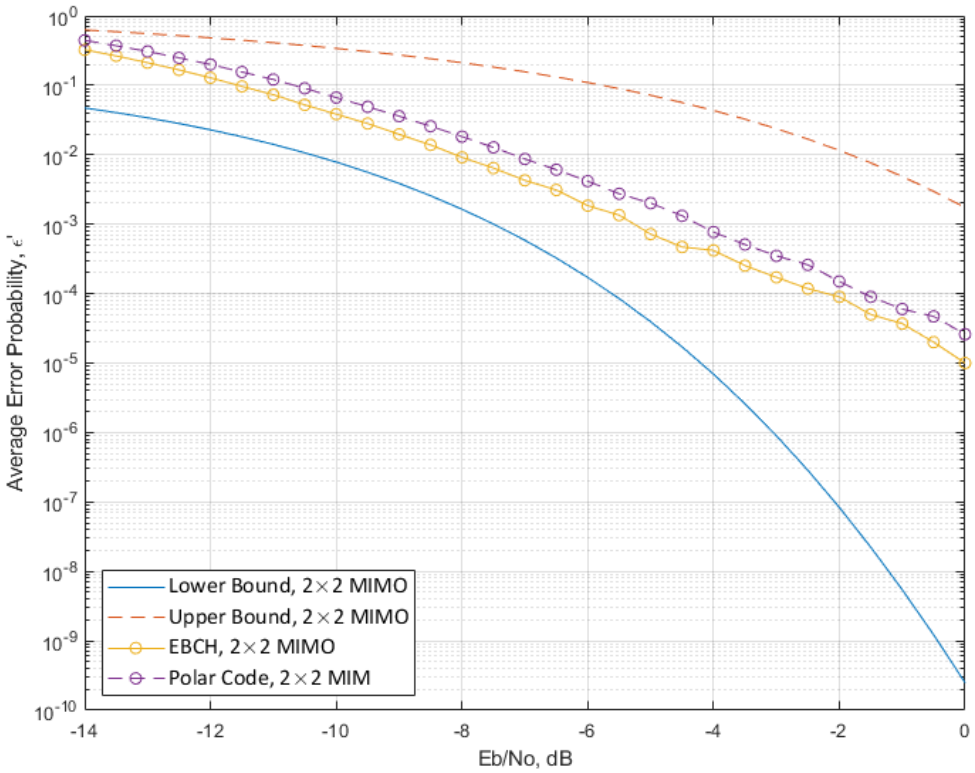

Figure 4.8: The lower and upper bounds for $(128, 2^{64}, \epsilon')$ codes for the RIS MIMO system over a Rayleigh fading channel, the number of RIS elements $N_{ris} = 16$, and the BPSK modulation scheme with the number of antennas $t = r = 2$ and $t = r = 3$, respectively.

increases. In Fig. 4.11, we change the number of the transmit antennas to $t = 2$ and choose $N_{ris} = 4$ and 32. As SNR increases, there exists a limit of the achievable rate for each modulation scheme and the number of transmitter and receiver antennas, i.e., for 2×1 MIMO with BPSK modulation, the limit $t \log |\mathcal{A}| = 2$ and for 3×1 MIMO with QPSK modulation, the limit $t \log |\mathcal{A}| = 6$. Moreover, the effect of the number of RIS elements on the achievable rate is that the speed approaching the limit increases as the number of RIS elements increases.

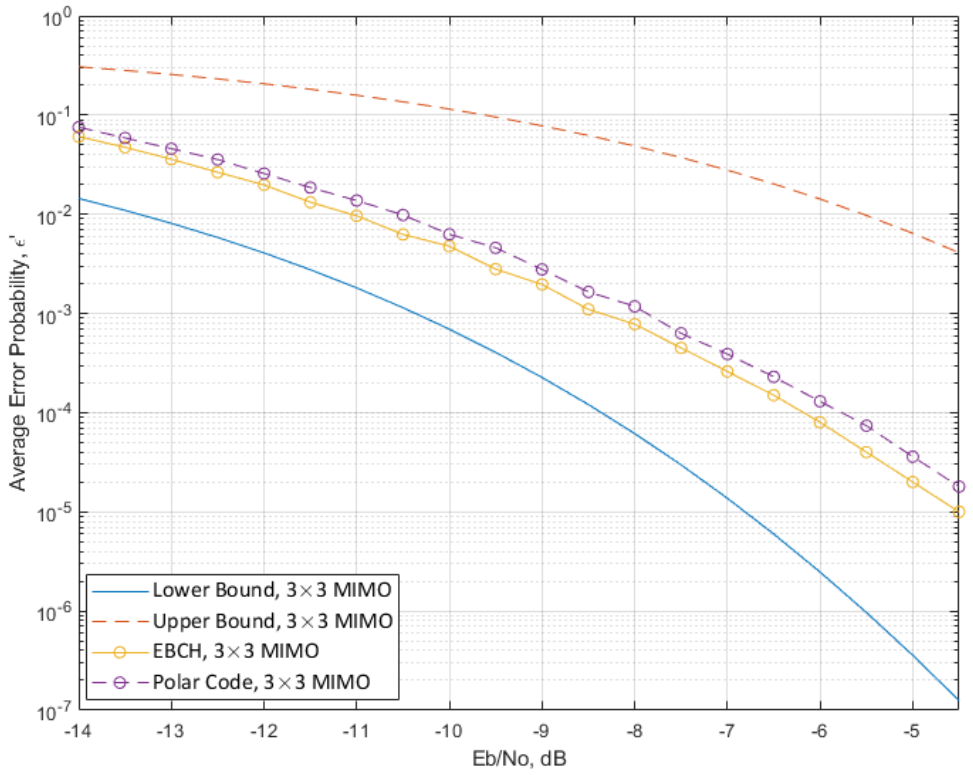

Figure 4.9: The lower and upper bounds for $(128, 2^{64}, \epsilon')$ codes for the RIS MIMO system over a Rayleigh fading channel, the number of RIS elements $N_{ris} = 16$, and the QPSK modulation scheme with the number of antennas $t = r = 2$ and $t = r = 3$, respectively.

4.6 Summary

In this chapter, we have established achievability and converse bounds on the maximal achievable rate R at a given blocklength n and a maximal error probability ϵ for an RIS MIMO system. The analytical results demonstrated that the number of transmit and receive antennas and the channel variance $U(X;Y)$ would affect the convergence speed to the maximal achievable rate as the blocklength n increases. For the future work, we will investigate our derived results into the new surfaces, such as the intelligent omni-surface [57].

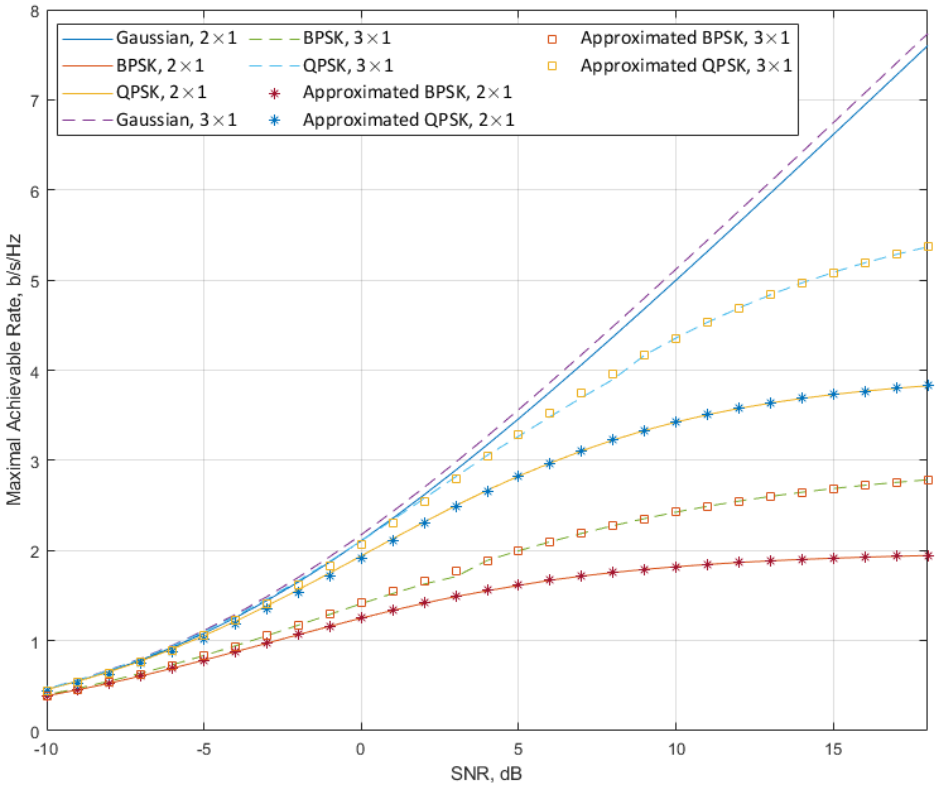

Figure 4.10: The maximal rate achieved by Gaussian inputs, QPSK, and BPSK for an RIS MIMO system over a Rayleigh fading channel with the number of RIS elements $N_{ris} = 4$, and single receive antennas $r = 1$ with $t = 2$ and $t = 3$, respectively.

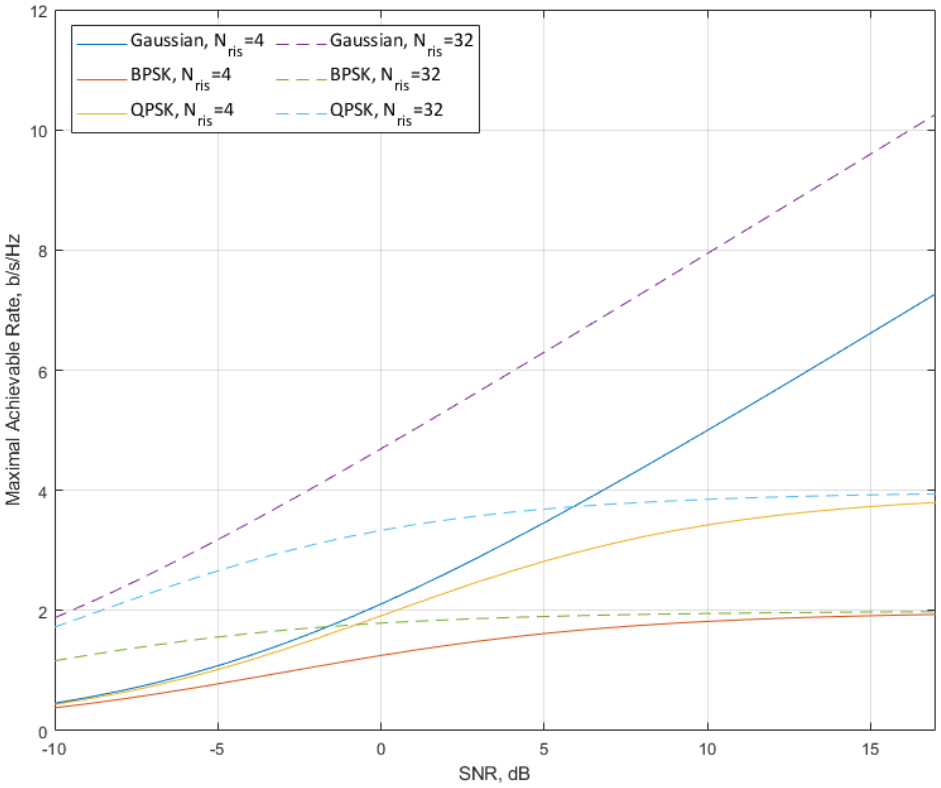

Figure 4.11: The maximal rate achieved by Gaussian inputs, QPSK, and BPSK for an RIS MIMO system over a Rayleigh fading channel and single receive antennas $r = 1$ and $t = 2$ with the number of RIS elements $N_{ris} = 4$, and $N_{ris} = 32$, respectively.

Chapter 5

Performance Analysis of Multiple-Antenna Ambient Backscatter Systems at Finite Blocklengths

5.1 Introduction

In this chapter, we use the Berry-Esseen theorem as a fundamental basis to provide achievability and converse bounds on the achievable rate R for a legacy system with multiple transmit and receive antennas. For our achievability bound, we utilize the Berry-Esseen theorem, the mutual information, and the information variance under the condition of the probability of the tag symbol to get the bound. Furthermore, we exploit the Mellin transform and Meijer G-function to obtain a maximum on the auxiliary channel's probability density function (PDF), a product of m copies of PDF of Gamma distributed variables. Then, we apply the Lebesgue measure to

get the maximum of its output space. To complete our achievability and converse bounds, we utilize the different modulation schemes in our legacy system.

To reduce the complexity of multiple integrals for deriving the mutual information and the information variance, we use the saddle point approximation and the Taylor expansion to obtain closed-form expressions of the mutual information and the information variance.

We apply a low-complexity ML detection to compute the average error probability of the tag symbol based on the received signal and estimated RF source signal for a variety of transmitter and receiver antennas. We determine the relationship between the average error probability of the tag symbol and the maximal error probability of the RF source signal as a function of the blocklength n and the number of transmitter and receiver antennas t and r. We utilize different modulation schemes, i.e., BPSK and QPSK, and different coding methods, i.e., the EBCH code and the polar code, in our legacy system and AmBC system to validate the derived bounds and the error probability of the tag symbol.

5.2 System Model

Let us consider input and output sets $\mathcal{A}^n$, $\mathcal{D}$ and $\mathcal{B}^n$, $\hat{\mathcal{D}}$ and the conditional probability measures $P_{Y|X} : \mathcal{A}^n \mapsto \mathcal{B}^n$, and $P_{\hat{d}|d} : \hat{\mathcal{D}} \mapsto \mathcal{D}$. We denote an RF source's codebook with M codewords by $(c_1, \ldots, c_M)$. An RF source signal decoder, which is defined as a random transformation $P_{Z|Y} : \mathcal{B}^n \mapsto \{1, \ldots, M\}$, satisfies a maximal error probability of the RF source signal as follows:

$$P_{Z|\mathbf{X}}(i|\mathbf{C}_i) \geq 1 - \epsilon_{source}, \quad i = 1, \ldots, M \tag{5.1}$$

where ϵ_{source} is the maximal error probability of the RF source signal. Additionally, a tag symbol decoder, which is a random transformation $P_{\hat{d}|d}$, satisfies an error

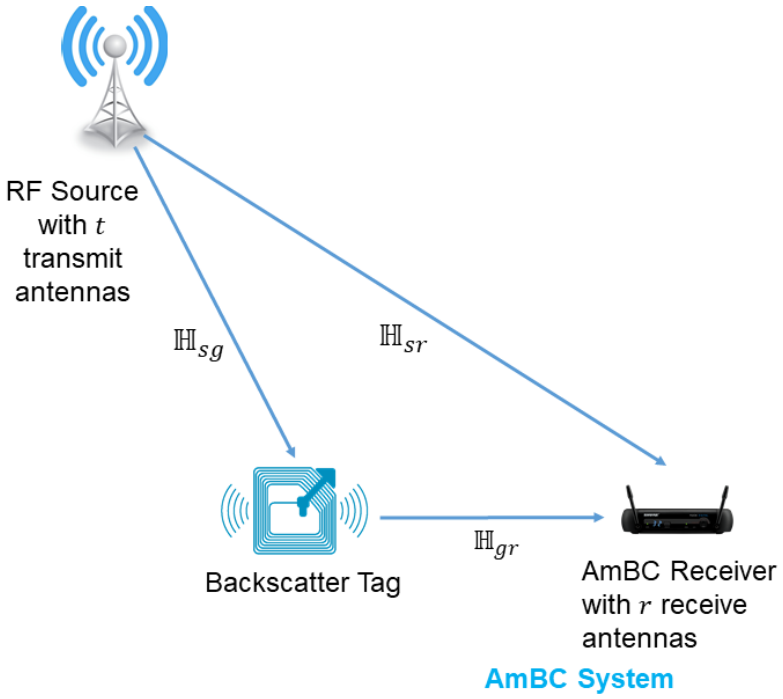

Figure 5.1: System model for ambient backscatter communications.

probability of the tag symbol as follows:

$$\epsilon_{tag} = 1 - \frac{1}{|\mathcal{D}|} \sum_{i=0}^{|\mathcal{D}|-1} P_{\hat{d}|d}(\hat{d}_i|d_i), \tag{5.2}$$

where $\hat{d}_i \in \mathcal{D}$ and $d_i \in \mathcal{D}$, and ϵ_{tag} is the error probability of the tag symbol. The RF source's codebook and decoder whose maximal error probability is smaller than ϵ_{source} are called an $(n, M, \epsilon_{source})$ code and its corresponding coding rate is defined as $R = \frac{\log M}{n}$.

We consider an AmBC MIMO system with one RF source, one receiver and one backscatter tag with no battery as depicted in Fig. 5.1. In the legacy system, the RF source and the receiver have t and r antennas, respectively and the tag has a single antenna. We let $m \triangleq \min(t, r)$ and denote by $\mathbf{H}_{sg}$, $\mathbf{H}_{gr}$ and $\mathbf{H}_{sr}$ the channel coefficient matrices between the RF source and tag, the tag and receiver, the RF source and receiver, respectively. We have $\mathbf{H}_{sg} \in \mathbb{C}^{t\times 1}, \mathbf{H}_{gr} \in \mathbb{C}^{1\times r}, \mathbf{H}_{sr} \in \mathbb{C}^{t\times r}$ [58].

A part of the tag received signal will be harvested to power the circuit of the

tag, the rest would be backscattered to accomplish "0" and " + 1" transmission. Without loss of generality, we assume that the tag symbol remains unchanged for one block data transmission from the RF source. We denote the tag symbol as $d_0, d_1 \in \mathcal{D}$, where $\mathcal{D} = \{0, +1\}$. The AmBC receiver receives both the RF source and tag symbol. Suppose the time delay between the RF source and the tag is negligible. Then, the received signal $\mathbf{Y}$ can be expressed by

$$\mathbf{Y} = \mathbf{X}(\mathbf{H}_{sr} + \mathbf{H}_{sg}\mathbf{H}_{gr}Ad) + \mathbf{W}, \tag{5.3}$$

where $\mathbf{X} \in \mathbb{C}^{n\times t}$ is the signal transmitted over n channel uses; $\mathbf{Y} \in \mathbb{C}^{n\times r}$ is the corresponding received signal; channel coefficients $\mathbf{H}_{sg}$, $\mathbf{H}_{gr}$ and $\mathbf{H}_{sr}$ are random but remain constant over the n channel uses [59] [19]. $\mathbf{W} \in \mathbb{C}^{n\times r}$ is the additive noise at the receiver, which is independent of $\mathbf{H}_{sg}$, $\mathbf{H}_{gr}$ and $\mathbf{H}_{sr}$ and has i.i.d. $\mathcal{CN}(0, 1)$ entries; A is the scattering efficiency of the tag and since the tag only contains passive components, therefore the thermal noise at the tag is negligible.

Now let us denote $\mathbf{H}_0 = \mathbf{H}_{sr}$ and $\mathbf{H}_1 = \mathbf{H}_{sr} + A\mathbf{H}_{sg}\mathbf{H}_{gr}$, then (5.3) can be written as

$$\mathbf{Y} = \begin{cases} \mathbf{X}\mathbf{H}_0 + \mathbf{W}, & d = 0, \\ \mathbf{X}\mathbf{H}_1 + \mathbf{W}, & d = +1. \end{cases} \tag{5.4}$$

5.3 Performance Analysis

In this section, we provide the definitions of achievability and converse bounds. The achievability and converse bounds are essential to the proof of the channel coding theorem. The achievability bound is a lower bound on the size of a code that can be guaranteed to exist with a given arbitrary blocklength and error probability. The converse bound is an upper bound on the size of any code with a given arbitrary blocklength and error probability. Moreover, compared with the original work

in [17], our achievability and converse bounds examine the legacy MIMO system with finite alphabet constraints, i.e., BPSK and QPSK modulated signal. Due to the high complexity of multiple integrals in the calculation, we obtain the closed-form expression by applying the saddle point approximation to let our bounds have practical implementation. Furthermore, in the second subsection, we examine the relation between the error probability of the RF source signal, ϵ_{source}, and the error probability of the tag symbol, ϵ_{tag}, with respect to the blocklength n. Combining our derived bounds and the relation between ϵ_{source} and ϵ_{tag}, we would find an $(n, M, \epsilon_{source})$ code to achieve a specific level of ϵ_{tag}.

5.3.1 Achievability and Converse Bounds

In this subsection, our achievability and converse bounds for the legacy MIMO system are presented below.

Theorem 9. *We consider a communication system having the finite input alphabet $\mathcal{A}$ and $\mathcal{D}$, and the continuous output alphabet $\mathcal{B}$. Let $p(\mathbf{Y}, \mathbf{H}|\mathbf{X})$ be the corresponding conditional PDF on $\mathcal{B}$ for all $\mathbf{X} \in \mathcal{A}$, where $\mathbf{H}$ is a channel matrix. The input distribution $P(\mathbf{X}) \triangleq [\mathbf{q}_0, \ldots, \mathbf{q}_t]^T$, where $\mathbf{q}_i = [q_{i,0}, \ldots, q_{i,|\mathcal{A}|}]$ is equiprobable.*

Thus for the legacy MIMO channel and arbitrary $0 < \epsilon_{source} < 1$, we have the achievability and converse bounds

$$I(X;Y|D) - \sqrt{\frac{U(X;Y|D)}{n}} Q^{-1}(\epsilon_{source}) + \mathcal{O}(n^{-3/2}) \leq R$$
$$\leq I(X;Y|D) - \sqrt{\frac{U(X;Y|D)}{n}} Q^{-1}(\epsilon_{source}) + \frac{m+1}{2}\frac{\log n}{n} + \mathcal{O}(n^{-3/2}). \quad (5.5)$$

where $I(X;Y|D)$ and $U(X;Y|D)$ denote the mutual information and the information variance with respect to D, respectively and Q is the complementary Gaussian cumulative distribution function $Q(x) = \int_x^\infty \frac{1}{\sqrt{2\pi}} \exp(-\frac{u^2}{2}) du$.

The proof of the achievability part of Theorem 9 can be found in Section 2.2.1 and the converse part can be found in Appendix A.

In order to apply Th. 9 in our system model, we make the assumption that the tag symbol d is predetermined. We then apply a two-step decoding process: the first step is to decode the received signal Y with the knowledge of d, and the second step is to decode the tag symbol d with the use of the decoded received signal. According to Section 5.2, we know that the set of d consists of two different values, which are "0" and " + 1", respectively. One way to obtain the mutual information $I(X;Y|D)$ and the information variance $U(X;Y|D)$ is by taking a weighted sum on the probability of occurrence of that particular value of d.

1. Case 1: when $d = 0$, we have

$$
\begin{aligned}
I(X;Y|d=0) \triangleq & \int_0^\infty \int_{-\infty}^\infty \sum_{\mathbf{X}\in\mathcal{A}^t} \big(P(\mathbf{X})p(\mathbf{Y},\mathbf{H}_0|\mathbf{X})\cdot \\
& \log\big\{\frac{p(\mathbf{Y},\mathbf{H}_0|\mathbf{X})}{\sum_{\mathbf{X}'\in\mathcal{A}^t} P(\mathbf{X}')p(\mathbf{Y},\mathbf{H}_0|\mathbf{X}')}\big\}\big) d\mathbf{Y} d\mathbf{H}_0 \\
= & \sum_{\mathbf{X}\in\mathcal{A}^t} \frac{q_{\mathbf{X}}}{det(\pi\mathbf{I}_r)} \underbrace{\int_0^\infty \cdots \int_0^\infty}_{\substack{\text{m-dimensions} \\ \text{(w.r.t. } \mathbf{h}_0\text{)}}} \underbrace{\int_{-\infty}^\infty \cdots \int_{-\infty}^\infty}_{\substack{\text{m-dimensions} \\ \text{(w.r.t. } \mathbf{y}\text{)}}} \prod_{i=0}^{m-1} p(\mathbf{h}_{0,i})\cdot \\
& \exp\{-\frac{1}{2}||\mathbf{y}_i - \mathbf{h}_{0,i}\mathbf{x}_i||^2\}\Big(- \log e \sum_{j=0}^{m-1} \frac{1}{2}||\mathbf{y}_j - \mathbf{h}_{0,i}\mathbf{x}_j||^2 \\
& - \log\big\{\sum_{k=0}^{m-1} \sum_{\mathbf{x}'_k\in\mathcal{A}} \mathbf{q}_k \exp\{-\frac{1}{2}||\mathbf{y}_k - \mathbf{h}_{0,k}\mathbf{x}'_k||^2\}\big\}\Big) d\mathbf{y} d\mathbf{h}_0 \qquad (5.6)
\end{aligned}
$$

and

$$
\begin{aligned}
U(X;Y|d=0) \triangleq & \int_0^{\infty}\int_{-\infty}^{\infty}\sum_{\mathbf{X}\in\mathcal{A}^t}\big(P(\mathbf{X})p(\mathbf{Y},\mathbf{H}_0|\mathbf{X})\cdot \\
& \log^2\big\{\frac{p(\mathbf{Y},\mathbf{H}_0|\mathbf{X})}{\sum_{\mathbf{X}'\in\mathcal{A}^t}P(\mathbf{X}')p(\mathbf{Y},\mathbf{H}_0|\mathbf{X}')}\big\}\big)d\mathbf{Y}d\mathbf{H}_0 \\
= & \sum_{\mathbf{X}\in\mathcal{A}^t}\frac{q_{\mathbf{X}}}{det(\pi\mathbf{I}_r)}\underbrace{\int_0^{\infty}\cdots\int_0^{\infty}}_{\substack{\text{m-dimensions}\\(\text{w.r.t. }\mathbf{h}_0)}}\underbrace{\int_{-\infty}^{\infty}\cdots\int_{-\infty}^{\infty}}_{\substack{\text{m-dimensions}\\(\text{w.r.t. }\mathbf{y})}}\prod_{i=0}^{m-1}p(\mathbf{h}_{0,i})\cdot \\
& \exp\{-\frac{1}{2}||\mathbf{y}_i-\mathbf{h}_{0,i}\mathbf{x}_i||^2\}\Big(-\log e\sum_{j=0}^{m-1}\frac{1}{2}||\mathbf{y}_j-\mathbf{h}_{0,i}\mathbf{x}_j||^2 \\
& -\log\big\{\sum_{k=0}^{m-1}\sum_{\mathbf{x}'_k\in\mathcal{A}}\mathbf{q}_k\exp\{-\frac{1}{2}||\mathbf{y}_k-\mathbf{h}_{0,k}\mathbf{x}'_k||^2\}\big\}\Big)^2 d\mathbf{y}d\mathbf{h}_0 \\
& -[I(X;Y)]^2, \qquad (5.7)
\end{aligned}
$$

where $P(\mathbf{X}) = [\mathbf{q}_0,\ldots,\mathbf{q}_t]^T$ denotes the input distribution, $\mathbf{q}_i = [\frac{1}{2},\frac{1}{2}]$ and $\mathbf{q}_i = [\frac{1}{4},\frac{1}{4},\frac{1}{4},\frac{1}{4}]$, for BPSK and QPSK respectively, and $p(\mathbf{h}_{0,i})$ denotes the PDF of the channel between one transmit antenna and one receive antenna. In this case, we can assume that the PDF of $\mathbf{h}_{0,i}$ obeys the Rayleigh distribution.

In order to reduce the complexity of multiple integrals in the mutual information and the information variance, we give the closed-formed approximation of (5.6) and (5.7) as follow

$$
\begin{aligned}
I(X;Y|d=0) \approx & \, t\log|\mathcal{A}| - \mathbb{E}_{\mathbf{h}_0}\Big[\frac{1}{|\mathcal{A}|^t}\sum_{i=1}^{|\mathcal{A}|^t}\log\Big[\sum_{i'=1}^{|\mathcal{A}|^t} \\
& \exp\Big\{-\frac{\big\|\mathbf{h}_0(\mathbf{x}_i-\mathbf{x}_{i'})\big\|^2}{3-\exp\{-\big\|\mathbf{h}_0(\mathbf{x}_i-\mathbf{x}_{i'})\big\|^2/4\}}\Big\}\Big]\Big] \qquad (5.8)
\end{aligned}
$$

and

$$
\begin{aligned}
U(X;Y|d=0) \approx & -\big[(t\log|\mathcal{A}|)-I(X;Y)\big]^2 \\
& +\mathbb{E}_{\mathbf{h}_0}\Big[\frac{1}{|\mathcal{A}|^t}\sum_{i=1}^{|\mathcal{A}|^t}\log^2\Big[\sum_{i'=1}^{|\mathcal{A}|^t}\exp\Big\{-\frac{\big\|\mathbf{h}_0(\mathbf{x}_i-\mathbf{x}_{i'})\big\|^2}{6-\exp\{-\big\|\mathbf{h}_0(\mathbf{x}_i-\mathbf{x}_{i'})\big\|^2/16\}}\Big\}\Big]\Big], \qquad (5.9)
\end{aligned}
$$

where the proof of (5.8) and (5.9) can be found in Appendix B.

2. Case 2: when $d = +1$, in order to obtain the mutual information and the information variance $I(X;Y|d=+1)$ and $U(X;Y|d=+1)$, we just change $\mathbf{h}_0$ in (5.8) and (5.9) to $\mathbf{h}_1$.

After getting the mutual information and the information variance of each case, then applying Theorem 9, we have

$$I(X;Y|D) - \sqrt{\frac{U(X;Y|D)}{n}}Q^{-1}(\epsilon_{source}) + \mathcal{O}(n^{-3/2}) \leq R$$
$$\leq I(X;Y|D) - \sqrt{\frac{U(X;Y|D)}{n}}Q^{-1}(\epsilon_{source}) + \frac{m+1}{2}\frac{\log n}{n} + \mathcal{O}(n^{-3/2}), \quad (5.10)$$

where

$$I(X;Y|D) = \sum_{i=0}^{|\mathcal{D}|-1} \mathbb{P}[d=d_i]I(X;Y|d=d_i) \quad (5.11)$$

$$U(X;Y|D) = \sum_{i=0}^{|\mathcal{D}|-1} \mathbb{P}[d=d_i]U(X;Y|d=d_i). \quad (5.12)$$

To compare with our result, we calculate the capacity of the channel whose input is a circularly symmetric complex Gaussian with zero mean and covariance $\frac{P}{t}\mathbf{I}_t$. The Theorem is shown below.

Theorem 10. *[21] Under the power constraint P, we assume the same channel with the same number of transmitting and receiving antennas as our system model. Its capacity, as determined by the complex Gaussian input, is equal to*

$$C = \mathbb{P}[d=0]\mathbb{E}_{\mathbf{g}_0}[\log(1+\frac{P}{t}g_0)] + \mathbb{P}[d=+1]\mathbb{E}_{\mathbf{g}_1}[\log(1+\frac{P}{t}g_1)], \quad (5.13)$$

where g_0 and g_1 denote the eigenvalues of the matrix $\mathbf{H}_0^H\mathbf{H}_0$ and $\mathbf{H}_1^H\mathbf{H}_1$, respectively, where $\mathbf{H}_0$ and $\mathbf{H}_1$ are from (5.4), and their PDFs are given by

$$p_{g_0}(x) = \frac{1}{2m}\sum_{i=1}^{m}\frac{(i-1)!}{(i-1+\max\{r,t\}-m)!}\Big(L_{i-1}^{\max\{r,t\}-m}(\frac{x}{2})\Big)^2(\frac{x}{2})^{\max\{r,t\}-m}\exp\{-\frac{x}{2}\}, \quad (5.14)$$

and

$$p_{g_1}(x) = \frac{1}{m}\sum_{i=1}^{m} \frac{(i-1)!}{(i-1+\max\{r,t\}-m)!}\big(L_{i-1}^{\max\{r,t\}-m}(x)\big)^2 x^{\max\{r,t\}-m}\exp\{-x\}, \tag{5.15}$$

where $L_k^a(x)$ *is the associated Laguerre polynomial of order* k*. Thus we have*

$$\begin{aligned} C = \frac{\mathbb{P}[d=0]}{2}\int_0^\infty \log(1+\frac{P}{t}g_0)\sum_{i=1}^{m}\frac{(i-1)!}{(i-1+\max\{r,t\}-m)!}\cdot \\ \Big(L_{i-1}^{\max\{r,t\}-m}(\frac{g_0}{2})\Big)^2(\frac{g_0}{2})^{\max\{r,t\}-m}\exp\{-\frac{g_0}{2}\} \\ +\mathbb{P}[d=+1]\int_0^\infty \log(1+\frac{P}{t}g_1)\sum_{i=1}^{m}\frac{(i-1)!}{(i-1+\max\{r,t\}-m)!}\cdot \\ \big(L_{i-1}^{\max\{r,t\}-m}(g_1)\big)^2 g_1^{\max\{r,t\}-m}\exp\{-g_1\}. \end{aligned} \tag{5.16}$$

5.3.2 The Capacity Analysis of the AmBC System

In this subsection, we analyze the capacity of the AmBC system. We define $C_{AmBC}(D;Y)$ as the capacity of the AmBC system. We assume that the input distribution $P(\mathbf{X})$ is equiprobable and that the RF source signal is known in advance. Then we can obtain the conditional capacity of the AmBC system. By taking a weighted sum on the probability of occurrence of that particular value of $\mathbf{X}$, $P(\mathbf{X})$, we have

$$\begin{aligned} C_{AmBC}(D;Y|\mathbf{x}_j) &= \int_0^\infty\int_{-\infty}^\infty \sum_{i=0}^{1}\mathbb{P}[d=i]p(\mathbf{Y},\mathbf{H}_i|\mathbf{X})\cdot \\ &\qquad \log\frac{p(\mathbf{Y},\mathbf{H}_i|\mathbf{X})}{\sum_{i'=0}^{1}\mathbb{P}[d=i']p(\mathbf{Y},\mathbf{H}_{i'}|\mathbf{X})}d\mathbf{Y}d\mathbf{H} \qquad (5.17) \\ &= \mathbb{E}_{\mathbf{h}_i}\Big[\sum_{i=0}^{1}p(\mathbf{h}_i)\mathbb{P}[d=i]\log\Big(\sum_{i'=0}^{1}\mathbb{P}[d=i']\cdot \\ &\qquad \exp\Big\{-\frac{||\mathbf{x}_j(\mathbf{h}_i-\mathbf{h}_{i'})||^2}{3-\exp\{-||\mathbf{x}_j(\mathbf{h}_i-\mathbf{h}_{i'})||^2/4\}}\Big\}\Big)\Big], \qquad (5.18) \end{aligned}$$

where the proof of (5.18) can be easily obtained by the similar method in Appendix B. Then, we have

$$C_{AmBC}(D;Y) = \sum_{j=1}^{|\mathcal{A}|^t} \frac{1}{|\mathcal{A}|^t} C_{AmBC}(D;Y|\mathbf{x}_j). \tag{5.19}$$

5.3.3 The Relation between ϵ_{source} and ϵ_{tag}

In this subsection, we provide the relation between the maximal error probability of the RF source signal, ϵ_{source}, and the average error probability of the tag symbol, ϵ_{tag}, with respect to the blocklength n. Due to the fact that the tag symbol affects the channel instead of being directly sent to the receiver end, we do not directly use the maximum-likelihood (ML) detection to estimate the tag symbol $\hat{d}$. According to [60], the computational complexity of the ML detector is $|\mathcal{A}|^{\log M}|\mathcal{D}|$, which grows exponentially as the alphabet size of the modulation scheme increases. To reduce the complexity, we propose a low-complexity ML detection to decode the tag symbol from the received signal $\mathbf{Y}$. The computational complexity of low-complexity ML detection is $\log M|\mathcal{A}||\mathcal{D}|$, which is lower than that of the original ML detection.

The estimated tag symbol $\hat{d}$ is given as follows:

$$\hat{d} \triangleq \arg\min_{d} \left\| \mathbf{Y} - \hat{\mathbf{X}}\mathbf{H}_{sr} - d\hat{\mathbf{X}}\mathbf{G} \right\|^2, \tag{5.20}$$

where $\hat{\mathbf{X}}$ is the estimated RF source signal at the receiver side and $\mathbf{G} = A\mathbf{H}_{sg}\mathbf{H}_{gr}$. Then, we let

$$Z = \frac{1}{n}\text{Trace}\{\frac{\mathbf{G}^H\hat{\mathbf{X}}^H}{\|\mathbf{G}\|^2}(\mathbf{Y} - \hat{\mathbf{X}}\mathbf{H}_{sr})\} \tag{5.21}$$

$$= \frac{1}{n}\text{Trace}\{\frac{\mathbf{G}^H\hat{\mathbf{X}}^H\mathbf{X}\mathbf{G}}{\|\mathbf{G}\|^2}\}d + \frac{1}{n}\text{Trace}\{\frac{\mathbf{G}^H(\hat{\mathbf{X}}^H\mathbf{X} - \hat{\mathbf{X}}^H\hat{\mathbf{X}})\mathbf{H}_{sr}}{\|\mathbf{G}\|^2}\} + \omega, \tag{5.22}$$

where

$$\omega = \frac{1}{n}\text{Trace}\{\frac{\mathbf{G}^H\hat{\mathbf{X}}^H\mathbf{W}}{\|\mathbf{G}\|^2}\} \tag{5.23}$$

and $\omega \sim \mathcal{CN}(0, 1/(n\|\mathbf{G}\|^2))$.

Due to the low-complexity ML detection, if $Z > Z_{th}$, $\hat{d} = +1$, otherwise, $\hat{d} = 0$, where Z_{th} is the decision threshold.

1. Case 1: when $\hat{\mathbf{X}} = \mathbf{X}$, we have $1 - \delta < \frac{1}{n}\text{Trace}\{\mathbf{G}^H\hat{\mathbf{X}}^H\mathbf{X}\mathbf{G}/\|\mathbf{G}\|^2\} < 1 + \delta$, where $\delta \leq 1$, and $\frac{1}{n}\text{Trace}\{\mathbf{G}^H\hat{\mathbf{X}}^H\mathbf{X}\mathbf{G}/\|\mathbf{G}\|^2\}$ is a discrete real number, then we can treat this value as the coefficient of d, thus

$$Z = \frac{1}{n}\text{Trace}\{\mathbf{G}^H\hat{\mathbf{X}}^H\mathbf{X}\mathbf{G}/\|\mathbf{G}\|^2\}d + \omega. \tag{5.24}$$

The coefficient of d only has value in the real part which means $\Im\{\text{Trace}\{\mathbf{G}^H\hat{\mathbf{X}}^H\mathbf{X}\mathbf{G}/\|\mathbf{G}\|^2\} = 0$. Thus it shows that Z obeys Gaussian distribution. Therefore, under $\hat{\mathbf{X}} = \mathbf{X}$, the error probability of the event $\hat{d} \neq d$ can be expressed as below

$$\mathbb{P}[\hat{d} \neq d|\hat{\mathbf{X}} = \mathbf{X}] = Q\Big(\sqrt{n}\|\mathbf{G}\|\left(-Z_{th,1} + \frac{1}{n}\mathbb{E}\big[\text{Trace}\{\mathbf{G}^H\hat{\mathbf{X}}^H\mathbf{X}\mathbf{G}/\|\mathbf{G}\|^2\}\big]\right)\Big). \tag{5.25}$$

Remark. *For 2×2 MIMO, we select $Z_{th,1} = 0.75$, while for 3×3 MIMO, we select $Z_{th,1} = 0.95$.*

2. Case 2: when $\hat{\mathbf{X}} \neq \mathbf{X}$, we have $-\delta < \frac{1}{n}\text{Trace}\{\mathbf{G}^H\hat{\mathbf{X}}^H\mathbf{X}\mathbf{G}/\|\mathbf{G}\|^2\} < +\delta$, where $\delta \leq 1$, and $\frac{1}{n}\text{Trace}\{\mathbf{G}^H\hat{\mathbf{X}}^H\mathbf{X}\mathbf{G}/\|\mathbf{G}\|^2\}$ is a discrete complex number, thus we have,

$$Z = \frac{1}{n}\text{Trace}\{\mathbf{G}^H\hat{\mathbf{X}}^H\mathbf{X}\mathbf{G}/\|\mathbf{G}\|^2\}d + \frac{1}{n}\text{Trace}\{\frac{\mathbf{G}^H(\hat{\mathbf{X}}^H\mathbf{X} - \hat{\mathbf{X}}^H\hat{\mathbf{X}})\mathbf{H}_{sr}}{\|\mathbf{G}\|^2}\} + \omega. \tag{5.26}$$

Thus for $d = +1$, we have

$$\mathbb{P}[\hat{d} = 0, d = +1|\hat{\mathbf{X}} \neq \mathbf{X}] = Q\Bigg(\sqrt{n}\|\mathbf{G}\|\Big(-Z_{th,2} + \frac{1}{n}\mathbb{E}\big[\Im\{\text{Trace}\{\frac{\mathbf{G}^H\hat{\mathbf{X}}^H\mathbf{X}(\mathbf{G} + \mathbf{H}_{sr})}{\|\mathbf{G}\|^2} + \frac{\mathbf{G}^H\hat{\mathbf{X}}^H\hat{\mathbf{X}}\mathbf{H}_{sr}}{\|\mathbf{G}\|^2}\}\}\big]\Big)\Bigg) \tag{5.27}$$

and for $d = 0$, we have

$$\mathbb{P}[\hat{d} = +1, d = 0 | \hat{\mathbf{X}} \neq \mathbf{X}] = Q\bigg(\sqrt{n}\|\mathbf{G}\| \Big(Z_{th,2} - \frac{1}{n}\mathbb{E}\big[\Im\{\text{Trace}\{ \frac{\mathbf{G}^H\hat{\mathbf{X}}^H\mathbf{X}(\mathbf{G}+\mathbf{H}_{sr})}{\|\mathbf{G}\|^2} + \frac{\mathbf{G}^H\hat{\mathbf{X}}^H\hat{\mathbf{X}}\mathbf{H}_{sr}}{\|\mathbf{G}\|^2}\}\}\big]\Big)\bigg). \quad (5.28)$$

Remark. *For* 2×2 *MIMO, we select* $Z_{th,2} = 0.75$*, while for* 3×3 *MIMO, we select* $Z_{th,2} = 0.95$*.*

Once getting the error probability of the tag symbol for both cases of $\hat{\mathbf{X}} = \mathbf{X}$ and $\hat{\mathbf{X}} \neq \mathbf{X}$, we have the equation which expresses the relationship between ϵ and the error probability of the tag symbol, ϵ_{tag} by combining (5.25), (5.27) and (5.28).

$$\begin{aligned}\epsilon_{tag} = (1-\epsilon_{source})Q\bigg(\sqrt{n}\|\mathbf{G}\| \Big(- Z_{th,1} + \frac{1}{n}\mathbb{E}\big[\text{Trace}\{\mathbf{G}^H\hat{\mathbf{X}}^H\mathbf{X}\mathbf{G}/\|\mathbf{G}\|^2\}\big]\Big)\bigg) \\ + \epsilon_{source}\Bigg[\mathbb{P}[d=+1]Q\bigg(\sqrt{n}\|\mathbf{G}\| \Big(- Z_{th,2} + \frac{1}{n}\mathbb{E}\big[\Im\{\text{Trace}\{\frac{\mathbf{G}^H\hat{\mathbf{X}}^H\mathbf{X}(\mathbf{G}+\mathbf{H}_{sr})}{\|\mathbf{G}\|^2} \\ + \frac{\mathbf{G}^H\hat{\mathbf{X}}^H\hat{\mathbf{X}}\mathbf{H}_{sr}}{\|\mathbf{G}\|^2}\}\}\big]\Big)\bigg) + \mathbb{P}[d=0]Q\bigg(\sqrt{n}\|\mathbf{G}\| \Big(Z_{th,2} - \frac{1}{n}\mathbb{E}\big[\Im\{\text{Trace}\{ \\ \frac{\mathbf{G}^H\hat{\mathbf{X}}^H\mathbf{X}(\mathbf{G}+\mathbf{H}_{sr})}{\|\mathbf{G}\|^2} + \frac{\mathbf{G}^H\hat{\mathbf{X}}^H\hat{\mathbf{X}}\mathbf{H}_{sr}}{\|\mathbf{G}\|^2}\}\}\big]\Big)\bigg)\Bigg]. \quad (5.29)\end{aligned}$$

Therefore, given a specific maximal error probability of the RF source signal ϵ_{source}, after getting the lower and upper bounds for the channel code rate R, we can obtain the relationship between the channel code rate R and the error probability of the tag symbol ϵ_{tag} from (5.29).

5.4 Numerical Results

In this section, we resort to numerical simulation to evaluate the proposed studies. We consider a legacy system consisting of multiple transmitter antennas, the tag with a single antenna and multiple receiver antennas. We assume all the channels,

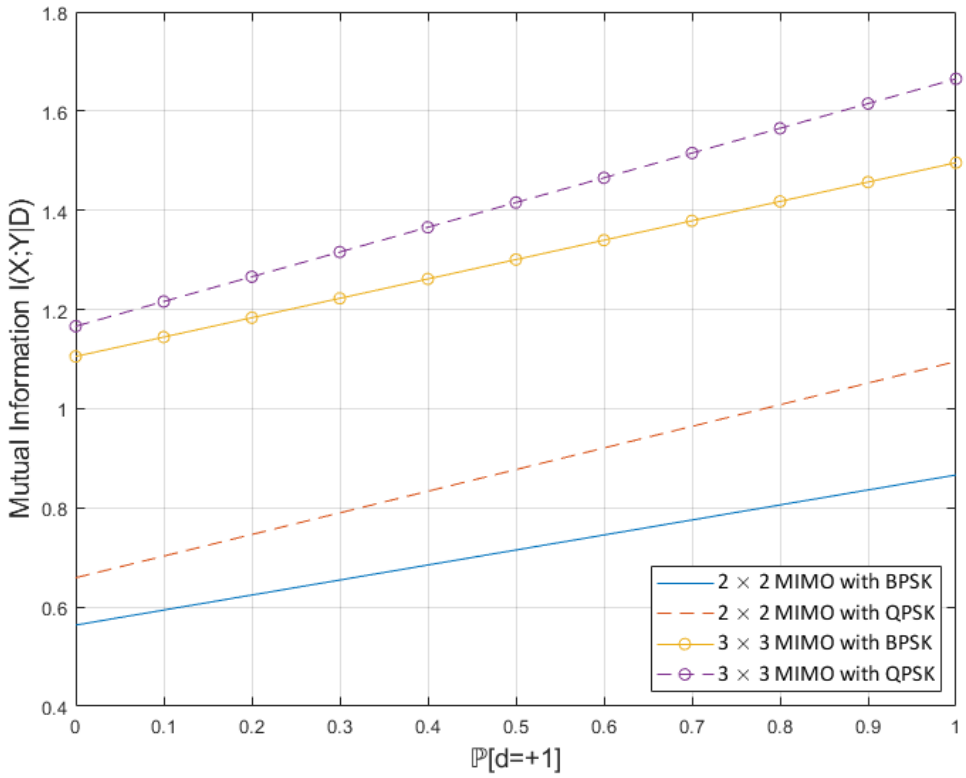

Figure 5.2: The comparison between 2×2 MIMO and 3×3 MIMO with BPSK and QPSK modulated signal, respectively.

i.e., the channels between the transmitter and the tag, the tag and the receiver, and the transmitter and the receiver, are independent, Assuming that all the channels are Rayleigh fading channels, and the SNR is -5 dB. Fig. 5.2 shows the mutual information of the legacy system in (5.11) for the BPSK and QPSK modulated signal for $\mathbb{P}[d = +1]$ from 0 to 1 with 2×2 MIMO and 3×3 MIMO, respectively. We observe that as the probability of the tag symbol $d = +1$ increases, $I(X; Y|D)$ increases accordingly, regardless of the modulation scheme of the RF source signal and the number of transmitter and receiver antennas. Additionally, the gap between different modulated signals decreases as the number of transmitter and receiver antennas increases. Fig. 5.3 demonstrates the value of $C_{AmBC}(D; Y)$ in (5.19) for

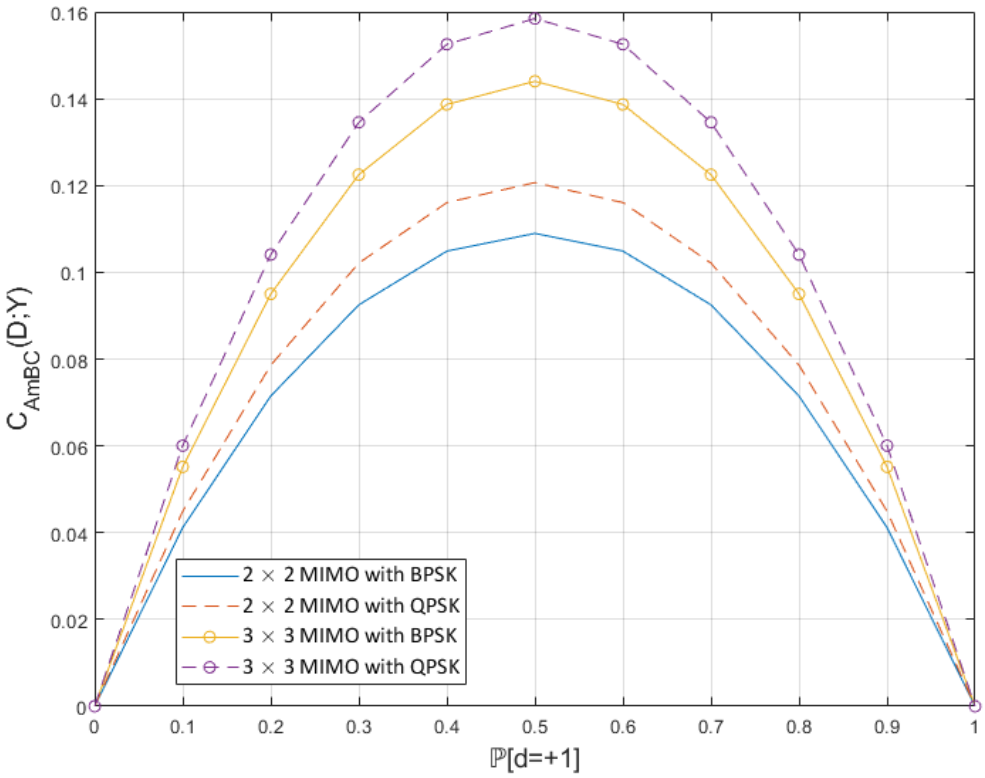

Figure 5.3: The comparison between 2×2 MIMO and 3×3 MIMO with BPSK and QPSK modulated signal, respectively.

BPSK and QPSK modulated RF source signal with $\mathbb{P}[d = +1]$ from 0 to 1 over the 2×2 MIMO and 3×3 MIMO systems, respectively. By comparing the results in Fig. 5.2, we easily observe that under the same level of SNR, i.e., SNR$= -5$ dB, the mutual information of the legacy system $I(X;Y|D)$ is much larger than the capacity of the AmBC system $C_{AmBC}(D;Y)$. The mutual information of the legacy system as shown in Fig. 5.2 increases as $\mathbb{P}[d = +1]$ increases. While the mutual information of the AmBC system $C_{AmBC}(D;Y)$ reaches the peak when $\mathbb{P}[d = +1] = 0.5$, see Fig. 5.3, therefore, in the following simulations, we choose $\mathbb{P}[d = +1] = 0.5$.

We consider the same legacy MIMO system as above, and we set the maximal error probability $\epsilon = 10^{-3}$. Assuming that all the channels are Rayleigh fading

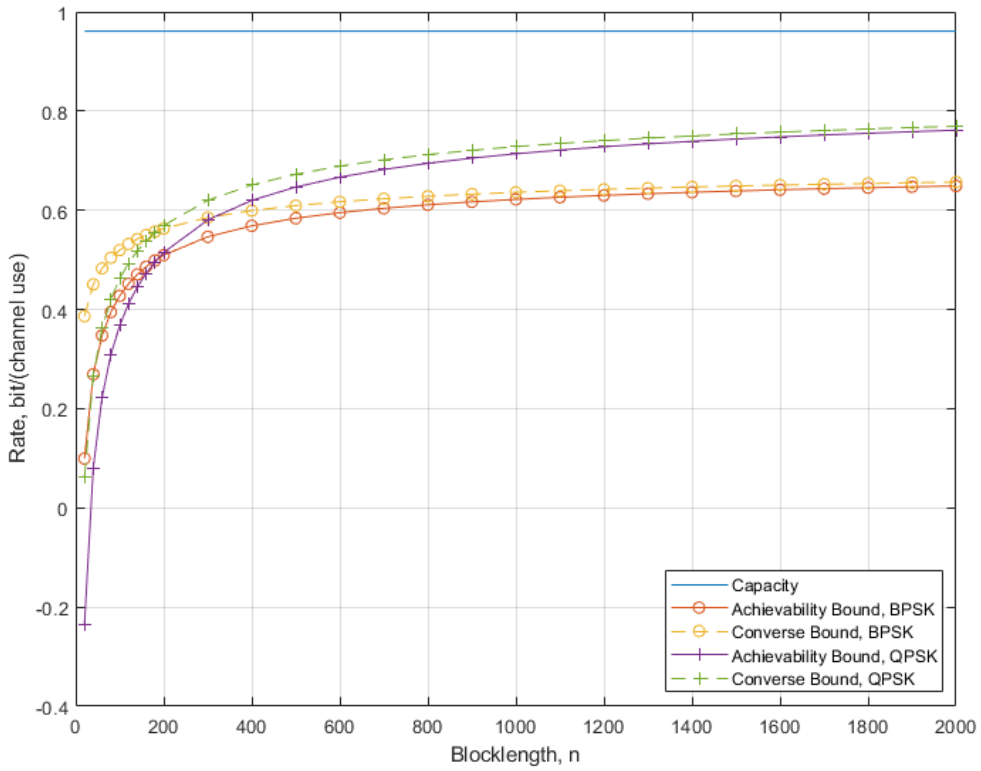

Figure 5.4: Achievability and converse bounds for $(n, M, \epsilon_{source})$ codes for an AmBC MIMO system over a Rayleigh fading channel and transmit antennas $t = 2$ and receive antennas $r = 2$ for $\epsilon_{source} = 10^{-3}$, SNR$= -5$ dB and with BPSK and QPSK modulation, repectively.

channels, $\mathbb{P}[d = 0] = \mathbb{P}[d = +1] = 0.5$ and the SNR is -5 dB. Figs. 5.4 and 5.5 show the numerical results of the derived bounds with BPSK and QPSK modulated signals and the capacity for $t = r = 2$ and $t = r = 3$, respectively. From Fig. 5.4), we can see that the capacity is 0.9611 bit/(channel use), which is calculated from (5.16) and the maximal achievable rate for the BPSK modulated signal is 0.7151 bit/(channel use), which is obtained based on (5.11). The blocklength n required to achieve above 70% and 80% of its maximal achievable rate start at $n = 180$ and $n = 420$, respectively. The gap between the capacity and its maximal achievable rate is 0.2460 bit/(channel use). With the QPSK modulation, the maximal achiev-

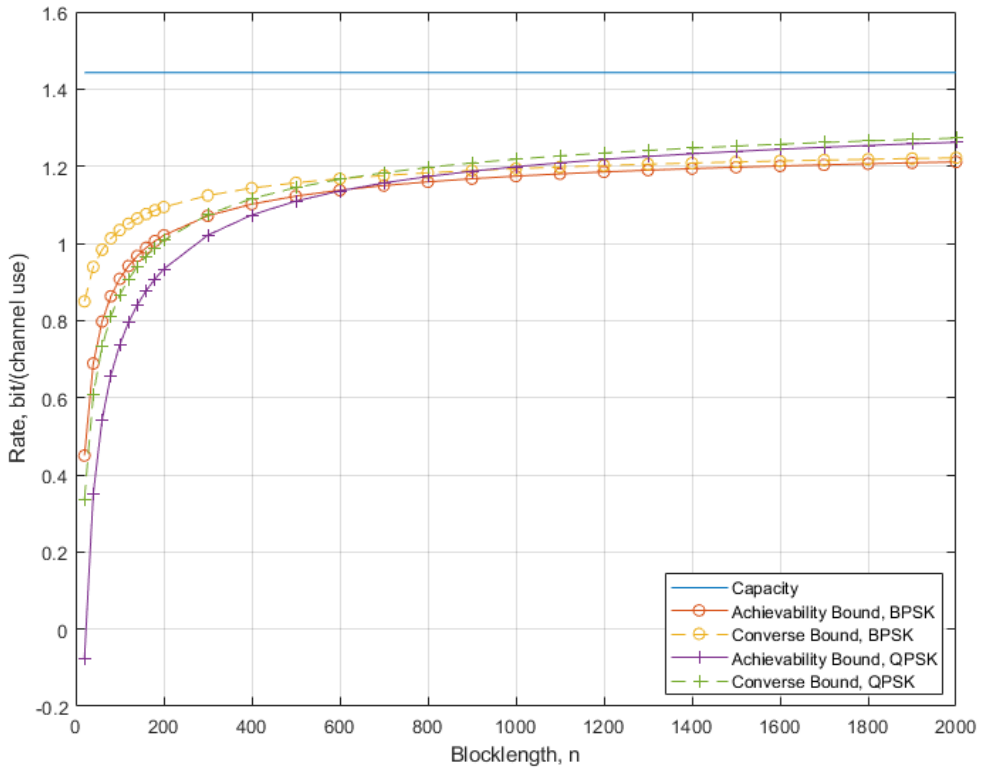

Figure 5.5: Achievability and converse bounds for $(n, M, \epsilon_{source})$ codes for an AmBC MIMO system over a Rayleigh fading channel and transmit antennas $t = 3$ and receive antennas $r = 3$ for $\epsilon_{source} = 10^{-3}$, SNR$= -5$ dB and with BPSK and QPSK modulation, repectively.

able rate is 0.8772 bit/(channel use), and the blocklength n required to achieve above 70% and 80% of its maximal achievable rate start at $n = 380$ and $n = 860$, respectively. The gap in the QPSK case is 0.0839 bit/(channel use). In Fig. 5.5, we only change the number of transmitter and receiver antennas from $t = r = 2$ to $t = r = 3$, and the rest parameters remain the same. The capacity, in this case, is 1.4425 bit/(channel use). The BPSK modulated signal's maximal achievable rate is 1.3006 bit/(channel use). The blocklength n, which can surpass 70% and 80% of its maximal achievable rates, decreases dramatically to 100 and 240, respectively, compared with the case of 2×2 MIMO. Moreover, the gap between the capacity

and the maximal achievable rate decreases to 0.1419 bit/(channel use). For QPSK modulation, its maximal achievable rate is 1.415 bit/(channel use), and the blocklength $n = 260$ and $n = 580$ are required to achieve above 70% and 80% of its maximal achievable rate, respectively. The gap also falls to 0.0269 bit/(channel use) compared with the case for 2×2 MIMO. The findings are summarized in Table 5.1. From Figs. 5.4-5.5, we can conclude that: 1) as the number of transmitter and receiver antennas increases, the maximal achievable rates of the BPSK and QPSK modulated signal accelerate, which indicates that the gap between the maximal achievable rate for different modulation schemes and the capacity decreases at the same SNR level; 2) the required blocklength n falls significantly to achieve a given fraction of the maximal achievable rate as the number of transmitter and receiver antennas increases.

The information variance $U(X;Y|D)$ in (5.12) shows how quickly the performance converges to the maximal achievable rate as blocklength n grows. In the case of the BPSK and QPSK modulations shown in Fig. 5.4, the information variances for the BPSK and QPSK modulated signal are 0.9281 and 2.8267, respectively. From Fig. 5.5, we can see that the information variances are 1.6990 and 4.9729, respectively.

Additionally, if the target is to transmit at a fraction of the maximal achievable rate $0 < \eta < 1$ with a pre-determined ϵ_{source}, the relationship between the required blocklength n and the information variance is given as follows:

$$n \approx \frac{U(X;Y|D)}{(I(X;Y|D))^2}\Big(\frac{Q^{-1}(\epsilon_{source})}{1-\eta}\Big)^2.$$

To validate our results, we transform the achievability and converse bounds in Th. 9 to the lower and upper bounds on the average error probability of the RF source signal. From Th.9, We have the achievability and converse bounds on maximal error probability. Since there always exists an $(n, M, \epsilon_{source})$-code in the maximal

Table 5.1: Required blocklength to achieve a given fraction of the maximal achievable rate for an AmBC MIMO system over a Rayleigh fading channel, SNR= -5dB and $\epsilon = 10^{-3}$, and $P(d) = [0.5, 0.5]$.

	2×2 MIMO		3×3 MIMO	
	BPSK	QPSK	BPSK	QPSK
Required n to Achieve 70% of The Maximal Achievable Rate	180	380	100	260
Required n to Achieve 80% of The Maximal Achievable Rate	420	860	240	580

error probability ϵ_{source} that guarantees the existence of an $(n, M', \epsilon'_{source})$-code in the average error probability ϵ'_{source}, for any $\epsilon'_{source} < \epsilon_{source} < 1$ and $0 < \xi < 1$, where $M' = 2^{nR/(1-\xi)}$ and $\epsilon'_{source} = \xi\epsilon_{source}$. From (5.10), we have $I(X;Y|D) - \sqrt{U(X;Y|D)/n}Q^{-1}(\epsilon_{source}) + \mathcal{O}(n^{-3/2}) \leq R \leq I(X;Y|D) - \sqrt{U(X;Y|D)/n}$ $Q^{-1}(\epsilon_{source}) + (m+1)\log n/(2n) + \mathcal{O}(n^{-3/2})$.

We transform the achievability and converse bounds into the lower and upper bounds on the maximal error probability of the RF source signal as follows.

$$Q\Big(\frac{I(X;Y|D) + \frac{m+1}{2}\frac{\log n}{n} - R}{\sqrt{\frac{U(X;Y|D)}{n}}}\Big) \leq \epsilon_{source} \leq Q\Big(\frac{I(X;Y|D) - R}{\sqrt{\frac{U(X;Y|D)}{n}}}\Big).$$

Therefore, we obtain the lower and upper bounds on the average error probability of the RF source signal, i.e., ϵ'_{source}, which is shown below.

$$\xi Q\Big(\frac{I(X;Y|D) + \frac{m+1}{2}\frac{\log n}{n} - R(1-\xi)}{\sqrt{\frac{U(X;Y|D)}{n}}}\Big) \leq \epsilon'_{source} \leq \xi Q\Big(\frac{I(X;Y|D) - R(1-\xi)}{\sqrt{\frac{U(X;Y|D)}{n}}}\Big).$$

By utilizing the polar code with a successive cancellation list (SCL) decoder and the extended BCH code with an ordered statistic decoder (OSD), we validate our derived results.

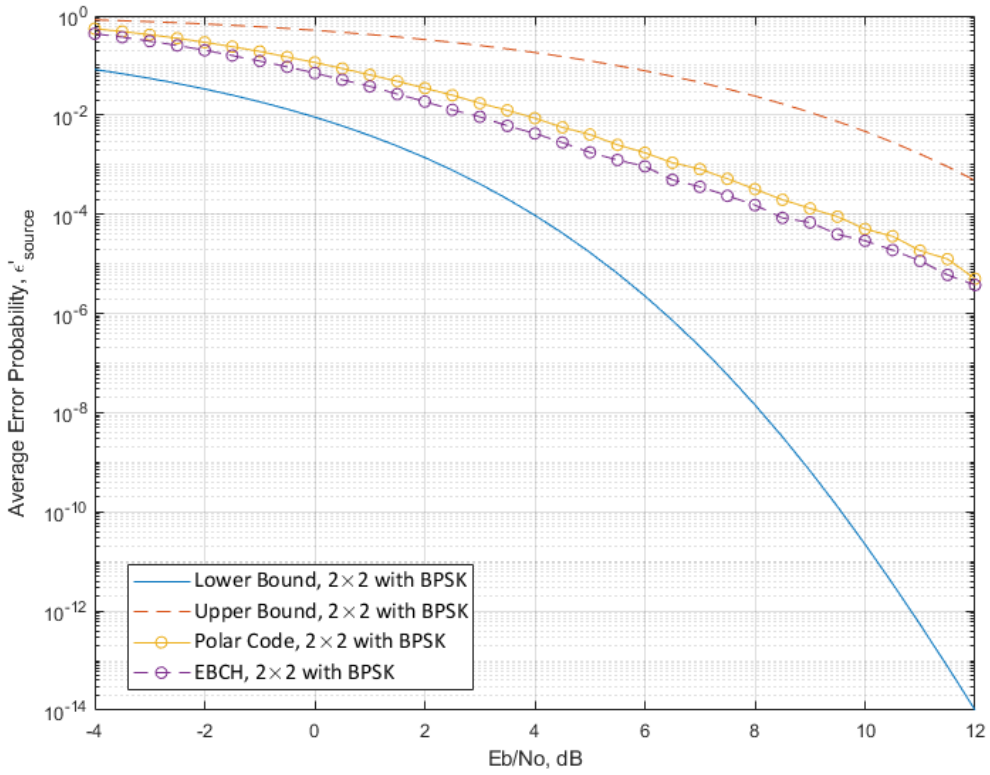

Figure 5.6: Lower and upper bounds for $(128, 2^{64}, \epsilon'_{source})$ codes for a legacy system over a Rayleigh fading channel and transmit antennas $t = 2$ and receive antennas $r = 2$ with BPSK modulated RF source signal, repectively.

In Fig. 5.6, we set the number of the transmitter and receiver antennas to 2, the modulation scheme to BPSK, the coding rate $R = 0.5$, and the blocklength $n = 128$. All the simulations are averaged over 10^6 Monte Carlo realizations. We choose two coding methods: one is the $(128, 2^{64})$-polar code with SCL decoder (the list size is $L = 32$), and the other is the $(128, 2^{64})$-EBCH code with OSD decoder (the order is chose to 4). We observe that for the EBCH code, at the average error probability level of 10^{-2} and 10^{-4}, the gap between the simulation result and the lower bound increases from 2.5 dB to 4 dB, respectively. As EbNo increases, the gap increases accordingly. The simulation result of the EBCH code is slightly better than the one of the polar code. However, it still shows that the EBCH code is still better

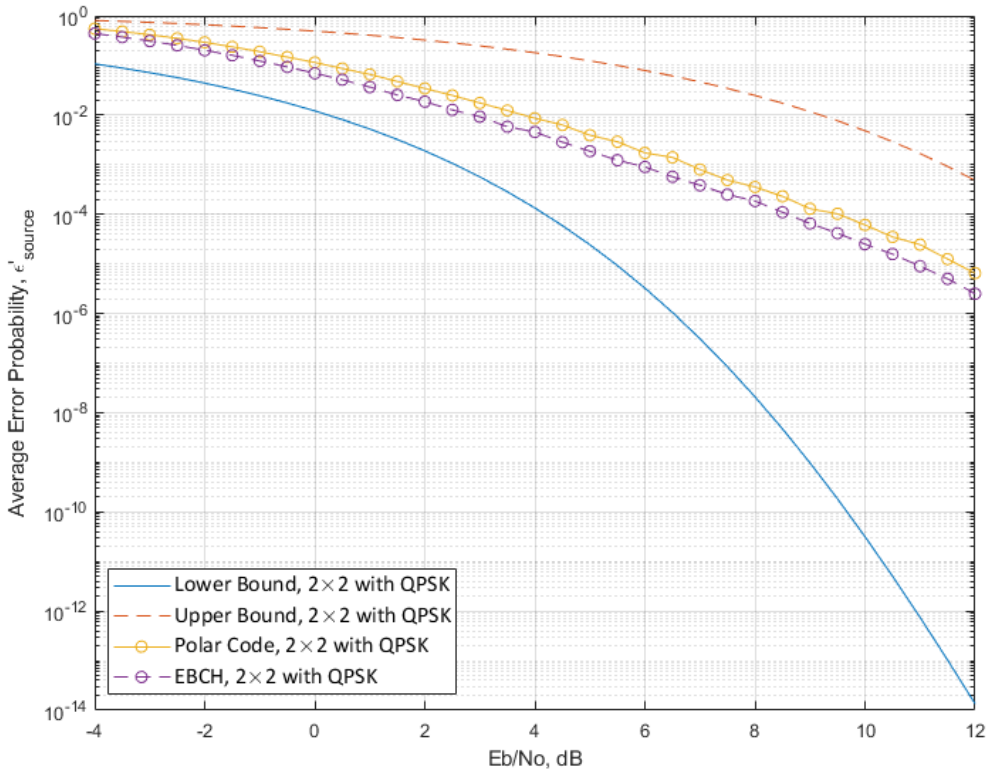

Figure 5.7: Lower and upper bounds for $(128, 2^{64}, \epsilon'_{source})$ codes for a legacy system over a Rayleigh fading channel and transmit antennas $t = 2$ and receive antennas $r = 2$ with QPSK modulated RF source signal, repectively.

than the polar code at the blocklength $n = 128$. In Fig. 5.7, we set the modulation scheme to QPSK and keep the rest parameters the same as in Fig. 5.6. We observe that the overall performance between the BPSK modulation scheme and the QPSK modulation scheme in the 2×2 MIMO system is similar. The simulation results and our derived bounds validate the observation. In Fig. 5.8, we change the number of the transmitter and receiver antennas to 3, the modulation scheme to BPSK, and remain the rest parameters the same as in Figs. 5.6 and 5.7. At first, we compare the performance of two codes in different MIMO systems, i.e., 2×2 MIMO and 3×3 MIMO systems. At the same EbNo level of -4 dB, the average error probability drops from 0.4375 to 0.0907 for the EBCH code and from 0.5509 to 0.1089 for the

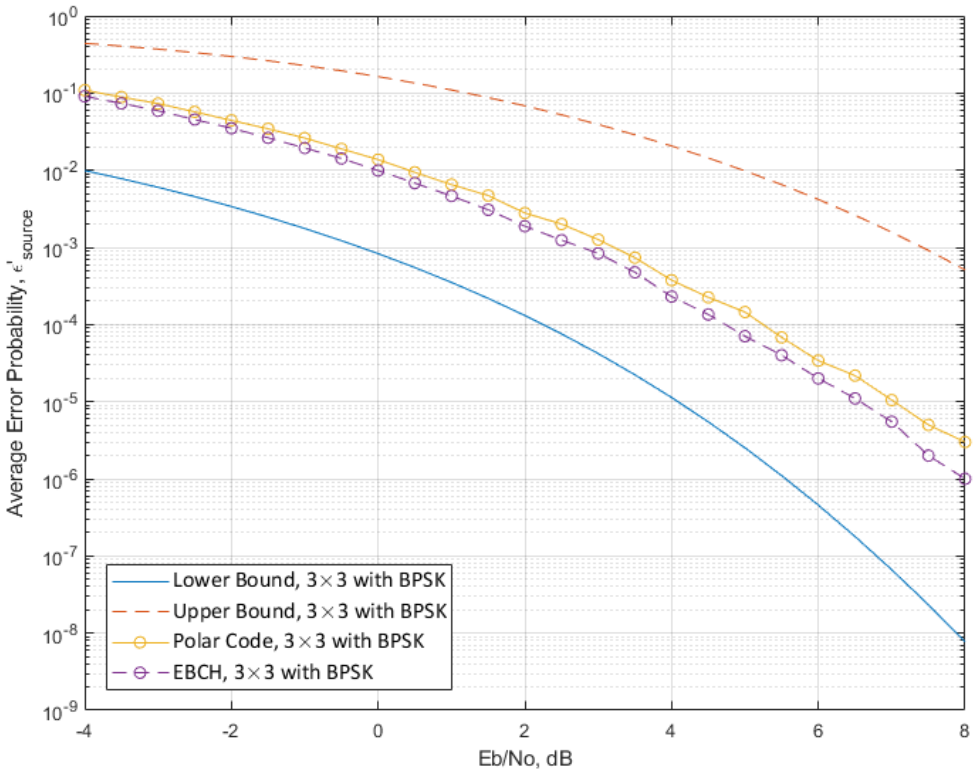

Figure 5.8: Lower and upper bounds for $(128, 2^{64}, \epsilon'_{source})$ codes for a legacy system over a Rayleigh fading channel and transmit antennas $t = 3$ and receive antennas $r = 3$ with BPSK modulated RF source signal, repectively.

polar code. At the same average error probability level of 10^{-2}, the gaps between different MIMO systems are 3 dB and 3.5 dB for the EBCH code and polar code, respectively. We observe that the bounds are closer in the 3×3 MIMO system than in the 2×2 MIMO system. In Fig. 5.9, we change the modulation scheme from BPSK to QPSK, and remain the rest parameters the same as in Fig. 5.8. The comparison between these two figures shows that the gap between the performance of the two codes in different modulation schemes becomes larger, i.e., 1 dB and 2 dB (at the same average error probability level of 10^{-2}) for the EBCH code and polar code, respectively. In Fig. 5.10, we set the number of the transmitter and receiver antennas to 2 and 3, respectively, the RF source signal modulation scheme

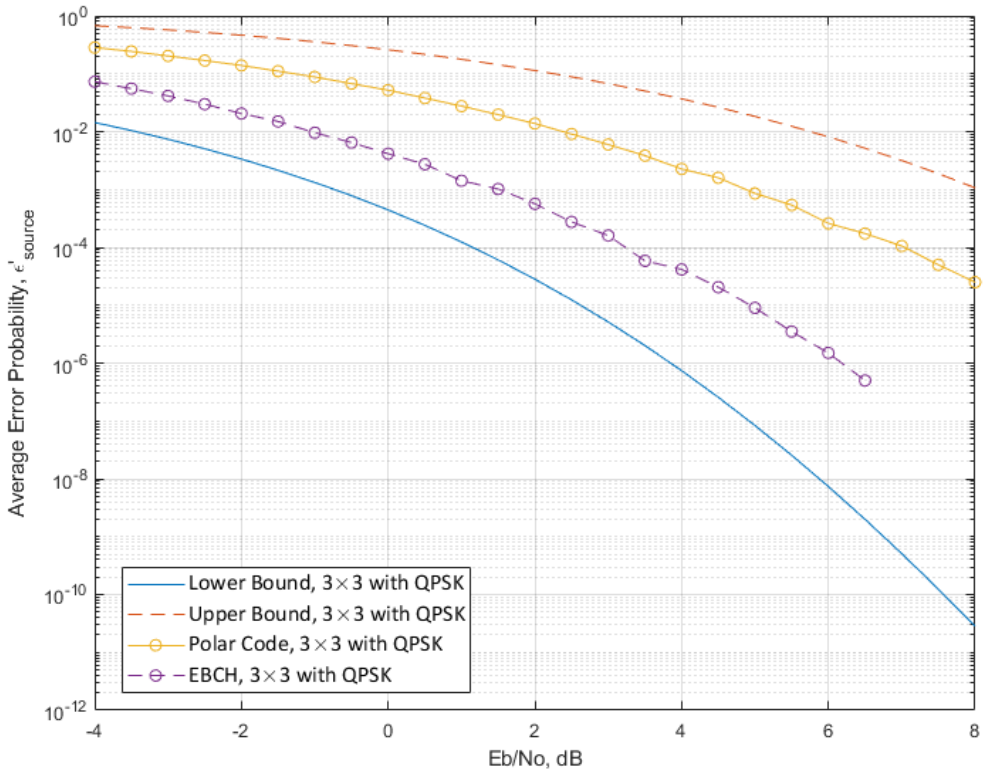

Figure 5.9: Lower and upper bounds for $(128, 2^{64}, \epsilon'_{source})$ codes for a legacy system over a Rayleigh fading channel and transmit antennas $t = 3$ and receive antennas $r = 3$ with QPSK modulated RF source signal, repectively.

to BPSK, and keep the rest parameters the same as in Figs. 5.6-5.9. We compare the performance of our proposed method and ML detection with different coding methods of the RF source signal, i.e., the EBCH code and polar code. When EbNo is small, the gaps between these two methods are 0.5 dB and 0.8 dB for the 2×2 MIMO and 3×3 MIMO system, respectively. As EbNo increases, the gap slightly increases to 1 dB and 1.2 dB for 2×2 MIMO and 3×3 MIMO systems, respectively. Additionally, we observe that as EbNo increases, the gap between different codes vanishes for both 2×2 MIMO and 3×3 MIMO systems.

Fig. 5.11-5.13 demonstrates the relation between the blocklength n and the probability of $\mathbb{P}[\hat{d} \neq d|\hat{\mathbf{X}} = \mathbf{X}]$, $\mathbb{P}[\hat{d} = 0, d = +1|\hat{\mathbf{X}} \neq \mathbf{X}]$, and $\mathbb{P}[\hat{d} = +1, d = 0|\hat{\mathbf{X}} \neq$

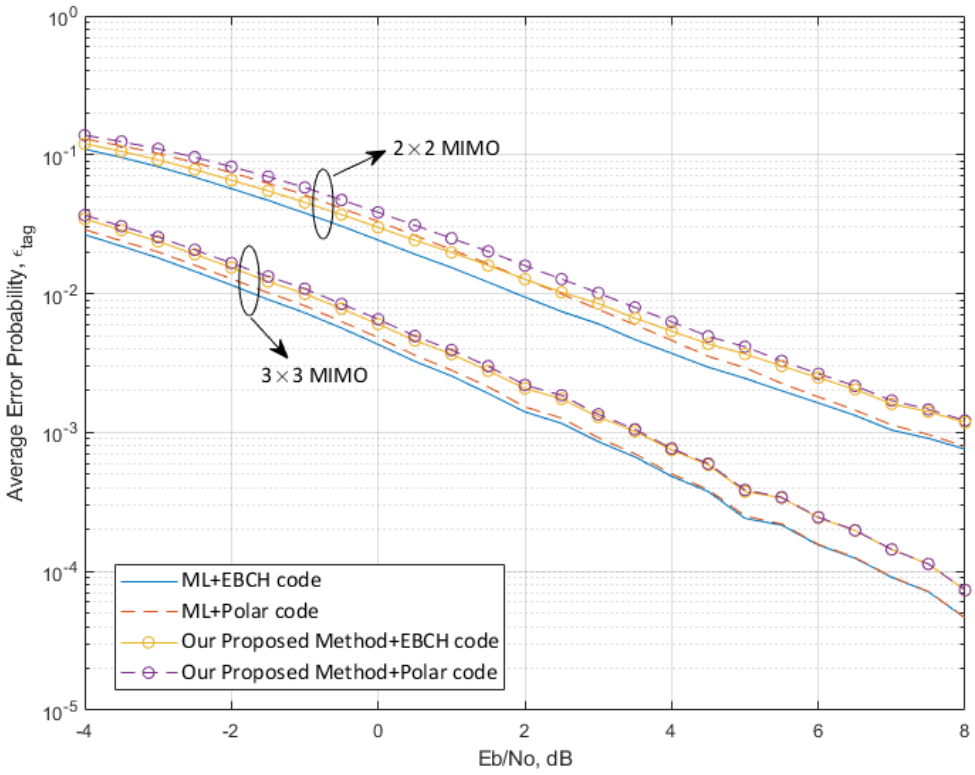

Figure 5.10: The comparison between ML detection and our proposed method with different coding methods with BPSK modulation over a Rayleigh fading channel and transmit antennas $t = 2$ and receive antennas $r = 2$, and transmit antennas $t = 3$ and receive antennas $r = 3$, respectively.

$\mathbf{X}$], which are obtained from (5.25), (5.27), and (5.28), respectively. From Fig. 5.11, we observe that under the condition of $\hat{\mathbf{X}} = \mathbf{X}$, the conditional probability of $\hat{d} \neq d$ decreases as the blocklength n increases regardless of the number of transmitter and receiver antennas. When $n = 200$, $\mathbb{P}[\hat{d} \neq d|\hat{\mathbf{X}} = \mathbf{X}]$ for 2×2 MIMO is 6.56×10^{-4}, while the one for 3×3 MIMO is 9.53×10^{-6}. When n moves to 1000, the probability for 2×2 MIMO decreases to 4.29×10^{-5} while the one for 3×3 MIMO drops to 1.23×10^{-7}. Furthermore, when n increases to 2000, the conditional probability, $\mathbb{P}[\hat{d} \neq d]$ under the condition of $\hat{\mathbf{X}} = \mathbf{X}$ for 2×2 MIMO case decreases to 1.30×10^{-5} in the meanwhile, that probability for 3×3 MIMO case falls to 2.41×10^{-8}. The

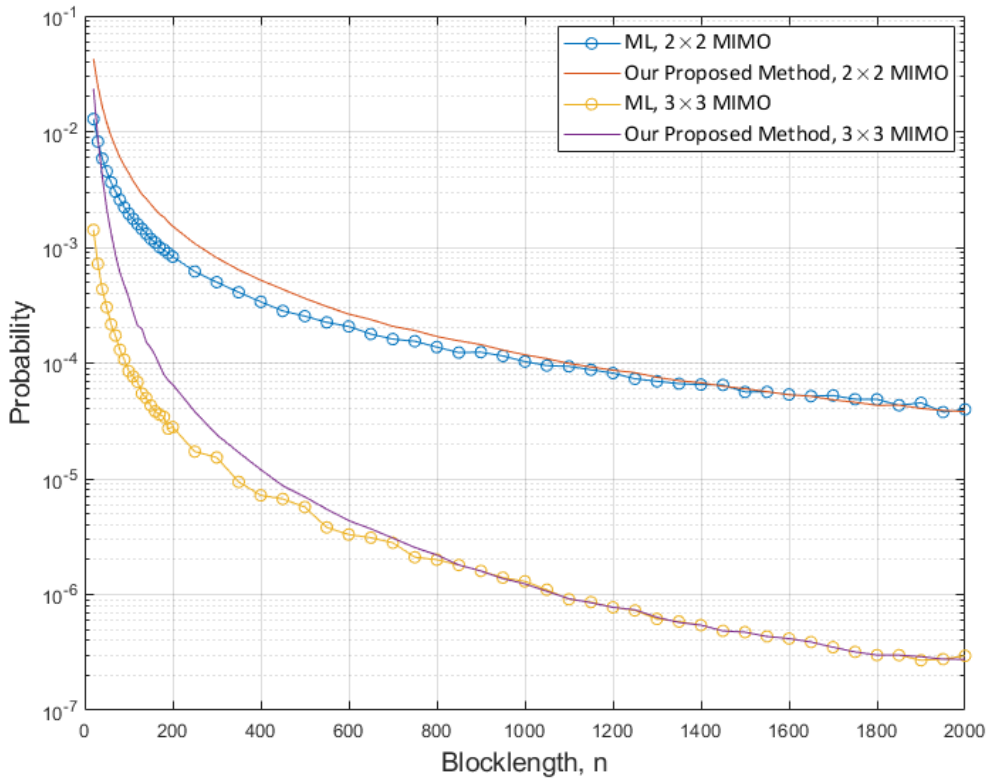

Figure 5.11: $\mathbb{P}[\hat{d} \neq d|\hat{\mathbf{X}} = \mathbf{X}]$ in (5.25) over 2×2 MIMO and 3×3 MIMO, respectively.

decreasing trend of 2×2 MIMO is much slower than that for 3×3 MIMO from $n = 0$ to 1000. After $n = 1000$, the tendencies for both cases are flattened. Compared with ML detection, when n is less than 800, there is a small gap between the low-complexity ML detection that we mainly use in this paper and the ML detection for 2×2 and 3×3 MIMO. As n grows larger, the performances of the two methods, i.e., the ML and the low-complexity ML detection methods, are basically the same. Fig. 5.12 and 5.13 show that under the condition of $\hat{\mathbf{X}} \neq \mathbf{X}$ and $d = +1$, the conditional probability of $\hat{d} \neq d$ increases as the blocklength n increases regardless of the number of the transmitter and receiver antennas. Moreover, the figures also demonstrate that under the condition of $\hat{\mathbf{X}} \neq \mathbf{X}$ and $d = 0$, the conditional probability of $\hat{d} \neq d$

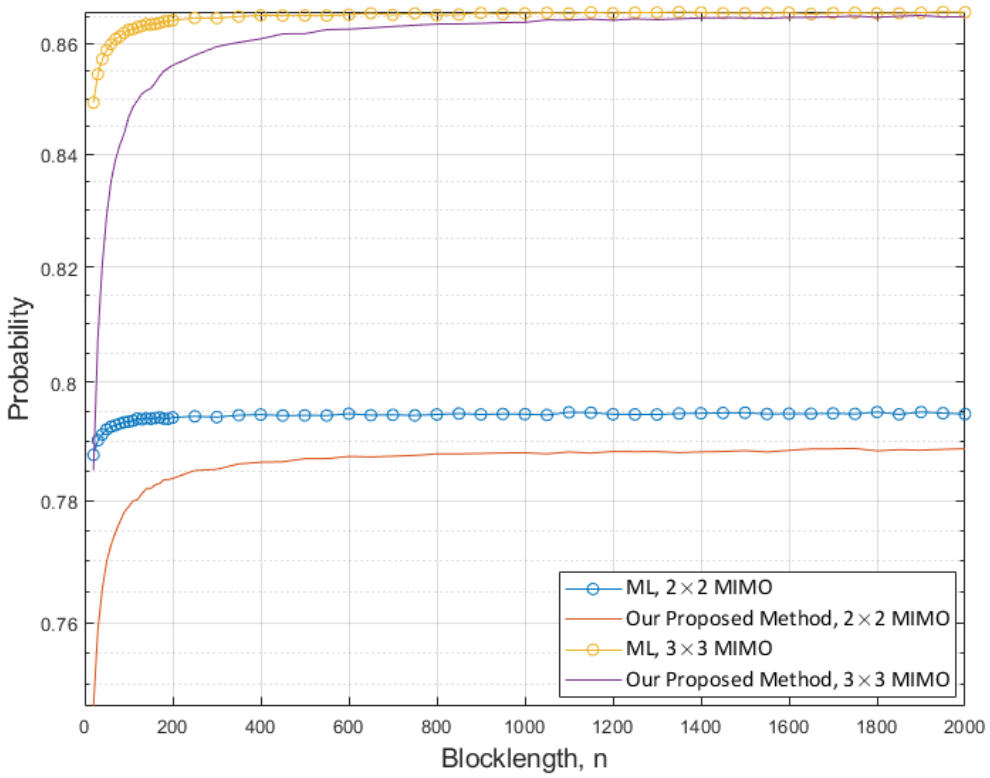

Figure 5.12: $\mathbb{P}[\hat{d} = 0, d = +1|\hat{\mathbf{X}} \neq \mathbf{X}]$ in (5.27) over 2×2 MIMO and 3×3 MIMO, respectively.

decreases as the blocklength n increases regardless of the number of transmitter and receiver antennas. Compared with the ML detection, for 2×2 MIMO case, when n increases from 0 to 2000, the gap between the ML and the low-complexity ML detection shrinks to a constant, while the gap for 3×3 MIMO falls to a very small margin. Basically, when n goes beyond 1000, the performances of the two detections are the same for 3×3 MIMO case.

Fig. 5.14 demonstrates the error probability of the tag symbol ϵ_{tag} in (5.29) with different blocklength n and the error probability of the RF source signal ϵ_{source} for 2×2 MIMO and 3×3 MIMO, respectively. The relationship between ϵ_{source} and the blocklength n is given by Theorem 9 and (5.10). Moreover, (5.29) illustrates the

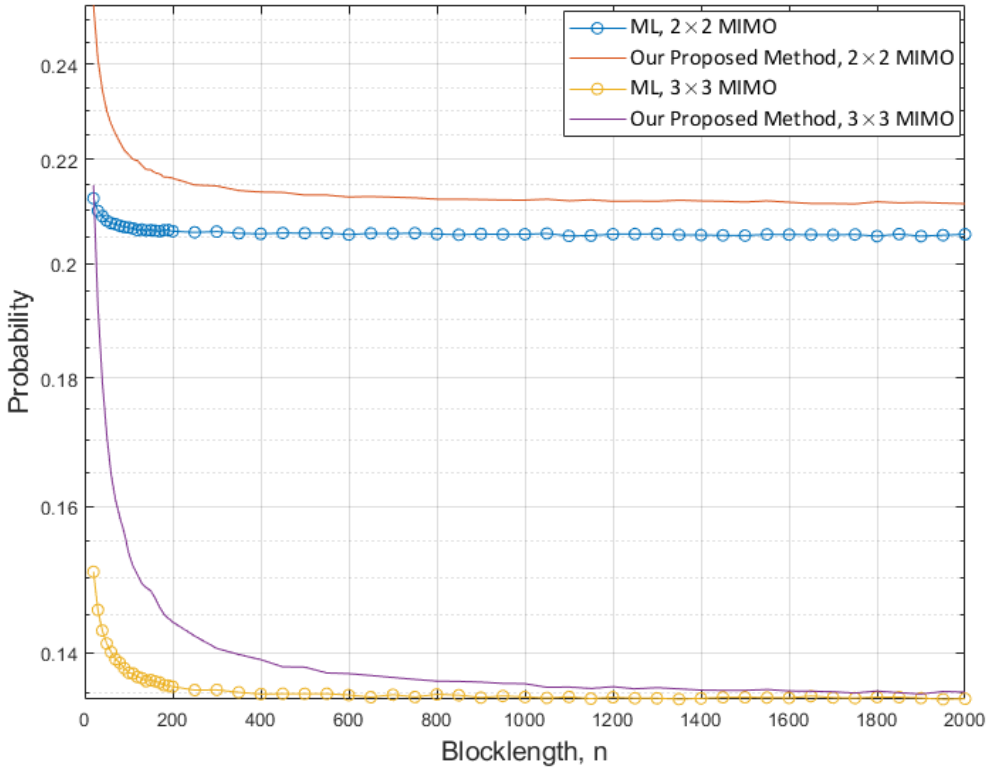

Figure 5.13: $\mathbb{P}[\hat{d} = +1, d = 0 | \hat{\mathbf{X}} \neq \mathbf{X}]$ in (5.28) over 2×2 MIMO and 3×3 MIMO, respectively.

relation between ϵ_{source} and ϵ_{tag} and the blocklength n. Therefore, we plot (5.29) in a 2D plane with the x-axis representing the blocklength n, the y-axis representing ϵ_{source}, and the z-axis representing ϵ_{tag}. From Fig. 5.14, we observe that for the same ϵ_{source}, 3×3 MIMO significantly outperforms 2×2 MIMO from the blocklength $n = 0$ to 1000. When n increases, the gap between these two cases shrinks. Furthermore, for the same blocklength n, when ϵ_{source} is less than 10^{-5}, the performance of 3×3 MIMO is substantially better than that of 2×2 MIMO. As ϵ_{source} becomes small, i.e., 10^{-10}, the gap between the performances of two cases decreases.

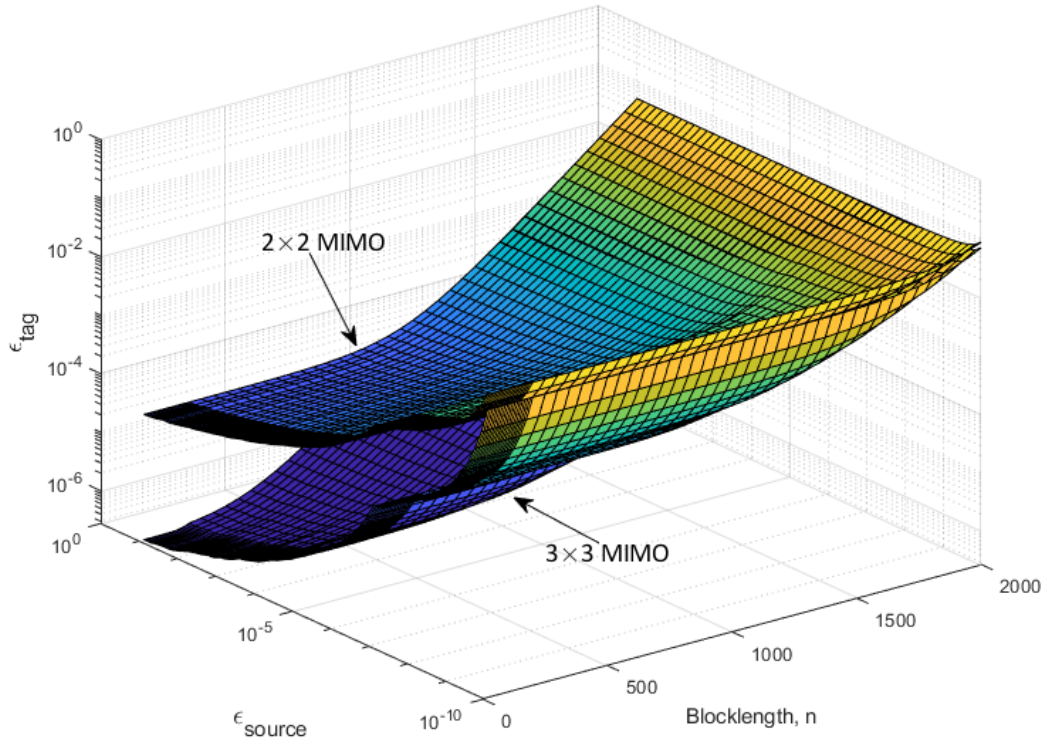

Figure 5.14: The comparison between the blocklength, n, the error probability of the RF source signal ϵ_{source} and the error probability of the tag symbol, ϵ_{tag}.

5.5 Summary

In this chapter, we established achievability and converse bounds on the maximal achievable rate R at a given blocklength n and a maximal error probability ϵ_{source} for an AmBC MIMO system. We derived the relationship between ϵ_{source} and ϵ_{tag} with respect to the blocklength n. The analytical results demonstrated that the number of transmit and receive antennas and the information variance $U(X;Y|D)$ would affect the convergence speed to the maximal achievable rate as the blocklength n increases.

Chapter 6

Conclusions

This thesis presents novel methods to analyze the performance and demonstrate the methods how to analyze the performance of RIS and AmBC systems. The key results and findings are summarized as follows.

In Chapter 3, we explore the lower and upper bounds of the optimal code's decoding error probability, for a specific length, SNR, and code rate, in a short blocklength regime, within an RIS-assisted communication system. Our approach primarily employs the sphere-packing technique to determine the lower and upper bounds, which are derived using closed-form expressions. Through our numerical analysis, we gain insights into the performance of various blocklengths within an RIS-assisted wireless system, given a specific code rate, and determine how the number of RIS elements could enhance signal quality at the receiver's end.

In Chapter 4, we derive both achievability and converse bounds on the maximal achievable rate R for a given blocklength n and maximal error probability ϵ in an RIS MIMO system. Our analysis reveals that the convergence speed to the maximal achievable rate is impacted by several factors, such as the number of transmit and receive antennas, as well as the channel variance $U(X;Y)$. Our analytical results

shed light on the important role these factors play in determining the achievable rate and the associated error probability in RIS MIMO systems, particularly as the blocklength n increases.

In Chapter 5, we develop both achievability and converse bounds on the maximal achievable rate R for a given blocklength n and maximal source error probability ϵ_{source}. Through our analysis, we establish the relationship between the source error probability ϵ_{source} and the tag error probability ϵ_{tag} with respect to the blocklength n. Our analytical results further demonstrate that the convergence speed to the maximal achievable rate is influenced by various factors, including the number of transmit and receive antennas and the information variance $U(X;Y|D)$, especially as the blocklength n increases. These findings provide important insights into the factors that impact the achievable rate and associated error probabilities in AmBC MIMO systems.

6.1 Future Work

In this section, some remaining research problems are listed which will be carried out in the future:

1. We will investigate our mathematics framework into the state-of-the-art communication systems, such as the Intelligent Omni-surface in [57] and the Reconfigurable Holographic Surfaces in [61].

2. We will investigate our derived results at the finite blocklength regime into the differential privacy due to the fact that Rebollo-Mondero et al. connect Equation 4 in [62], which represents the risk-distortion function, to Shannon's rate-distortion problem in information theory [63]. Shannon's theory addresses the compression of data while minimizing the average distortion in the recon-

structed signal. It aims to create a concise code that efficiently represents the original signal or data, with low distortion. The rate-distortion theory determines the expected distortion level D given the desired information rate R of the code, or vice versa, using the rate-distortion function $R(D)$ similar to Equation 4. This function defines the infimum of the rates of codes that maintain a distortion bounded by D. By the above connection, we can apply our derived results at the finite blocklength regime to find the relationship between the size of the dataset and the differential privacy.

Appendix A

Proofs for Chapter 4

In this appendix, we give the proof of the converse part of Theorem 7 and Theorem 9 in Chapter 4 and Chapter 5, respectively. We assume the transmitter is not aware of the realizations of the channel matrix $\mathbf{H}$. We denote the average power constraint

$$\mathbf{p}(\mathbf{X}) \stackrel{\Delta}{=} \frac{1}{n}\mathbf{X}\mathbf{X}^H. \tag{A.1}$$

Based on [64–66], to evaluate the converse bound of an auxiliary channel, we need to obtain the lower bound of ϵ', where ϵ' is the maximal error probability over the corresponding auxiliary channel. We thus denote the auxiliary channel Q as:

$$Q_{\mathbf{Y}|\mathbf{X},\mathbf{H}} \stackrel{\Delta}{=} \prod_{j=1}^{n} Q_{Y_j|\mathbf{X},\mathbf{H}}, \tag{A.2}$$

where

$$Q_{Y_j|\mathbf{X},\mathbf{H}} = \mathcal{CN}(0, \mathbf{I}_r + \mathbf{H}\mathbf{p}(\mathbf{X})\mathbf{H}^H), \tag{A.3}$$

We denote $\mathbf{B} \stackrel{\Delta}{=} \mathbf{I}_r + \mathbf{H}\mathbf{p}(\mathbf{X})\mathbf{H}^H$ and let its eigenvector $\boldsymbol{\omega} = [\omega_1, \ldots, \omega_m] = \lambda_{max}(\mathbf{B})$. Note that $\mathbf{P} = \mathbf{p}(\mathbf{X})$ is the only factor that affects the output of the $Q_{\mathbf{Y}|\mathbf{X},\mathbf{H}}$ channel. Let the space $\mathbf{S} \stackrel{\Delta}{=} \mathbf{p}(\mathbf{Y}) = \frac{1}{n}\mathbf{Y}\mathbf{Y}^H$ and its entry is defined as the square of the norm of $\mathbf{Y}$ and is then normalized by the blocklength n, which is

shown below

$$S_j = \frac{\omega_j}{n} \sum_{i=1}^{n} |Z_{j,i}|^2, \quad j = 1, \ldots, m, \tag{A.4}$$

where $Z_{j,i} \sim \mathcal{CN}(0,1)$. $\mathbf{S}$ can be seen as the statistical expression of the receiver's detection of $\mathbf{X}$ from $(\mathbf{Y}, \mathbf{H})$. Thus the auxiliary channel $Q_{\mathbf{Y}|\mathbf{X},\mathbf{H}}$ can be seen as $Q_{\mathbf{S}|\mathbf{B}}$. From (A.4), we note that the S_j follows the Gamma distribution, and its corresponding PDF is given by

$$q_{S_j|B_j}(s_j|\omega_j) = \frac{n^n}{(\omega_j)^n \Gamma(n)} s_j^{n-1} \exp\Big\{ - \frac{n s_j}{\omega_j} \Big\}. \tag{A.5}$$

Moreover, as $Q_{\mathbf{S}|\mathbf{B}}$ is a product of m copies of the PDF of S_j. We can obtain the PDF of $Q_{\mathbf{S}|\mathbf{B}}$ by the theorem shown below [67].

Theorem 11. *Given N independent Gamma-distributed RVs x_i and that their shape parameter k and scale parameter θ are all the same, we have the PDF of x_i as*

$$f_i(x_i) = \frac{1}{\Gamma(k)\theta^k} x_i^{k-1} e^{-\frac{x_i}{\theta}}. \tag{A.6}$$

We denote z as the product of N independent gamma variables x_i. Therefore, the PDF of $z = x_1 x_2 \ldots x_N$ is a normalized Meijer G-function as

$$g(z) = \mathcal{K} G_{0,N}^{N,0}\big({}_{k-1} \,\big|\, \frac{z}{\theta^N} \big), \tag{A.7}$$

where $\mathcal{K}$ is a normalizing factor which is

$$\mathcal{K} = (\frac{1}{\theta})^N \prod_{i=1}^{N} \frac{1}{\Gamma(k)}, \tag{A.8}$$

and

$$G_{p,q}^{m,n}\big({}^{j_1,j_2,\ldots,j_p}_{k_1,k_2,\ldots,k_q} \,\big|\, z \big) = \frac{1}{2\pi i} \int_{c-i\infty}^{c+i\infty} z^{-s} \cdot \frac{\prod_{j=1}^{m} \Gamma(s + k_j) \cdot \prod_{j=1}^{n} \Gamma(1 - j_j - s)}{\prod_{j=n+1}^{p} \Gamma(s + j_j) \cdot \prod_{j=m+1}^{q} \Gamma(1 - k_j - s)} ds, \tag{A.9}$$

where c is a vertical contour in the complex plane chosen to separate the poles of $\Gamma(s + k_j)$ from those of $\Gamma(1 - j_k) - s$.

We set two parameters, the shape parameter $k = n$ and the scale parameter $\theta_j = \frac{\omega_j}{n}$. The number of copies in our case is $N = m$. Then we can apply Theorem 11 to calculate the PDF of $Q_{\mathbf{S}|\mathbf{B}}$ as

$$q_{S_j|B_j}(s_j|\omega_j) = \mathcal{K} G_{0,m}^{m,0}\Big({}_{n-1} \Big| \, s_j(\frac{n}{\omega_j})^m \Big), \tag{A.10}$$

where

$$\mathcal{K} = (\frac{n}{\omega_j})^m \prod_{i=1}^{m} \frac{1}{\Gamma(n)}, \tag{A.11}$$

and

$$G_{0,m}^{m,0}\Big({}_{n-1} \Big| \, s_j(\frac{n}{\omega_j})^m \Big) = \frac{1}{2\pi i} \int_{c-i^\infty}^{c+i^\infty} (s_j(\frac{n}{1+\omega_j})^m)^{-z} \prod_{j=1}^{m} \Gamma(z+n-1) dz. \tag{A.12}$$

Consider an arbitrary code for the auxiliary channel Q. The decoding sets corresponding to the M codewords is denoted by $D_i, i = 1, ..., M$. ϵ' is the maximal error probability over the auxiliary channel Q. Then we have

$$\begin{aligned} 1 - \epsilon' &= \frac{1}{M} \mathbb{E}_{\mathbf{H}} \Bigg[\sum_{i=0}^{M} \int_{D_i} q_{\mathbf{S}|\mathbf{B}}(\mathbf{s}) d\mathbf{s} \Bigg] \\ &\leq \mathbb{E}_{\mathbf{H}} \Bigg[\int_{D_0} q_{\mathbf{S}|\mathbf{B}}(\mathbf{s}) d\mathbf{s} \Bigg] \leq \mathbb{E}_{\mathbf{H}} \Bigg[\max\{q_{\mathbf{S}|\mathbf{B}}(\mathbf{s})\} \times Leb(D_0) \Bigg]. \end{aligned}$$

Next we need to provide the maximum of the output space of an arbitrary decoding set, $Leb(D_0)$. Due to the power allocation vector $\mathbf{p}(\mathbf{X})$, the space $\mathbf{P}$ can be bounded by a certain ball in $\mathbb{R}^m$. Based on the definition of $\mathbf{S}$, its space is a slightly larger ball than the space $\mathbf{P}$. Thus we can obtain the maximum of the Lebesgue measure [68] of D_0,

$$Leb(D_0) \leq Leb(\mathbf{S}) \leq \frac{K}{M}, \tag{A.13}$$

where K is a constant.

Then the decoding set of any codeword has a Lebesgue measure space which is always smaller than $\frac{K}{M}$. Therefore, we have

$$1-\epsilon' \leq \mathbb{E}_{\mathbf{H}}\left[\max\{q_{\mathbf{S}|\mathbf{B}}(\mathbf{s})\} \times \frac{K}{M}\right] \tag{A.14}$$

$$= \frac{1}{M}\left(\frac{(n-1)^n \exp\{-(n-1)\}}{\Gamma(n)}\right)^m \times \int_0^\infty \prod_{i=1}^{m}(\omega_j)p(g)dg \tag{A.15}$$

$$\leq \frac{n^{m/2}}{M}. \tag{A.16}$$

According to Theorem 4, we have

$$\Lambda(\epsilon) \geq \frac{1}{\lambda}\Big(\epsilon - \mathbb{P}\big[i(X^n;Y^n) \leq \log\lambda\big]\Big) \geq \frac{1}{\lambda}\Big(\epsilon - \frac{6T(X;Y)}{\sqrt{n}U(X;Y)^{\frac{3}{2}}} - Q(\tau)\Big), \tag{A.17}$$

where $\Lambda(\epsilon)$ denotes the maximal probability of error under $P_{\mathbf{Y}|\mathbf{X},\mathbf{H}}$ if the probability of error under $Q_{\mathbf{Y}|\mathbf{X},\mathbf{H}}$ is ϵ and (A.17) follows from (2.40) in Subsection 2.2.1. Then,

$$\log\Lambda(\epsilon) \geq -nI(X;Y) + \tau\sqrt{nU(X;Y)} + \log\Big(\epsilon - \frac{6T(X;Y)}{\sqrt{n}U(X;Y)^{\frac{3}{2}}} - Q(\tau)\Big), \tag{A.18}$$

where (A.18) follows from (2.39) in Subsection 2.2.1. We assume $\tau = Q^{-1}(\epsilon(1+\frac{1}{\sqrt{n}}) - \frac{6T(X;Y)}{\sqrt{n}U(X;Y)^{\frac{3}{2}}})$. Thus,

$$\log\Lambda(\epsilon) \geq -nI(X;Y) + \sqrt{nU(X;Y)}Q^{-1}(\epsilon(1+\frac{1}{\sqrt{n}}) - \frac{6T(X;Y)}{\sqrt{n}U(X;Y)^{\frac{3}{2}}}) - \frac{1}{2}\log n. \tag{A.19}$$

Due to the fact that $\log\Lambda(\epsilon) \leq \log(1-\epsilon')$, we have

$$-nI(X;Y) + \sqrt{nU(X;Y)}Q^{-1}(\epsilon + \frac{\epsilon}{\sqrt{n}}) - \frac{1}{2}\log n + \mathcal{O}(\frac{1}{\sqrt{n}}) \leq 1-\epsilon'. \tag{A.20}$$

Thus substituting (A.20) into (A.16), we have

$$R \leq I(X;Y) - \sqrt{\frac{U(X;Y)}{n}}Q^{-1}(\epsilon + \frac{\epsilon}{\sqrt{n}}) + \frac{(m+1)\log n}{2n} + \mathcal{O}(n^{-\frac{3}{2}}). \tag{A.21}$$

Appendix B

Proofs for Chapter 5

In this appendix, we give the proof of saddle point approximation [69] of (5.8) and (5.9) in Chapter 5.

$$I(X;Y|d=0) = t\log|\mathcal{A}| + \frac{1}{|\mathcal{A}|^t}\sum_{i=1}^{|\mathcal{A}|^t}\int_0^\infty\int_{-\infty}^\infty \frac{1}{det(\pi\mathbf{I}_r)}p(\mathbf{h}_0)\exp\{-\frac{1}{2}\|\mathbf{y}-\mathbf{h}_0\mathbf{x}_i\|^2\}\cdot \log\{\frac{\exp\{-\frac{1}{2}\|\mathbf{y}-\mathbf{h}_0\mathbf{x}_i\|^2\}}{\sum_{i'=1}^{|\mathcal{A}|^t}\exp\{-\frac{1}{2}\|\mathbf{y}-\mathbf{h}_0\mathbf{x}_{i'}\|^2\}}\}d\mathbf{y}d\mathbf{h}_0 \quad \text{(B.1)}$$

$$= t\log|\mathcal{A}| - \frac{1}{|\mathcal{A}|^t\ln 2}\sum_{i=1}^{|\mathcal{A}|^t}\sum_{p=1}^{\infty}\frac{1}{p}\sum_{q=0}^{p}\frac{p!(-1)^q}{q!(p-q)!}\frac{1}{det(\pi\mathbf{I}_r)}\cdot \int_0^\infty\int_{-\infty}^\infty p(\mathbf{h}_0)\Big(\mathbf{\Pi}(\mathbf{y},\mathbf{h}_0)\Big)^{-q}d\mathbf{y}d\mathbf{h}_0, \quad \text{(B.2)}$$

where (B.2) comes from Taylor series expansion of (B.1) and

$$\mathbf{\Pi}(\mathbf{y},\mathbf{h}_0) = \sum_{i'=1}^{|\mathcal{A}|^t}\exp\Big\{\frac{\big\|\mathbf{y}-q\mathbf{h}_0(\mathbf{x}_i-\mathbf{x}_{i'})\big\|^2}{2q} - \frac{(q+1)\big\|\mathbf{h}_0(\mathbf{x}_i-\mathbf{x}_{i'})\big\|^2}{2}\Big\}.$$

Before utilizing the saddle point approximation, we need to guarantee the existence of the saddle point. For convenience of notation, we use vector $\mathbf{c}_{i,i'}$ to represent $\mathbf{h}_0(\mathbf{x}_i-\mathbf{x}_{i'})$. Since q is positive integers, it is easy for us to validate that $\mathbf{\Pi}^{-q}(\mathbf{y}) > 0$, $\lim_{\mathbf{y}\to\infty}\{\mathbf{\Pi}^{-q}(\mathbf{y})\} = 0$ and $\lim_{\mathbf{y}\to-\infty}\{\mathbf{\Pi}^{-q}(\mathbf{y})\} = 0$.

Thus there exists a maximum value of $\mathbf{\Pi}^{-q}(\mathbf{y})$, which satisfies the condition of the saddle point approximation. Then we can assume that $\mathbf{\Pi}^{-q}(\mathbf{y})$ achieves its maximum at $\mathbf{y} = \mathbf{y}_0$, which $\mathbf{y}_0$ satisfies $\frac{\partial}{\partial \mathbf{y}} \mathbf{\Pi}^{-q}(\mathbf{y})|_{\mathbf{y}=\mathbf{y}_0} = 0$

$$\sum_{i'=1}^{|\mathcal{A}|^t} \frac{2(\mathbf{y}_0 - q\mathbf{c}_{i,i'})}{2q} \exp\{\frac{\left\|\mathbf{y}_0 - q\mathbf{c}_{i,i'}\right\|^2}{2q} - \frac{(q+1)\left\|\mathbf{c}_{i,i'}\right\|}{2}\} = 0. \tag{B.3}$$

After solving (B.3), we have $\mathbf{y}_0 = \sum_{i'=1}^{|\mathcal{A}|^t} q\rho_{i,i'}\mathbf{c}_{i,i'}$, where $\rho_{i,i'} = \mathbf{\Pi}(\mathbf{y}_0)/\sum_{i'=1}^{|\mathcal{A}|^t} \mathbf{\Pi}(\mathbf{y}_0)$ is a positive number from $(0,1)$ and satisfies that $\sum_{i'=1}^{|\mathcal{A}|^t} \rho_{i,i'} = 1$. Therefore, we have for a non-zero number q, the multiple integrals over the complex number vector $\mathbf{y}$ can be approximated by the saddle point approximation

$$\int_{-\infty}^{\infty} \frac{1}{det(\pi \mathbf{I}_r)} \Big(\mathbf{\Pi}(\mathbf{y}, \mathbf{h}_0)\Big)^{-q} d\mathbf{y} \approx \Big[\sum_{i'=1}^{|\mathcal{A}|^t} \exp\{-\frac{\left\|\mathbf{h}_0(\mathbf{x}_i - \mathbf{x}_{i'})\right\|^2}{3 - \exp\{-\left\|\mathbf{h}_0(\mathbf{x}_i - \mathbf{x}_{i'})\right\|^2/4\}}\}\Big]^{-q}. \tag{B.4}$$

Combining (B.2) and (B.4), we eliminate the multiple integrals over the complex vector $\mathbf{y}$ as

$$I(X;Y|d=0) \approx t\log|\mathcal{A}| - \frac{1}{|\mathcal{A}|^t \ln 2} \sum_{i=1}^{|\mathcal{A}|^t} \sum_{p=1}^{\infty} \frac{1}{p} \sum_{q=0}^{p} \frac{p!(-1)^q}{q!(p-q)!} \int_0^{\infty} p(\mathbf{h}_0) \cdot \Big[\sum_{i'=1}^{|\mathcal{A}|^t} \exp\Big\{-\frac{\left\|\mathbf{h}_0(\mathbf{x}_i - \mathbf{x}_{i'})\right\|^2}{3 - \exp\{-\left\|\mathbf{h}_0(\mathbf{x}_i - \mathbf{x}_{i'})\right\|^2/4\}}\Big\}\Big]^{-q} d\mathbf{h}_0. \tag{B.5}$$

Then by observing (B.5), we take advantage of inverse Taylor series expansion and we obtain

$$I(X;Y|d=0) \approx t\log|\mathcal{A}| - \int_0^{\infty} p(\mathbf{h}_0) \frac{1}{|\mathcal{A}|^t} \sum_{i=1}^{|\mathcal{A}|^t} \log\Big[\sum_{i'=1}^{|\mathcal{A}|^t} \exp\Big\{-\frac{\left\|\mathbf{h}_0(\mathbf{x}_i - \mathbf{x}_{i'})\right\|^2}{3 - \exp\{-\left\|\mathbf{h}_0(\mathbf{x}_i - \mathbf{x}_{i'})\right\|^2/4\}}\Big\}\Big] d\mathbf{h}_0. \tag{B.6}$$

Moreover, we need to obtain the approximation of the unconditional variance $U(X;Y)$. The steps are basically same with the process of the approximation of

$I(X;Y)$, then we have

$$U(X;Y|d=0) \approx -[I(X;Y) - (t\log|\mathcal{A}|)]^2 + \int_0^\infty p(\mathbf{h}_0)\frac{1}{|\mathcal{A}|^t}\sum_{i=1}^{|\mathcal{A}|^t} \log^2[\sum_{i'=1}^{|\mathcal{A}|^t}\exp\{-\frac{\left\|\mathbf{h}_0(\mathbf{x}_i-\mathbf{x}_{i'})\right\|^2}{6-\exp\{-\left\|\mathbf{h}_0(\mathbf{x}_i-\mathbf{x}_{i'})\right\|^2/16\}}\}]d\mathbf{h}_0. \quad \text{(B.7)}$$

Bibliography

[1] M. Di Renzo et al., "Reconfigurable Intelligent Surfaces vs. Relaying: Differences, Similarities, and Performance Comparison," in *IEEE Open J. Commun. Soc.*, vol. 1, pp. 798-807, 2020.

[2] Ludek Subrt and Pavel Pechac. "Controlling propagation environments using intelligent walls," in *Eur. Conf. Antennas Propag.*, pages 1–5. IEEE, 2012.

[3] Ludek Subrt and Pavel Pechac. "Intelligent walls as autonomous parts of smart indoor environments," in *IET Commun.*, 6(8):1004–1010, 2012.

[4] Kihun Chang, Sang il Kwak, and Young Joong Yoon. "Equivalent circuit modeling of active frequency selective surfaces," in *IEEE Radio Wireless Symp.*, pages 663–666, 2008.

[5] Harry Stockman. "Communication by means of reflected power," in *Proc. IRE*, 36(10):1196–1204, 1948.

[6] L. Yan, Y. Zhang, L. T. Yang, and H. Ning, *The Internet of Things: From RFID to the Next-Generation Pervasive Networked Systems.* Boca Raton, FL, USA: Auerbach Publications, 2008.

[7] H. Jayakumar, K. Lee, W. S. Lee, A. Raha, Y. Kim, and V. Raghunathan, "Powering the Internet of Things," in *Proc. Int. Symp. Low Power Electron. Design*, La Jolla, CA, USA, Aug. 2014, pp. 375–380.

[8] V. Liu, A. Parks, V. Talla, S. Gollakota, D. Wetherall, and J. R. Smith, "Ambient backscatter: Wireless communication out of thin air," in *Proc. ACM SIGCOMM*, Hong Kong, Aug. 2013, pp. 39–50.

[9] A. Parks, A. Liu, S. Gollakota, and J. R. Smith, "Turbocharging ambient backscatter communication," in *Proc. ACM SIGCOMM*, Chicago, IL, USA, Aug. 2014, pp. 619–630.

[10] C. Boyer and S. Roy, "Backscatter communication and RFID: Coding, energy, and MIMO analysis," in *IEEE Trans. Commun.*, vol. 62, no. 3, pp. 770–785, Mar. 2014.

[11] G. Yang, Y.-C. Liang, R. Zhang, and Y. Pei, "Modulation in the air: Backscatter communication over ambient OFDM carrier," in *IEEE Trans. Commun.*, vol. 66, no. 3, pp. 1219–1233, Mar. 2018.

[12] J. Qian, Y. Zhu, C. He, F. Gao and S. Jin, "Achievable Rate and Capacity Analysis for Ambient Backscatter Communications," in *IEEE Trans. Commun.*, vol. 67, no. 9, pp. 6299-6310, Sept. 2019.

[13] D. Darsena, G. Gelli, and F. Verde, "Modeling and performance analysis of wireless networks with ambient backscatter devices," in *IEEE Trans. Commun.*, vol. 65, no. 4, pp. 1797–1814, Jan. 2017.

[14] Shancang Li, Li Da Xu, and Shanshan Zhao. "The Internet of Things: A survey," in *Inf. Syst. Front.*, 17(2):243–259, 2015.

[15] Y. -C. Liang, Q. Zhang, E. G. Larsson and G. Y. Li, "Symbiotic Radio: Cognitive Backscattering Communications for Future Wireless Networks," in *IEEE Trans. on Cogn. Commun. Netw.*, vol. 6, no. 4, pp. 1242-1255, Dec. 2020

[16] C. E. Shannon, "Probability of error for optimal codes in a Gaussian channel," in *Bell Syst. Tech.l J.*, vol. 38, no. 3, pp. 611-656, May 1959.

[17] Y. Polyanskiy, H. V. Poor, and S. Verdú, "Channel coding rate in the finite blocklength regime," in *IEEE Trans. Inf. Theory*, vol. 56, no. 5, pp. 2307–2359, May 2010.

[18] D. Gesbert, M. Shafi, Da-shan Shiu, P. J. Smith and A. Naguib, "From theory to practice: an overview of MIMO space-time coded wireless systems," in *IEEE J. Sel. Areas Commun.*, vol. 21, no. 3, pp. 281-302, April 2003,

[19] G. J. Foschini and M. J. Gans, "On limits of wireless communications in a fading environment when using multiple antennas," in *Wireless Pers. Commun.*, vol. 6, pp. 311–335, Mar. 1998.

[20]] G. J. Foschini, "Layered space–time architecture for wireless communication in a fading environment when using multielement antennas," in *Bell Labs Tech. J.*, pp. 41–59, Autumn 1996.

[21] İ. E. Telatar, "Capacity of multi-antenna Gaussian channels," in *Eur. Trans. Telecommun.*, vol. 10, pp. 585–595, Nov. 1999.

[22] G. Raleigh and J. M. Cioffi, "Spatial-temporal coding for wireless communications," in *IEEE Trans. Commun.*, vol. 46, pp. 357–366, 1998.

[23] H. Bölcskei, D. Gesbert, and A. J. Paulraj, "On the capacity of OFDM-based spatial multiplexing systems," in *IEEE Trans. Commun.*, vol. 50, pp. 225–234, Feb. 2002.

[24] E. Basar, M. Di Renzo, J. De Rosny, M. Debbah, M. -S. Alouini and R. Zhang, "Wireless Communications Through Reconfigurable Intelligent Surfaces," in *IEEE Access*, vol. 7, pp. 116753-116773, 2019.

[25] L. Yang, Y. Yang, M. O. Hasna and M. -S. Alouini, "Coverage, Probability of SNR Gain, and DOR Analysis of RIS-Aided Communication Systems," in *IEEE Wireless Commun. Lett.*, vol. 9, no. 8, pp. 1268-1272, Aug. 2020.

[26] S. Zeng, H. Zhang, B. Di, Z. Han and L. Song, "Reconfigurable Intelligent Surface (RIS) Assisted Wireless Coverage Extension: RIS Orientation and Location Optimization," in *IEEE Commun. Lett.*, vol. 25, no. 1, pp. 269-273, Jan. 2021.

[27] H. Guo, Y. -C. Liang, J. Chen and E. G. Larsson, "Weighted Sum-Rate Maximization for Intelligent Reflecting Surface Enhanced Wireless Networks," in *2019 IEEE Glob. Commun. Conf. (GLOBECOM)*, 2019.

[28] C. Huang, G. C. Alexandropoulos, A. Zappone, M. Debbah and C. Yuen, "Energy Efficient Multi-User MISO Communication Using Low Resolution Large Intelligent Surfaces," in *IEEE Glob. Wkshps. (GC Wkshps)*, 2018.

[29] H. Han, J. Zhao, D. Niyato, M. D. Renzo and Q. -V. Pham, "Intelligent Reflecting Surface Aided Network: Power Control for Physical-Layer Broadcasting," in *IEEE Int. Conf. Commun. (ICC)*, 2020.

[30] A. -A. A. Boulogeorgos and A. Alexiou, "Performance Analysis of Reconfigurable Intelligent Surface-Assisted Wireless Systems and Comparison With Relaying," in *IEEE Access*, vol. 8, pp. 94463-94483, 2020.

[31] H. Ren, K. Wang and C. Pan, "Intelligent Reflecting Surface-Aided URLLC in a Factory Automation Scenario," in *IEEE Trans. Commun.*, vol. 70, no. 1, pp. 707-723, Jan. 2022

[32] Vincent Liu, Aaron Parks, Vamsi Talla, Shyamnath Gollakota, David Wetherall, and Joshua R Smith. "Ambient backscatter: Wireless communication out of thin air," in *ACM SIGCOMM Comput. Commun. Rev.*, 43(4):39–50, 2013.

[33] Dinesh Bharadia, Kiran Raj Joshi, Manikanta Kotaru, and Sachin Katti. "Backfi: High throughput WiFi backscatter," in *ACM SIGCOMM Comput. Commun. Rev.*, 45(4):283–296, 2015.

[34] A. Valembois and M. P. C. Fossorier, "Sphere-packing bounds revisited for moderate block lengths," in *IEEE Trans. Inf. Theory*, vol. 50, pp. 2998–3014, 2004.

[35] G. Wiechman and I. Sason, "An Improved Sphere-Packing Bound for Finite-Length Codes Over Symmetric Memoryless Channels," in *IEEE Trans. Inf. Theory*, vol. 54, no. 5, pp. 1962-1990, May 2008.

[36] W. Yang, G. Durisi, T. Koch and Y. Polyanskiy, "Quasi-Static Multiple-Antenna Fading Channels at Finite Blocklength," in *IEEE Trans. Inf. Theory*, vol. 60, no. 7, pp. 4232-4265, Jul. 2014.

[37] A. Collins and Y. Polyanskiy, "Coherent Multiple-Antenna Block-Fading Channels at Finite Blocklength," in *IEEE Trans. Inf. Theory*, vol. 65, no. 1, pp. 380-405, Jan. 2019.

[38] Y. Polyanskiy, "Channel coding: Non-asymptotic fundamental limits," Ph.D. dissertation, *Dept. Elect. Eng., Princeton Univ.*, Princeton, NJ, USA, 2010.

[39] Y. Polyanskiy, H. V. Poor, and S. Verdú, "Dispersion of Gaussian channels," in *Proc. 2009 IEEE Int. Symp. Inf. Theory (ISIT)*, Seoul, Korea, Jul. 2009.

[40] W. Feller, *An Introduction to Probability Theory and Its Applications*, Second ed. New York: Wiley, 1971, vol. II.

[41] C. E. Shannon, R. G. Gallager, and E. R. Berlekamp, "Lower bounds to error probability for coding on discrete memoryless channels," in *Inform. Contr.*, pt. I, vol. 10, no. 1, pp. 65–103, Feb. 1967.

[42] Richard W Hamming. "Error detecting and error correcting codes," in *Bell Syst. Tech. J.*, 29(2):147–160, 1950.

[43] Arikan. "Channel polarization: A method for constructing capacity-achieving codes for symmetric binary-input memoryless channels," in *IEEE Trans. Inf. Theory*, 55(7):3051–3073, 2009.

[44] I. Tal and A. Vardy, "List Decoding of Polar Codes," in *IEEE Trans. Inf. Theory*, vol. 61, no. 5, pp. 2213-2226, May 2015.

[45] W. Tang et al., "Path Loss Modeling and Measurements for Reconfigurable Intelligent Surfaces in the Millimeter-Wave Frequency Band," in *IEEE Trans. Commun.*, vol. 70, no. 9, pp. 6259-6276, Sept. 2022

[46] William Kruskal, "The monotonicity of the ratio of two noncentral t density functions," in *Ann. Math. Stat.*, Vol. 25, pp. 162-165, 1954.

[47] T. J. Cui, M. Q. Qi, X. Wan, J. Zhao, and Q. Cheng, "Coding metamaterials, digital metamaterials and programmable metamaterials," in *Light, Sci. Appl.*, vol. 3, no. 10, p. e218, Oct. 2014.

[48] H. Yang et al., "A programmable metasurface with dynamic polarization, scattering and focusing control," in *Sci. Rep.*, vol. 6, no. 1, Oct. 2016, Art. no. 35692.

[49] S. Zhang and R. Zhang, "Capacity Characterization for Intelligent Reflecting Surface Aided MIMO Communication," in *IEEE J. Sel. Areas Commun.*, vol. 38, no. 8, pp. 1823-1838, Aug. 2020.

[50] S. Verdú and T. S. Han, "A general formula for channel capacity," in *IEEE Trans. Inf. Theory*, vol. 40, no. 4, pp. 1147–1157, Jul. 1994.

[51] I. Sason and S. Shamai, "On improved bounds on the decoding error probability of block codes over interleaved fading channels, with applications to turbo-like codes," in *IEEE Trans. Inf. Theory*, vol. 47, no. 6, pp. 2275-2299, Sept. 2001.

[52] S. Verdú, "Spectral efficiency in the wideband regime," in *IEEE Trans. Inf. Theory*, vol. 48, no. 6, pp. 1319–1343, Jun. 2002.

[53] Y. Wang and W. Zhang, "Generalized Nearest Neighbor Decoding," in *IEEE Trans. Inf. Theory*, vol. 68, no. 9, pp. 5852-5865, Sept. 2022.

[54] Z. Wang, L. Liu and S. Cui, "Channel Estimation for Intelligent Reflecting Surface Assisted Multiuser Communications: Framework, Algorithms, and Analysis," in *IEEE Trans. Wirel. Commun.*, vol. 19, no. 10, pp. 6607-6620, Oct. 2020.

[55] H. Guo and V. K. N. Lau, "Uplink Cascaded Channel Estimation for Intelligent Reflecting Surface Assisted Multiuser MISO Systems," in *IEEE Trans. Signal Process.*, vol. 70, pp. 3964-3977, 2022.

[56] Z. Zhou, N. Ge, Z. Wang and L. Hanzo, "Joint Transmit Precoding and Reconfigurable Intelligent Surface Phase Adjustment: A Decomposition-Aided Chan-

nel Estimation Approach," in *IEEE Trans. Commun.*, vol. 69, no. 2, pp. 1228-1243, Feb. 2021.

[57] S. Zeng et al., "Intelligent Omni-Surfaces: Reflection-Refraction Circuit Model, Full-Dimensional Beamforming, and System Implementation," in *IEEE Trans. Commun.*, vol. 70, no. 11, pp. 7711-7727, Nov. 2022.

[58] E. Biglieri, J. Proakis, and S. Shamai (Shitz), "Fading channels: Information-theoretic and communications aspects," in *IEEE Trans. Inf. Theory*, vol. 44, no. 6, pp. 2619–2692, Oct. 1998.

[59] D. N. C. Tse and P. Viswanath, *Fundamentals of Wireless Communication.* Cambridge, U.K.: Cambridge Univ. Press, 2005.

[60] G. Yang, Q. Zhang and Y. Liang, "Cooperative Ambient Backscatter Communications for Green Internet-of-Things," in *IEEE Internet Things J.*, vol. 5, no. 2, pp. 1116-1130, Apr. 2018.

[61] R. Deng et al., "Reconfigurable Holographic Surfaces for Future Wireless Communications," in *IEEE Wirel. Commun.*, vol. 28, no. 6, pp. 126-131, Dec. 2021.

[62] D. Rebollo-Monedero, J. Forné and J. Domingo-Ferrer, "From t-Closeness-Like Privacy to Postrandomization via Information Theory," in *IEEE Trans. Knowl. Data Eng.*, vol. 22, no. 11, pp. 1623-1636, Nov. 2010.

[63] T. M. Cover and J. A. Thomas. *Elements of Information Theory 2nd Edition.* Wiley-Interscience, Jul. 2006.

[64] J. Neyman and E. S. Pearson, "On the problem of the most efficient tests of statistical hypotheses," in *Philosoph. Trans. Roy. Soc. A*, vol. 231, pp. 289–337, Jan. 1933.

[65] H. V. Poor and S. Verdú, "A lower bound on the error probability in multi-hypothesis testing," in *IEEE Trans. Inf. Theory*, vol. 41, no. 6, pp. 1992–1993, 1995.

[66] R. E. Blahut, "Hypothesis testing and information theory," in *IEEE Trans. Inf. Theory*, vol. 20, no. 4, pp. 405–417, 1974.

[67] Springer, M. D., and W. E. Thompson. "The Distribution of Products of Beta, Gamma and Gaussian Random Variables," in *SIAM J. Appl. Math.*, vol. 18, no. 4, 1970, pp. 721–737.

[68] R. Ash, *Information Theory.* New York: Interscience Publishers, 1965.

[69] Liu, Y.; Zhang, J.; Zhang, D. "Saddle Point Approximation of Mutual Information for Finite-Alphabet Inputs over Doubly Correlated MIMO Rayleigh Fading Channels," in *Appl. Sci.*, 2021, 11, 4700.